Università Politecnica delle Marche
Facoltà di Ingegneria
Corso di Laurea Magistrale in Ingegneria Meccanica
curriculum Meccatronica

Algoritmi di ricostruzione di segnali sotto-campionati per la misura di vibrazioni con sistemi di visione

Reconstruction algorithms of down-sampled signals for vision based vibration measurements

Candidate:
Andrea Sabatini

Advisor:
Prof. Milena Martarelli

Coadvisor:
Eng. Davide Mastrodicasa

Academic Year 2023-2024

... smile at what you don't understand,
because the world can also deceive us that we are not miracles

Acknowledgments

I would like to thanks the Siemens Digital Industry Software, especially the Test Division team in Leuven, Belgium I worked with, during my 6 months internship. In particular, thanks to my supervisor at Siemens Davide Mastrodicasa, for his patience, availability and passion demonstrated. Thanks to the Professors Francesco Cosco, and Paolo Neri, for their intervention and suggestions during my work. Thanks to my Professors at Università Politecnica delle Marche Paolo Castellini and Milena Martarelli, for the possibility to have this experience abroad and also for continuing working in their research field as a PhD student.

Finally, thanks to my friends, the ones I met in Leuven that made me live one of the best experiences of my life, and the ones that have been always with me that fuel my energy and strength. Thanks to my family, that always supports me, in all my choices, and represents one of the most precious things I have.

Ancona, 28th of October 2024

Andrea Sabatini

Abstract

Complex mechanical products in automotive, aerospace and other mechanical industries are validated using vibration measurements and experimental modal analysis. These tests are mainly performed using pointwise sensors connected to the structure. A limited number of transducers might not be able to comprehensively measure the dynamic response, especially when dealing with large-size or very small structures. This is one of the reasons behind the development of image processing techniques, like Digital Image Correlation (DIC), to perform modal analysis.

A particular field of interest in using DIC for vibration analysis is in using cheap, light and low speed camera to detect structure's high frequency behavior. To overcome the low sampling rate, techniques such as under-sampling and remapping the time histories, random sampling and smart aliasing to measure above the camera Nyquist frequency limit can be employed.

Particularly, this thesis focuses on the use of signal reconstruction algorithms for bandlimited signals. It is possible, indeed, to go beyond the Nyquist Shannon frequency limit even without the use of high-speed cameras by exciting a structure using a bandlimited signal, reconstructing the output and perform modal analysis.

The two main studied algorithms are one in time domain and one in the frequency domain. Additional procedures for Frequency response function (FRF) branches assembly in bandlimited regions have been performed. The case study involves both numerical and experimental validations also with the use of affordable sensors such as accelerometers.
An appendix on a numerical study over Compressed Sensing, another signal reconstruction algorithm, is provided.

Sommario

Il presente sommario riassume il contenuto e i risultati della tesi redatta in lingua inglese.

Il mondo della misura di vibrazioni senza contatto rappresenta una delle frontiere di ricerca odierne. In particolari i vantaggi di questa tecnica sono legati a non aggiungere massa alla struttura, evitare numerosi cablaggi, poter misurare ad una certa distanza e quindi anche strutture ad alte temperature ed in rotazione. Rispetto a tecniche tradizionali come i classici accelerometri, questa è una tecnica full field, che utilizza telecamere a bassa o alta velocità. Il compromesso importante in queste due tipologie di telecamere riguarda velocità di acquisizione (frame rate o frequenza di campionamento) e risoluzione. Infatti avere alta frequenza di campionamento, oltre ad imcrementare il costo dello strumento, implica una minor risoluzione. Per questo motivo, come illustrato nella sezione 1.1, l'obiettivo di questa tesi è dimostrare come sia possibile utilizzare telecamere a bassa velocità, sottocampionando il segnale di spostamento misurato per poi utilizzare algoritmi di ricostruzione del segnale, ottenendo quello "corretto" e eseguire analisi modale. Lo scopo è quindi misurare ad alta risoluzione ma con una frequenza di campionamento che viola il teorema di Nyquist, andando in aliasing. Molteplici lavori in letteratura, come presentato nella sezione 1.2 hanno affrontato questo approccio variando nel dettaglio le tecniche di ricostruzione e gli approcci sperimentali.

Questa tesi parte dall'articolo di Paolo Neri [1] in cui si mostra una tecnica di ricostruzione di segnale sottocampionato con spettro a bandalimitata chiamato "Interpolation Method" e discusso teoricamente nella sezione 2.1 e implementato numericamente nella prima parte della sezione 2.2. A partire da questo metodo, che funziona nel dominio del tempo rielaborando la storia temporale del segnale sottocampionato, merito di questa tesi è stato sviluppare un metodo analogo ma nel dominio della frequenza chiamato "repMat Method". Il metodo è illustrato e discusso nella sezione 2.2. Questo metodo sfrutta il concetto di ripetizione di array, e tramite un operazione di "taglia e cuci" lo spettro ripetuto del segnale sottocampionato viene rielaborato fino ad ottenere quello originale. Il vantaggio principale è che non è necessario effettuare l'operazione di trasformata di Fourier inversa in quanto si possono calcoare cross-spettri, auto-spettri e coerenze direttamente nel dominio della frequenza per l'analisi modale.

Gli algoritmi sono stati numericamente validati, utilizzando sia generici segnali a banda limitata sia segnali provenienti da un modello massa molla smorzatore a 3 gradi di libertà che è stato eccitato con una forzante a banda limita. I risultati mostrano un'ottima corrispondenza col segnale originale, come riportato nella sezione 2.4, sono stati utilizzati dei coefficienti numerici per quantificare la bontà della ricostruzione, e questi si assestano a valori molto vicini al 100% di accuratezza di ricostruzione.

Successivamente nel capitolo 3, viene invece illustrata nel dettaglio una procedura ideata per la validazione sperimentale. Necessario è infatti, dopo aver correttamente pianificato il test, calcolare i parametri di acquisizione, tra cui la frequenza di sotto campionamento delle telecamere ed il numero di foto da acquisire nell'intervallo di tempo designato. Viene illustrato il setup sperimentale; i test sono stati effettuati su una trave piatta vincolata ad una estremità; l'eccitazione (necessariamente a banda limitata) è stata fornita attraverso uno shaker. La sezione 3.0.3 spiega invece come vengono elaborati i dati a partire dai segnali misurati. Infatti, dopo aver eseguito l'agoritmo di Digital Image Correlation (DIC) che fornisce il segnale degli spostamenti sottocampionati, è necessario ricostruire i segnali utilizzando gli algoritmi studiati precedentemente. Per la validazione, sono stati disposti sulla travetta 10 accelerometri, in modo da poter confrontare successivamente i risultati ottenuti invece con la DIC e conseguente ricostruzione.

Il capitolo 4 analizza i risultati. In primis un test con soli accelerometri è stato analizzato. Successivamente sono state analizzate le bande in frequenza del test con la DIC dove erano contenute le frequenze naturali misurate col test preliminare. I grafici mostrano come le FRF degli accelerometri, se integrate, siano congruenti a quelle ottenute dalla ricostruzione del segnale. Allo stesso modo, le forme modali corrispondono.

Successivamente sono illustrati i risultati dell'assemblaggio dei rami di FRF misurati, fino ad ottenere una unica FRF che ha come dominio in frequenza la totale banda di osservazione (nelle regioni di overlap delle bande, è stato scelto il ramo a maggior coerenza). Questa FRF finale è stata confrontata, per entrambi i metodi di ricostruzione, "Interpolation" e "repMat", con quella ottenuta globalmente nel test preliminare con soli accelerometri, le figure 4.23 e 4.24 mostrano un ottimo match nella ricostruzione. Del rumore è presente ad alte frequenze, ma la visualizzazione della forma modale del quinto modo osservato è chiaramente possibile. PolyMax è stato applicato all'FRF assemblata e la visualizzazione delle forme modali rimane chiara e visibile.

Studi futuri 5 potranno essere focalizzati in un migliaramento a livello di interazione script, con un occhio a possibili modifiche del software per l'automatizzazione

dell'intero processo. completamente l'intero processo. Investigare la natura del rumore ad alte frequenze per esempio utilizzando una validazione con telecamere high-speed può essere una ulteriore strada, insieme a test su strutture più complesse.

In appendice A, è presentato un lavoro di sintesi riguardo un ulteriore metodo di ricostruzione di segnali, che prevede un campionamento random, il Compressed Sensing. Un caso numerico, via script è stato studiato, valutandone l'efficacia.

Contents

List of Figures

List of Tables

Chapter 1.

Introduction

The thesis is structured into 5 chapters. Chapter 1 is the introduction, where a motivation section and a literature review are presented. Chapter 2 explains the theory of the reconstruction algorithm and their working principles. Chapter 3 explains the experimental procedure, before and after measuring, including the data acquisition generation and test management. Chapter 4 illustrates the results of the experiment over a cantilever beam. The conclusion and future works considerations are in chapter 5. A final appendix A is present, illustrating an additional reconstruction method.

1.1. Motivations

Using vision based method to measure vibrations (i.e. Digital Image Correlation [3]) has its advantages and disadvantages with respect to traditional methods such as using accelerometers and strain gauges. Firstly, using cameras is a no-contact technique that can be easily implemented on rotating structures or with complex geometry, and hot surfaces. No mass-load effect are present, but a speckle pattern needs to be sticked or painted on the structure. It also provides a more discretized geometry in terms of number of points. Accelerometers instead are cabled sensors that can cover a wide frequency range. The geometry is discretized depending on the number of accelerometers used (each accelerometer is one geometry point). Table 1.1 summarizes the advantages and disadvantages of the two techniques. The geometry effect is clearly visible from the figures 1.5 and 1.6, where also the sensors are showed. The aircraft in figure 1.3 and 1.4 is used for ground vibration testing (GVT [4]), both accelerometers and cameras are used.

In addition, one of the major differences of the two techniques is the output unit of measure. With accelerometers, the measured physical quantity is acceleration, whereas with the DIC is displacement. This brings out a fact: having a flat spectrum in force (i.e. exciting uniformly in amplitude over a large frequency range) means having a flat spectrum in acceleration. Passing from acceleration towards displacement requires a double integration i.e. a multiplication of the spectrum times $1/\omega^2 = 1/(2\pi f)^2$. From this operation, showed in figure 1.1 it is possible to understand that the obtained integrated displacement spectrum has a trend where

the amplitude decreases at higher frequency.

As a consequence, to be able to capture displacements at higher frequency high resolution camera are needed. Cameras can be divided into two categories, depending on the frame rate (i.e. the number of frames that the camera can acquire in one second, measured in frame per seconds *fps*) low speed and high speed cameras. The main issue is that resolution and frame rate limit each other: low speed cameras have high resolution but they are limited on the frame rate, while high speed cameras have high frame rate but lower resolution. As reported in [5], when the resolution increases, so does the amount of data that must be processed. This can place a load on the host processor's bandwidth, restricting the frame rate. Additionally, as the frame rate increases, the quantity of data that must be processed and communicated in a given period also increases, thus limiting the resolution that can be obtained. Figure 1.2 represents the trade off between resolution and frame rate when choosing between low speed and high speed cameras.

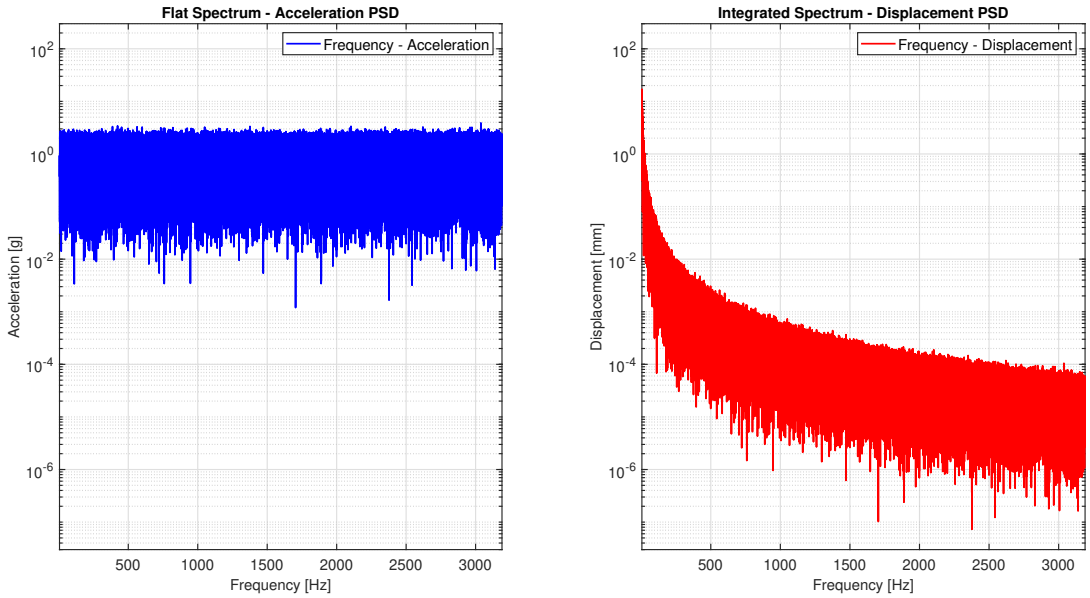

Figure 1.1.: A flat spectrum in terms of acceleration is a decreasing spectrum in displacement obtained by dividing by ω^2

The role of the reconstruction algorithms studied and applied for this thesis study is exactly to try to cover this limitation. The solution is then to use low speed cameras (having then high resolution), down-sampling high freqwuncy displacement (going in aliasing) and reconstructing the signal in post-processing to overcome the Nyquist theorem limitation.

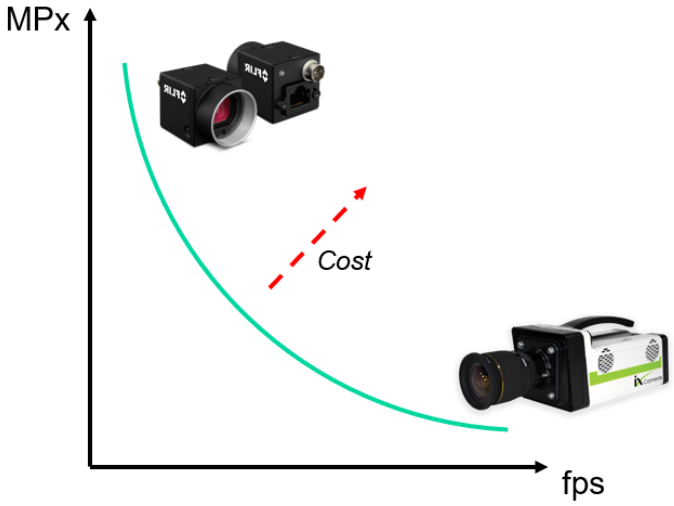

Figure 1.2.: Resolution (Mega Pixels) and frame rate (fps) limit each other

Figure 1.3.: Instrumented F16 - Sint-Truiden / Brustem Airfield – Belgium

Figure 1.4.: F16 with the speckle pattern placed on top of the wings and on the middle part of the fuselage

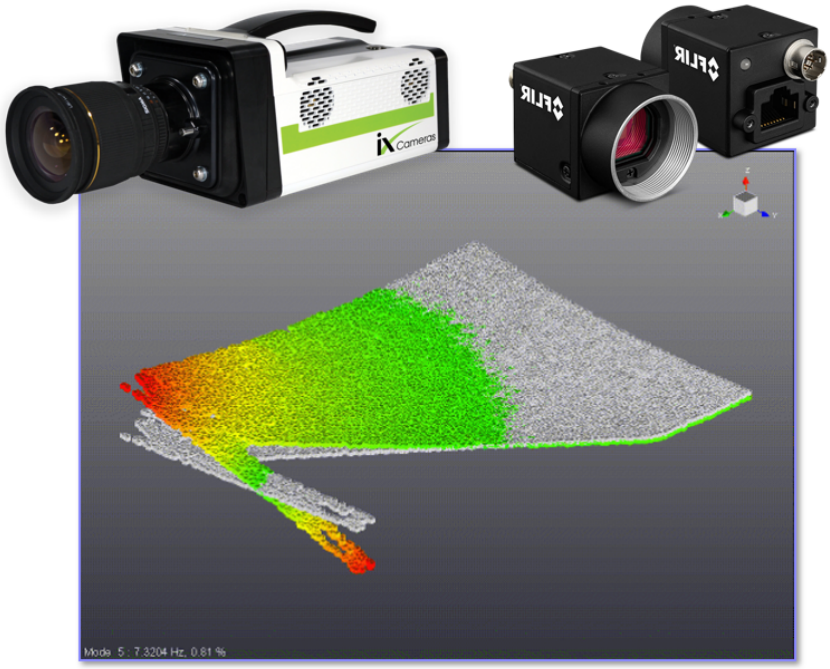

Figure 1.5.: High speed and low speed cameras together with a result view of a mode shape of the wing of the F16

-	Advantages	Disadvantages
Vision Based Methods (DIC)	• No wiring, contactless measurement, no mass loading • Full-field technique, easily measures 10000's points • Geometry is automatically available • Measure 3D displacement and planar strain field at the same time • Suitable for rotating structures, hot surfaces, membranes	• Line-of-sight measurements • Surface preparation and a well-designed lighting system • Primary measurement quantities are displacements, i.e. lower frequency range • Limited online processing capabilities • Big amount of data
Accelerometers	• Very high resolution across a wide frequency range • Easy to instrument and move around • Can measure any accessible location • Plug and play instrumentation • Data (and processing quantity) available in real-time	• Discrete measurement • Need sensor location and orientation to create a geometry • Cabling management and lengthy instrumentation • Mass loading (lightweight structures) • Special attention for high temperature and rotating structures

Table 1.1.: Advantages and disadvantages of both methods

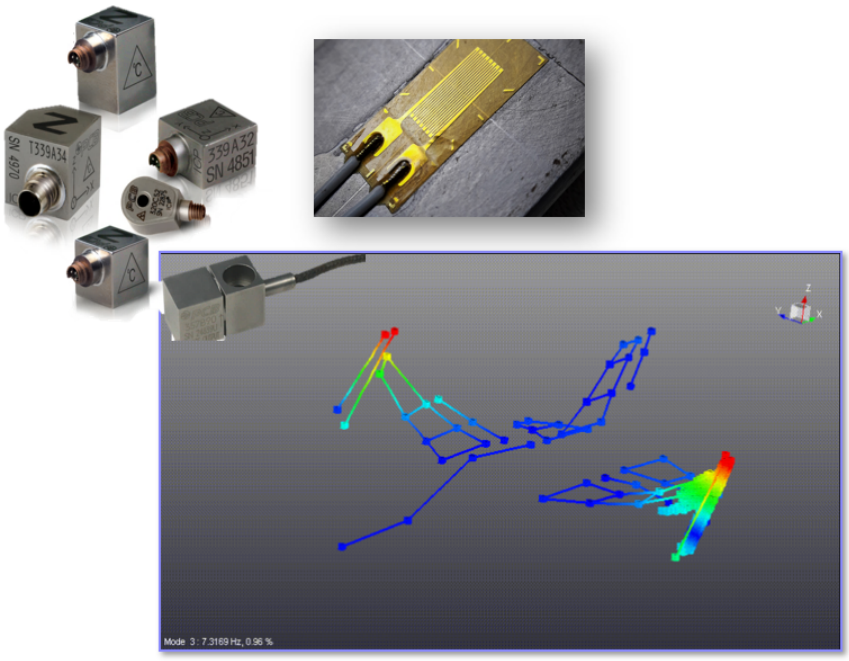

Figure 1.6.: Accelerometers and strain gauges sensors together with a result view of a mode shape of the F16

1.2. Literature Review

Literature exposes numerous and various approaches to exploit the motivation previously illustrated. There are different techniques based on under sampling, random sampling and smart aliasing with the purpose to use low-speed cameras, i.e. a full field measurement technique to capture high frequency behaviors.

A first work, worth mentioning is [6] where an impact test was performed over a cantilever plate and low-speed cameras allowed to characterize all the first mode shapes until 500 Hz, using a frame rate under 50 fps. The random sampling used technique involves the usage of an accelerometer for determine an initial guess. A random sampling technique called Compressed Sensing and very similar to the one used in [6] is discussed in A.
Many literature studies are related to the technique of knowing the aliased frequency and exciting using sinusoid of that specific frequency to measure via Digital Image Correlation (DIC). In [7] the concept of "fanfold" is presented, which is a direct and simple analogy of the revisited Nyquist Theorem discussed in 2.1.1.

Even if other optical processing technique such as spectral optical flow are being studied [8], the DIC is the main used full field technique that is finding multiple industrial application. Therefore it is worth mentioning [9] where the main concepts and working principle of the DIC are explained together with an experimental application with comparison with standard techniques such as accelerometers. The paper [10] illustrates also the calibration procedure for a rotatory component, where also the sub-sampling technique is used.
Different options of camera configurations are possible: in [11] a mono, single-camera set up is used to measure a turbine blade vibration, computing priorly the sampling frequency by knowing the natural frequencies of the structure. A similar experiment is carried out in [12] but in a stereo configuration. Also [13] is a case study of under-sampling technique that uses a designed trigger signal according to the know frequencies of the structure.

A very interesting approach is the one proposed in [14] where the assembly of bandlimited frequency excitation result is performed to reconstruct the full signal history of the displacement spectrum of a single DIC point. The main paper where this thesis work is inspired from is [1], later discussed in section 2.2. In addition to it, also [15] uses the same approach on a open bladed disk, and the result obtained are compared with LDV (laser doppler vibrometry) measurements showing high accuracy and low error of computation.

Chapter 2.

Reconstruction methods for bandlimited signals

This chapter illustrates two different methods of signal reconstruction for a bandlimited down-sampled signal.

- The first method exploits the reconstruction formula 2.23 theoretically demonstrated in section 2.1.3 and as a matter of fact it works in the time domain. We call it the "Interpolation" method.
- The second method instead makes use of the concept of frequency shift discussed in section 2.1.2 and as a matter of fact it works specifically in the frequency domain. We call it the "repMat" method.

These two methods are analyzed separately and a numerical validation over generic bandlimited signals such as chirp or pseudorandom are performed. Further investigations are also analyzed using a multi-degree of freedom (MDOF) system with fixed resonance frequencies, to also test the algorithms on an asymmetric spectrum.

2.1. Theory on down-sampled signal reconstruction

A theoretical summary report taken from the book [2] is provided, starting from the Sampling Theorem Revisited (pag. 269), passing by the formulation of the "frequency shift" (pag. 738) and arriving at the final reconstruction formulas.

2.1.1. Sampling Theorem Revisited

A bandlimited continuous-time signal, with the highest frequency (bandwidth) B hertz, can be uniquely recovered from its samples provided that the sampling rate $F_s \geq 2B$ samples per second. $x_a(t)$ is the analogic signal, and it can be recovered in time domain from its samples $x_a(nT)$, where nT is the time vector discretized over n samples:

$$x_a(t) = \sum_{n=-\infty}^{\infty} x_a(nT) \frac{\sin(\pi/T)(t-nT)}{(\pi/T)(t-nT)} = \sum_{n=-\infty}^{\infty} x_a(nT) \cdot \boldsymbol{g}(t-nT) \qquad (2.1)$$

Where:

$$\boldsymbol{g}(t) = \frac{\sin(\pi/T)t}{(\pi/T)t} = \frac{\sin(2\pi Bt)}{2\pi Bt} \tag{2.2}$$

2.1.2. Frequency Shift

If the analytic signal $x_+(t)$ is a bandpass signal, we can obtain an equivalent lowpass representation by performing a frequency translation of $X_+(F)$. Thus, we define $X_l(F)$ as:

$$X_l(F) = X_+ \left(F + F_c\right) \tag{2.3}$$

Where F_c is the central frequency defined in equation 2.12. The equivalent time-domain relation is:

$$x_l(t) = x_+(t)e^{-j2\pi F_c t} = [x(t) + j\hat{x}(t)]e^{-j2\pi F_c t} \tag{2.4}$$

Which is a complex signal and therefore it can be seen as:

$$x_l(t) = u_c(t) + ju_s(t) \tag{2.5}$$

If we substitute for $x_l(t)$ in equation 2.4 and equate real and imaginary parts on each side, we obtain:

$$\begin{aligned} \hat{x}(t) &= u_c(t)\sin 2\pi F_c t + u_s(t)\cos 2\pi F_c t \\ \boldsymbol{x(t) &= u_c(t)\cos 2\pi F_c t - u_s(t)\sin 2\pi F_c t} \end{aligned} \tag{2.6}$$

Equation 2.6 in bold is the desired form for the representation of a bandpass signal. The low-frequency signal components $u_c(t)$ and $u_s(t)$ can be viewed as amplitude modulations impressed on the carrier components $\cos(2\pi F_c t)$ and $\sin(2\pi F_c t)$, respectively. Since these carrier components are in phase quadrature, $u_c(t)$ and $u_s(t)$ are called the quadrature components of the bandpass signal $x(t)$. Performing the Fourier transform of $x(t)$:

$$X(F) = \int_{-\infty}^{\infty} x(t)e^{-j2\pi F_c t}dt = \int_{-\infty}^{\infty} \left\{ \mathrm{Re}\left[x(t)e^{j2\pi F_c t}\right] \right\} e^{-j2\pi F_c t}dt \tag{2.7}$$

And using the identity:

$$\mathrm{Re}(\xi) = \frac{1}{2}\left(\xi + \xi^*\right) \tag{2.8}$$

We obtain the result:

$$X(F) = \frac{1}{2}\int_{-\infty}^{\infty} \left[x(t)e^{j2\pi F_c t} + x^*(t)e^{-j2\pi F_c t}\right] \Big\} e^{-j2\pi Ft}dt \tag{2.9}$$

Therefore:

$$X(F) = \frac{1}{2}\left[X_l\left(F - F_c\right) + X_l^*\left(-F - F_c\right)\right] \tag{2.10}$$

Which means that the spectrum of the bandpass signal $x(t)$ can be obtained from the spectrum of the complex signal $x_l(t)$ by a **frequency translation**.

"Any bandpass signal $x(t)$ can be represented by an equivalent lowpass signal $x_l(t)$"

2.1.3. Sampling of Bandpass Signals

We define a bandpass signal as a signal $x(t)$ whose Fourier transform is:

$$X(j\omega) = \begin{cases} 0, |\omega| \leq \omega_L = 2\pi F_L \\ 0, |\omega| \geq \omega_H = 2\pi F_H \end{cases} \tag{2.11}$$

Where $B = F_H - F_L$ and its frequency components are in the band $F_L \leq F \leq F_H$. The central frequency of the band is defined:

$$F_c = \frac{F_L + F_H}{2} \tag{2.12}$$

A blind application of the "Sampling theorem revisited" (eq. 2.1 and 2.2) would have us sampling the signal at a rate of $2F_H$ samples per second. If that were the case and F_H was an extremely high frequency, it would certainly be advantageous to perform a frequency shift of the bandpass signal by F_c and sampling the equivalent lowpass signal. Such a frequency shift can be achieved by multiplying the bandpass signal by the quadrature carries $\cos(2\pi F_c t)$ and $\sin(2\pi F_c t)$ and lowpass filtering the products to eliminate the signal components at $2F_c$. These operations are in the analog domain, only then the outputs of the filters are sampled. The resulting equivalent lowpass signal has a bandwidth $B/2$, where $B = F_H - F_L$. Therefore, it can be represented uniquely by samples taken at the rate of B samples per second for each of the quadrature components. Thus the sampling can be performed on

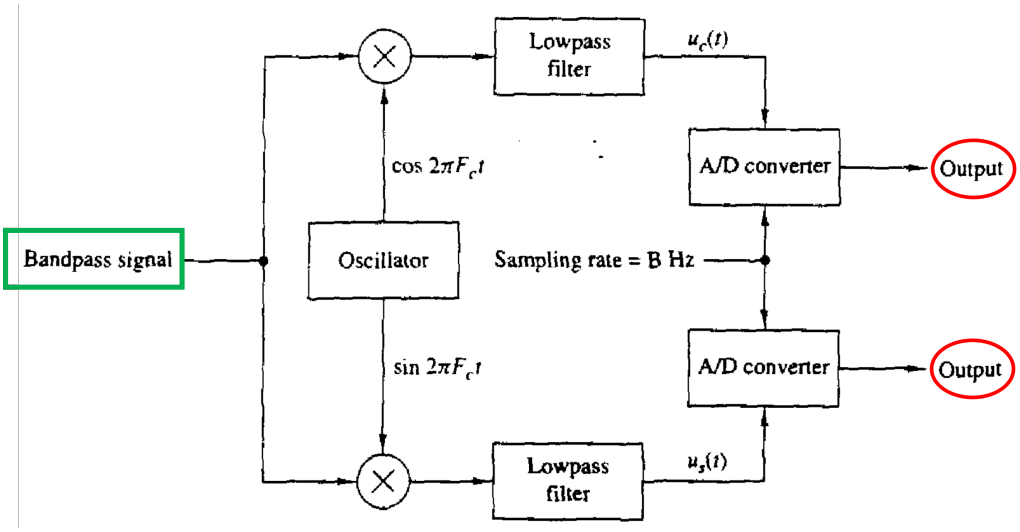

Figure 2.1.: Low pass operation, picture taken from the book [2]

each of the lowpass filter outputs at the rate of B samples per second. Therefore,

the resulting rate is $2B$ samples per second. If we suppose:

$$F_c + \frac{B}{2} = pB \quad \rightarrow \quad \boldsymbol{p = \frac{F_H}{B}} \tag{2.13}$$

With $\boldsymbol{p}$ a positive integer, when we sample $x(t)$ at the rate $2B = 1/T$ samples per second, we have

$$x(nT) = u_c(nT)\cos 2\pi F_c nT - u_s(nT)\sin 2\pi F_c nT \tag{2.14}$$

Substituting $F_c = pB - B/2$ and $T = 1/2B$:

$$x(nT) = u_c(nT)\cos\frac{\pi n(2p-1)}{2} - u_s(nT)\sin\frac{\pi n(2p-1)}{2} \tag{2.15}$$

Considering $T_1 = 2T = 1/B$.

For n **even**, say $n = 2m$, eq. 2.15 reduces to:

$$x(2mT) \equiv x\left(mT_1\right) = u_c\left(mT_1\right)\cos\pi m(2p-1) = (-1)^m \boldsymbol{u_c}\left(mT_1\right) \tag{2.16}$$

For n **odd**, say $n = 2m-1$, eq. 2.15 reduces to:

$$x(2mT - T) \equiv x\left(mT_1 - \frac{T_1}{2}\right) = \boldsymbol{u_s}\left(mT_1 - \frac{T_1}{2}\right)(-1)^{m+p+1} \tag{2.17}$$

Now the samples $u_c(mT_1)$ and the samples $u_s(mT_1 - T_1/2)$ can be used to reconstruct the equivalent lowpass signals. Thus according to the "Sampling theorem revisited" 2.1.1:

$$u_c(t) = \sum_{m=-\infty}^{\infty} u_c\left(mT_1\right)\frac{\sin\left(\pi/T_1\right)\left(t - mT_1\right)}{\left(\pi/T_1\right)\left(t - mT_1\right)} \tag{2.18}$$

$$u_s(t) = \sum_{m=-\infty}^{\infty} u_s\left(mT_1 - \frac{T_1}{2}\right)\frac{\sin\left(\pi/T_1\right)\left(t - mT_1 + T_1/2\right)}{\left(\pi/T_1\right)\left(t - mT_1 + T_1/2\right)} \tag{2.19}$$

If we substitute equations 2.17, 2.16, 2.18 and 2.19 in equation 2.6, we obtain:

$$\begin{aligned} x(t) = \sum_{m=-\infty}^{\infty} (-1)^m x(2mT)\frac{\sin(\pi/2T)(t-2mT)}{(\pi/2T)(t-2mT)}\cos 2\pi F_c t + \\ +(-1)^{m+p}x((2m-1)T)\frac{\sin(\pi/2T)(t-2mT+T)}{(\pi/2T)(t-2mT+T)}\sin 2\pi F_c t \end{aligned} \tag{2.20}$$

But

$$(-1)^m \cos 2\pi F_c t = \cos 2\pi F_c(t - 2mT) \tag{2.21}$$

and

$$(-1)^{m+p}\sin 2\pi F_c t = \cos 2\pi F_c(t - 2mT + T) \tag{2.22}$$

Obtaining finally the **reconstruction formula** for the bandpass signal $x(t)$, with samples taken at the rate of $2B$ samples per second, for the special case in which

the upper band frequency $F_c + B/2 = F_H$ is a multiple ($\boldsymbol{p}$ is integer) of the signal bandwidth B.

$$x(t) = \sum_{m=-\infty}^{\infty} x(mT) \frac{\sin(\pi/2T)(t-mT)}{(\pi/2T)(t-mT)} \cos 2\pi F_c(t-mT) \tag{2.23}$$

In the general case where only the condition $F_c \geq B/2$ is assumed to hold, let us define the integer part of the ratio $F_c + B/2$ to B as:

$$\boldsymbol{r} = \left\lfloor \frac{\boldsymbol{F_c} + \boldsymbol{B}/2}{\boldsymbol{B}} \right\rfloor = \left\lfloor \frac{F_H}{B} \right\rfloor = \text{floor}(p) \tag{2.24}$$

We increase the bandwidth from B to B' such that the ratio r is an integer value:

$$\boldsymbol{B'} = \frac{\boldsymbol{F_H}}{\boldsymbol{r}} \rightarrow \boldsymbol{r} = \frac{F_c + B/2}{B'} \tag{2.25}$$

It is convenient to define a new center frequency for the increased bandwidth signal as:

$$F_c' = F_c + \frac{B}{2} - \frac{B'}{2} \tag{2.26}$$

Now the upper cutoff frequency F_H is a multiple of B'. Consequently the signal reconstruction formula 2.23 holds with F_c replaced by F_c' and T replaced by $T' = 1/2B'$. Note that when the upper cutoff frequency $F_c + B/2$ is not an integer multiple of the bandwidth B, the sampling rate for the bandpass signal must be increased by a factor $\boldsymbol{p}/\boldsymbol{r}$. However as F_c/B increases, the ratio p/r tends towards unity In conclusion, we have demonstrated that a **bandpass signal can be represented uniquely by samples taken at a rate**:

$$2B \leq F_s < 4B \text{ where } F_s = 2B\frac{p}{r} \tag{2.27}$$

Where B is the bandwidth of the signal. The lower limit applies when the upper frequency $F_c + B/2$ is a multiple of B. The upper limit on F_s is obtained under worst-case conditions when $r = 1$ and $p \approx 2$.

2.2. Interpolation method

This method is analyzed and practically used by Paolo Neri in [1], a short recap is provided. The "Interpolation" method implements numerically the reconstruction formula 2.23 as follow:

$$x(t) \approx \sum_n x\left(nT_s\right) g_r\left(t - nT_s\right) \tag{2.28}$$

where $x(t)$ is the reconstructed signal, $x(nT_s)$ is the down-sampled signal and $g_r(t)$ is the modulated ideal bandlimited interpolation function, as described in [1]:

$$g_r(t) = \frac{\sin(\pi B t)}{\pi B t} \cos\left(2\pi F_c t\right) \tag{2.29}$$

F_c is the central frequency of the band B calculated as in equation 2.12. In comparison with the theoretical result discussed in section 2.1.3, the equation 2.28 is only an approximation, in fact, the sum is not until infinity (as theory says in equation 2.23) but over the n samples of the down-sampled signal. That is the reason of not putting the equal sign but only an "approx" sign. Note, in addition, that in equation 2.28 the $g_r(t)$ function is calculated in $(t - nT_s)$ which means, computationally speaking, that we are subtracting, for each element of the reconstructed signal time axis, the time step of the down-sampled time axis (i.e. *tsShort*) multiplied times the iterative variable n (the number of samples of the down-sampled signal). Algorithm 1 expresses the pseudocode for the script implementation.

Algorithm 1: Reconstruction Computation

for $1 \leq i \leq n$ **do**
  $reconstructed[i] \leftarrow downSampled[i] \times gFunc(time - (i-1) \times tsShort)$
end
$reconstructed \leftarrow sum(reconstructed)$

2.2.1. Numerical Validation

Figure 2.2 represents the generation of a bandlimited signal, a windowed chirp, and its down-sampled version. Downsampling the original signal (in this case the downsampling is done by using the "downsample" built-in MatLab function) causes a frequency back-shift of the spectrum. In fact, the sampling frequency of the original signal is $f_{s_{ori}} = 8000Hz$ and the sampling frequency of the down-sampled signal is $f_{s_{ds}} = 8Hz$. This means that the downsampling factor or the sampling frequencies is 1000 (i.e. $8000/8 = 1000$). If we apply the algorithm 1 to the down-sampled signal we obtain what is shown in figure 2.3. As reported in [2] and also put in practise in [1], this interpolation method works in the time domain, and it starts from the down-sampled time history to obtain the reconstructed one.

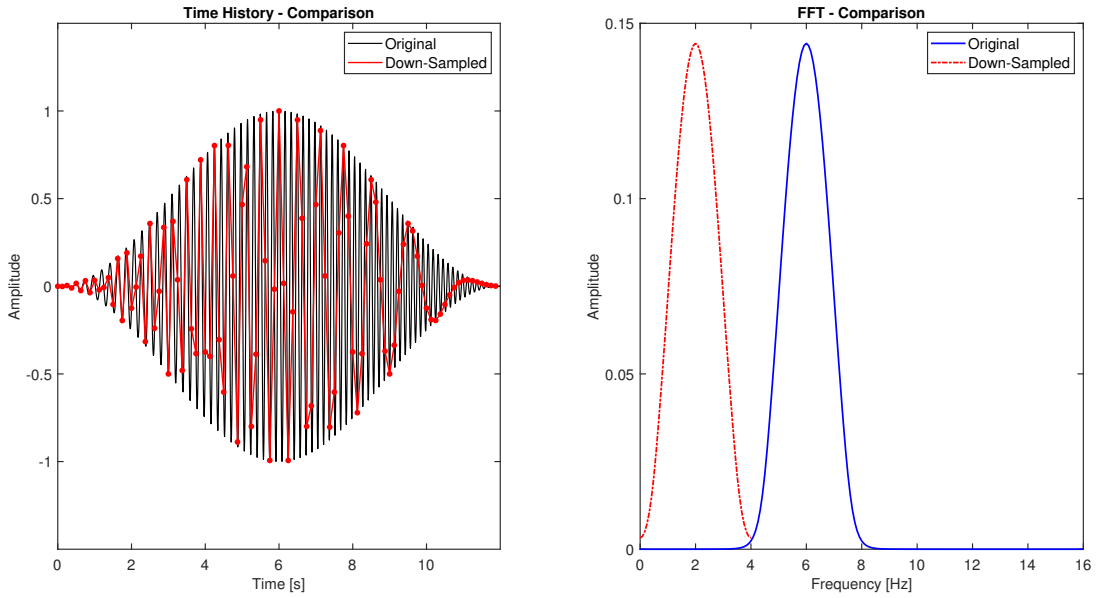

Figure 2.2.: Original and down-sampled signals - Windowed Chirp $F_L = 4Hz; F_H = 8Hz$

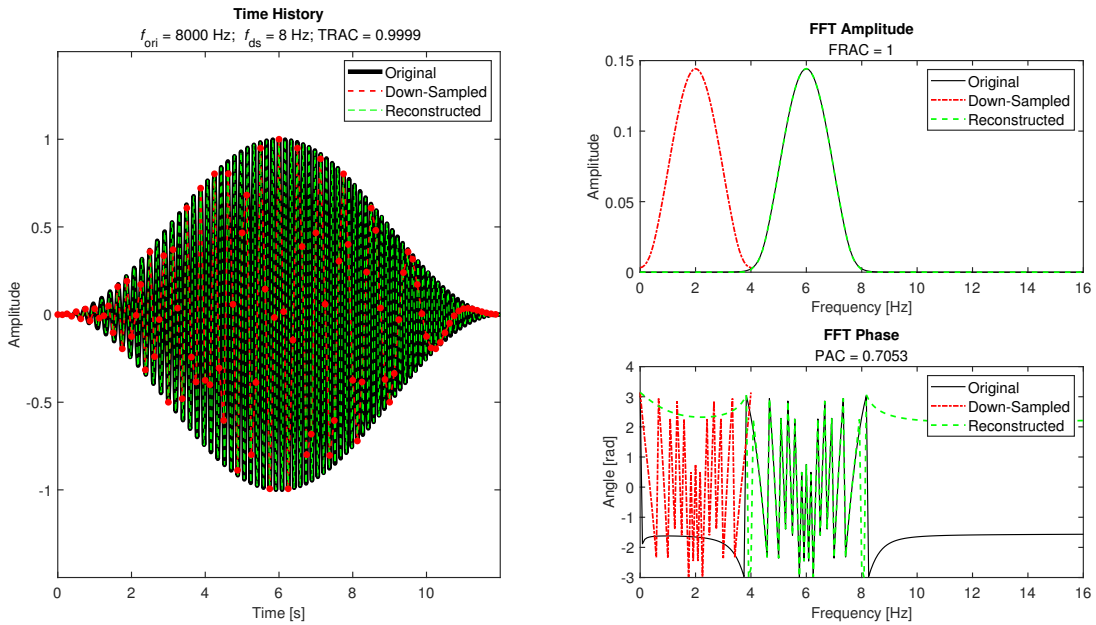

Figure 2.3.: Reconstructed signal via Interpolation method - Windowed Chirp $F_L = 4Hz; F_H = 8Hz$

2.3. repMat method

Studying the functioning of the interpolation method in the time domain it is possible to observe that the same result can be obtained by only working in the frequency domain. As a matter of fact, having a bandlimited down-sampled spectrum and reconstructing it, means exactly to perform a frequency shift of that spectrum by a specific known shift value.

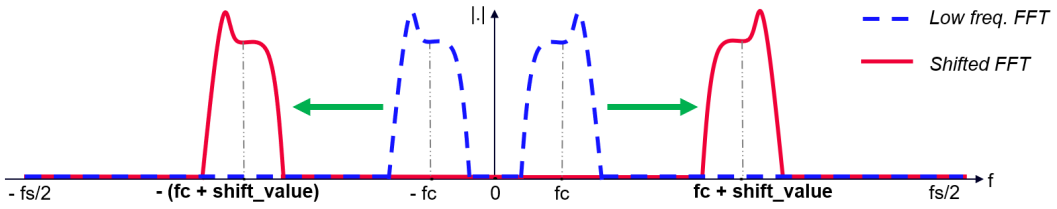

Figure 2.4.: Frequency Shift concept of a bandlimited spectrum

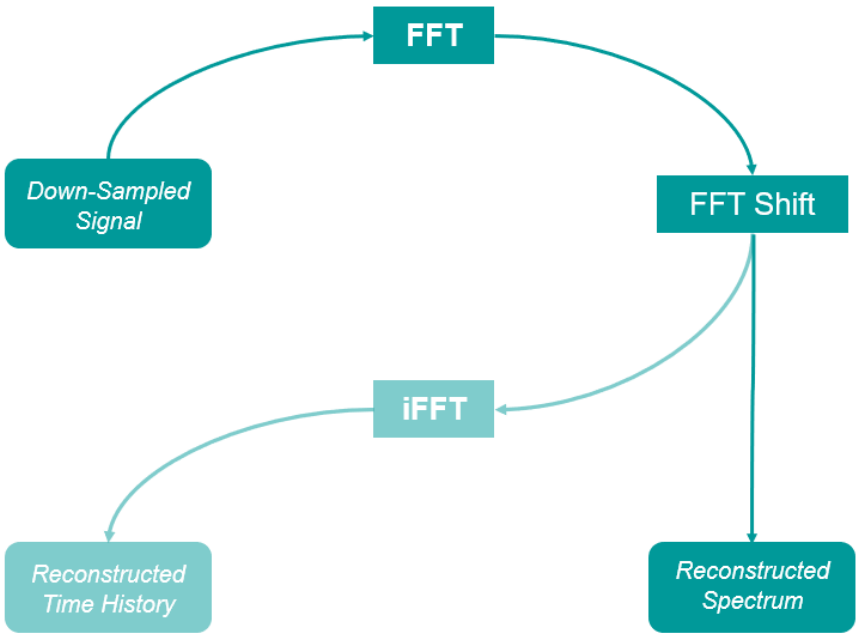

Figure 2.5.: Frequency Shift approach in the frequency domain

Figure 2.5 represents the described approach. It is possible to perform the translation of the spectrum as theoretically explained in 2.1.2 and not necessarily to come back in the time domain by performing the inverse operator (i.e. the inverse Fourier transform *iFFT*) obtaining at the end the shifted reconstructed spectrum. This approach is schematized in figure 2.4. The "repMat" algorithm is based on an array repetition: the FFT values of the down-sampled signal are repeated along the frequency axis and a successive selection of the correct peaks is performed. The

algorithm works by following in order three steps:

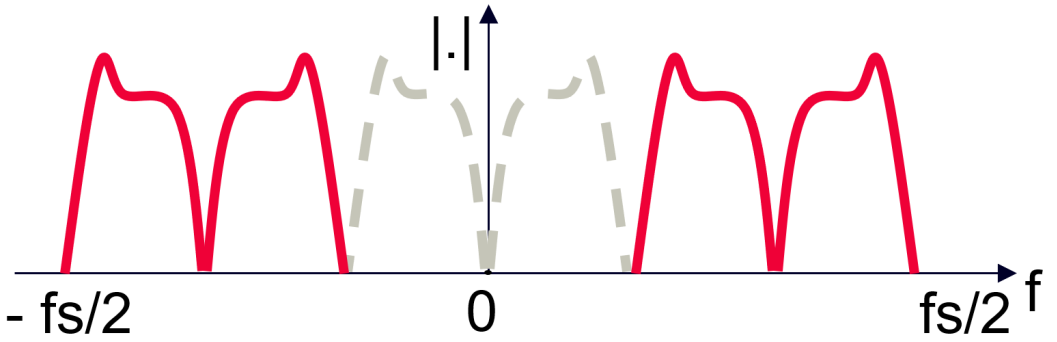

Figure 2.6.: **repMat algorithm - Step 1**: the spectrum of the down-sampled signal is repeated

The repetition of the spectrum happens along the frequency axis $[-f_s/2\ f_s/2]Hz$ where $f_s = f_{ori}$ is the sampling frequency of the reconstructed signal. To compute the correct number of times needed to repeat the spectrum the desired ratio between the down-sampling frequency f_{camera} and the original one f_{ori} is computed.

$$desired_{ratio} = \frac{f_{ori}}{f_{camera}} = \frac{N_{samples}}{n_{photos}} \tag{2.30}$$

Equation 2.30 represents a number (i.e. the desired ratio factor) that indicates the scaling in terms of both sampling frequencies and number of samples. The two relations are connected by the acquisition time dt because $N_{samples} = f_{ori} \cdot dt$ likewise $n_{photos} = f_{camera} \cdot dt$. The number of repetitions needed is computed as follows:

$$\boldsymbol{n}_{rep} = \text{floor}\left(desired_{ratio}\right) + 2 \tag{2.31}$$

It can happen, indeed, that the desired ratio is not integer, this means that a round of the decimal number is needed. The round is performed by taking the integer part of the ratio (i.e. using the floor operator) and adding 2 at that number as shown in equation 2.31. In this way, the inclusion of a fully repeated spectrum to cover the decimal part of the ratio is ensured. On the other hand, this will create an overextension of the repeated array that needs to be fixed after Step 2 of the algorithm. The repetition is practically done by using the built-in MatLab function called "repmat" itself.

$$\boldsymbol{rep}_{spectrum} = \text{repMAT}\left(ds_{spectrum}, 1, n_{rep}\right) \tag{2.32}$$

In equation 2.32, the first argument of the function is the spectrum of the down-sampled signal (i.e. $ds_{spectrum}$), the 1 represents the index towards which array dimension the repetition happens (in this case the repetition happens only "horizontally" along the frequency axis), the third argument is the number of times (it needs

to be an integer value) the array is repeated.

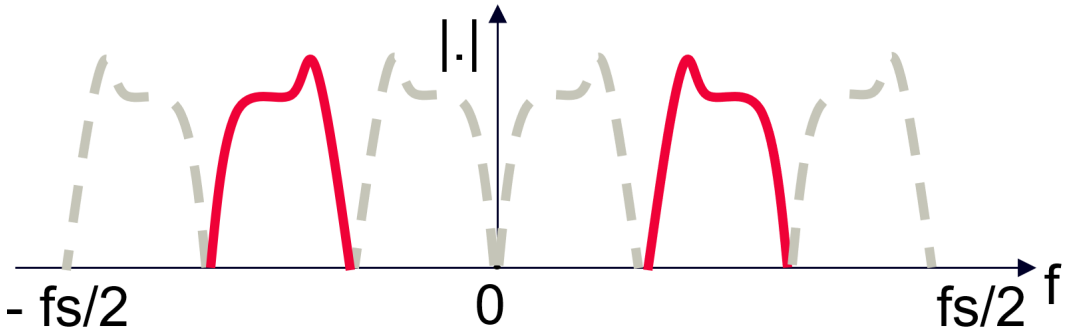

Figure 2.7.: **repMat algorithm - Step 2**: find the indexes of the frequency axis from where to zeros

As explained in Step 1, due to the round performed on the desired ratio an overextension of the array has occurred. After the repetition is then necessary to compute the entity of the overextension and re-size correctly the full repeated spectrum. The quantity of the overextension is the simple difference between the length of the output of 2.32 and the actual number of samples of the reconstructed signal computed as $N_{samples} = f_{ori} \cdot dt$ as explained in Step 1.

$$overExtension = \text{length}\left(rep_{spectrum}\right) - N_{samples} \tag{2.33}$$

Computationally it is necessary then to overwrite the variable of the repeated spectrum.

$$\begin{aligned} start_{cutoff} &= \frac{overExtension}{2} \\ end_{cutoff} &= \text{length}\left(rep_{spectrum}\right) - \frac{overExtension}{2} \\ \boldsymbol{rep}_{spectrum} &= rep_{spectrum}\left(start_{cutoff} : end_{cutoff}\right) \end{aligned} \tag{2.34}$$

Note that the operations 2.34 require a division by two of the length of the overextension. This means having an even number of samples of the down-sampled signal when implementing both numerically and experimentally the algorithm. Having an even number of samples of the down-sampled signal means having an even number of samples of its spectrum and, as a consequence, the length of the repeated spectrum will be an even number (being the repetition number an integer value). Working with even numbers of the downsampled spectrum allows the exact identification of the overextension value. This constraint will be one of the issues for the acquisition time optimization section. Successively the selection of the indexes of where to cut the repeated spectrum happens by identifying the index values of f_L and f_H (i.e. the extreme values of the observation band that defines the bandlimited signal) in the frequency axis array of interest. This is of course needed both in the positive semi-axis $[0\ f_s/2]Hz$ and in the negative one $[-f_s/2\ 0]Hz$. Taking into account that,

depending on the resolution adopted, the frequency axis might not have exactly the values of f_L and f_H. The algorithm proceeds by choosing the closest value to the effective value of f_L or f_H and finding its correspondent array index, to perform the cut. Computationally this happens via the "find" build-in MatLab function imposing a threshold on the equality as a percentage of the resolution. Here it is the script procedure for all the four indexes:

```
1    i_fl_pos = max(find(f_ax_simm <= fl+resolution*res_perc)) - 1;
2    i_fh_pos = max(find(f_ax_simm <= fh+resolution*res_perc)) + 1;
3    i_fl_neg = max(find(f_ax_simm <= -fl+resolution*res_perc)) + 1;
4    i_fh_neg = max(find(f_ax_simm <= -fh+resolution*res_perc)) - 1;
```

where the threshold value is set as the 1% of the resolution (res_perc = 0.01). A plus or minus 1 is added to the output of the find function to identify the cut-index at the previous sample ("-1" if the find is for $+f_L$ or $-f_H$) or at the next sample ("+1" if the find is for $+f_H$ or $-f_L$).

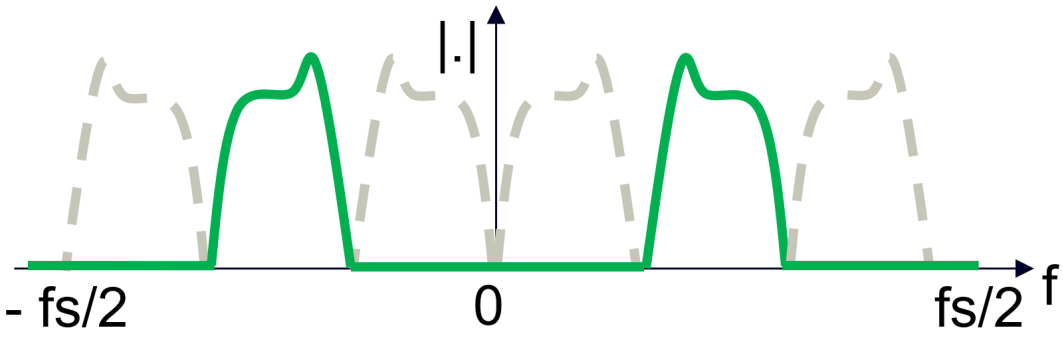

Figure 2.8.: **repMat algorithm - Step 3**: zero all the values identified outside the two desired peaks

Now that the four indexes in the frequency axis have been identified (i.e. the indexes of $-f_H$, $-f_L$, f_L and f_H). A zeroing procedure over the values outside the ranges defined by the indexes found in Step 2 is performed. The values of the spectrum are set at zero in the ranges: $[-f_s/2 \ -f_H]$, $[-f_L \ f_L]$ and $[f_H \ -f_s/2]$.

A general note that is good to take into account even if it does not affect the actual reconstruction inside the band, regards the value given to the zero. The mathematical zero "0" is different from the **eps** value of the calculator (i.e. the distance from 1.0 to the next larger double-precision number). The "eps" value for MatLab is $2.2204e^{-16}$ and using it in Step 3 instead of the actual zero "0" produces slightly different results in the phase of the FFT outside of the reconstruction band. To obtain a phase that is zero radiants outside of the observation band the use of "eps" or its multiples (e.g. $10 \cdot eps$) is needed. Using "0" instead creates phase fluctuations between $-\pi$ and π outside of the observation band.

2.3.1. Numerical Validation

Numerical validations have been conducted on a multi-degree of freedom system, shown in figure 2.9. The model is built with the following data:

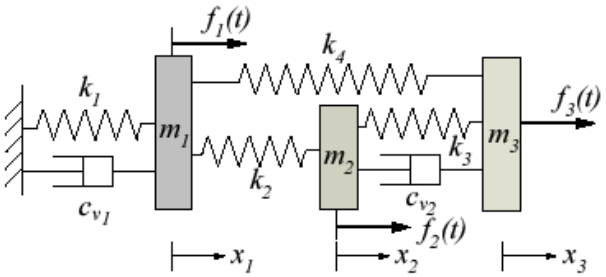

Figure 2.9.: Multi Degree of Freedom (MDOF) model used

$k_1 = k_2 = k_3 = k_4 = 900kN/m$; $m_1 = m_2 = 50kg$; $m_3 = 20kg$; $c_{v_1} = 25Ns/m$; $c_{v_2} = 10Ns/m$; $\boldsymbol{f_1 = f_2 = 0; f_3} = Chirp$. From the equations of the forces, it can be noted that the excitation is present only in the m_3 block and it is a windowed chirp defined in the bandlimited range $[50\ 75]Hz$. The signal taken into study is the displacement of the m_2 block.

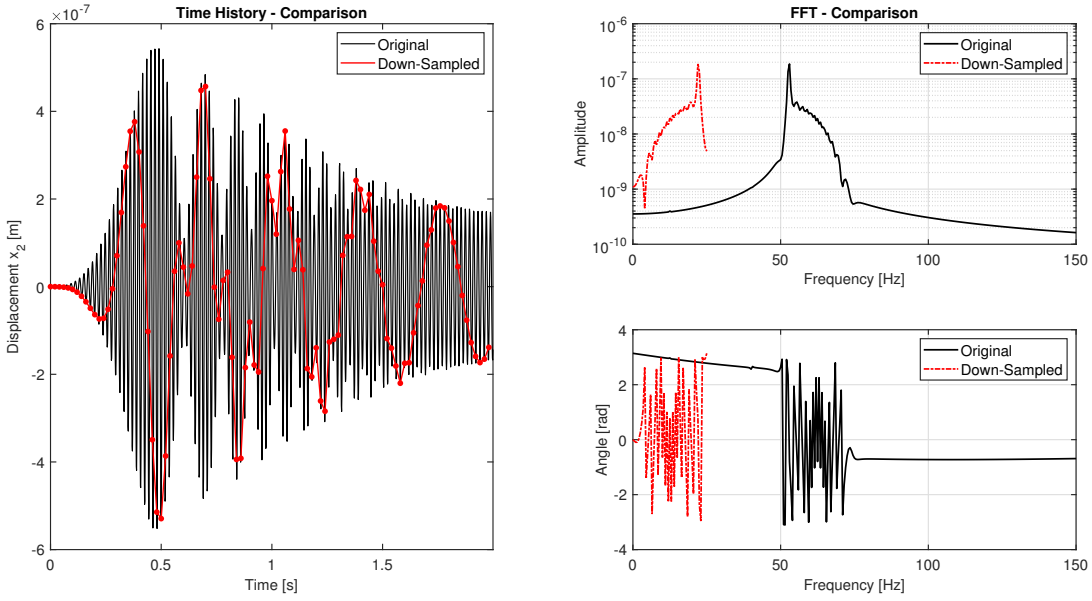

Figure 2.10.: Original signal and its down-sampled version of the MDOF system

Figure 2.10 shows the initialization of the original signal and its down-sampled version to test the reconstruction. In this type of numerical validation it is worth noting that the spectrum of the signal is not necessarily symmetric. In fact, having a MDOF system implies having resonance frequencies that create asymmetries in the FFT due to the resonance peaks. In this specific case, the observation band is set on

purpose to include one of the three resonance peaks located at $52Hz$. Figure 2.11

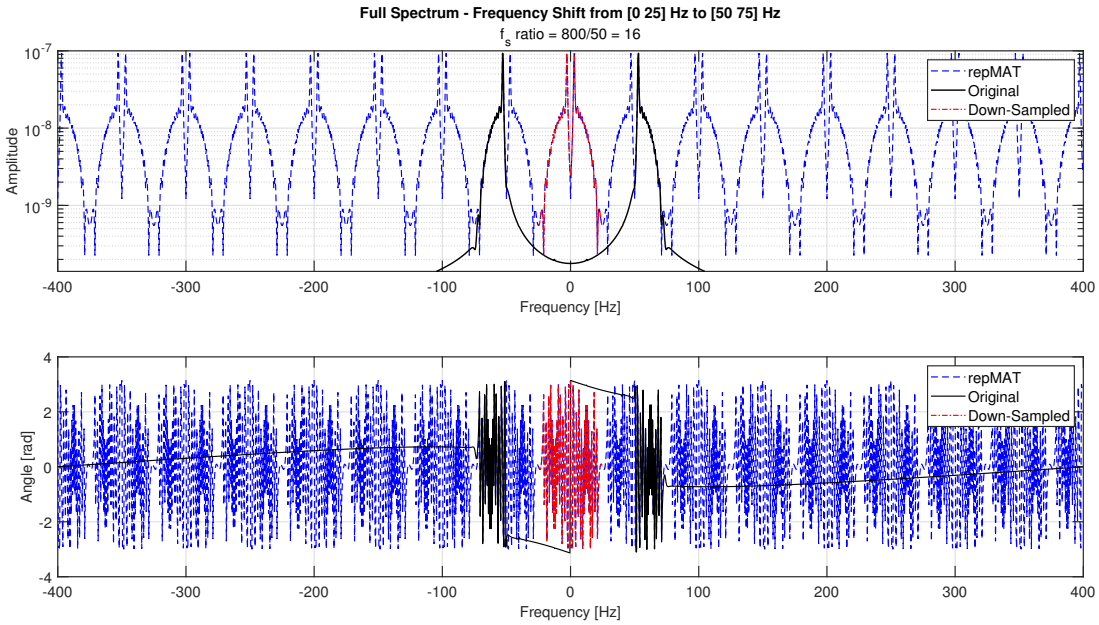

Figure 2.11.: Repeated down-sampled spectrum along the symmetric frequency axis

is the software implementation output of what exactly happens during the repMat algorithm. The goal of the algorithm as explained in the initial part of this section 2.3 is selecting the correct bands of the blue dotted spectrum and zeroing the rest of the values in the domain. Figure 2.12 is the output where also the reconstructed time-history is reported. As explained about the diagram 2.5 this procedure could be avoided for example in cases where modal analysis (i.e. FRF computation) needs to be performed: all the operations will remain in the frequency domain.

2.4. Numerical Validation Criteria

From figure 2.12 and figure 2.3 it is possible to see also numerical values that define the accuracy of the reconstruction. These numbers are respectively the TRAC (Time Response Assurance Criterion), the FRAC (Frequency Response Assurance Criterion) and the PAC (Phase Assurance Criterion). As reported in the "Appendix B" of [16] the formula considered is:

$$TRAC, FRAC, PAC = \frac{\left(\text{Ori} \cdot \text{Rec}^T \right)^2}{\left(\text{Ori} \cdot \text{Ori}^T \right) \cdot \left(\text{Rec} \cdot \text{Rec}^T \right)} \tag{2.35}$$

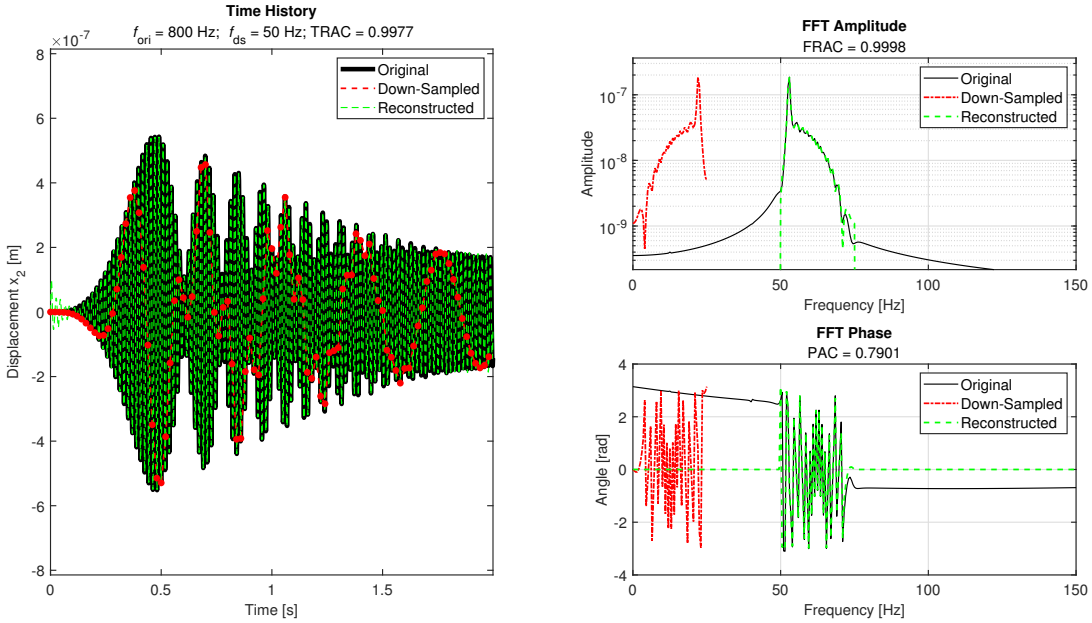

Figure 2.12.: Reconstructed signal via repMat method - MDOF excited via Windowed Chirp $F_L = 50Hz; F_H = 75Hz$

Where "Ori" represents the original signal and "Rec" the reconstructed one. For the TRAC, the ratio calculation is done by using the time histories of the two signals. For the FRAC, the ratio is performed between the two "abs" (i.e. the modules) of the FFTs of the two signals. For the PAC, the ratio is performed between the two "angle" (i.e. the phases) of the FFTs of the two signals.

Computationally this has been performed by the use of a single function that computes the ratio between two arrays as shown in equation 2.35. Of course, to compute a scalar result from the ratio function, the two arrays compared need to be of the same size[1].

The values computed are all very close to 1, this means that both reconstruction methods are numerically accurate. Note that the FRAC and the PAC are computed only in the specific band where the original signal is generated. This means that for example in figure 2.12 the computation of FRAC and PAC is performed only for the y-values in the x-axis between 50 and 75 Hz.

[1]Computationally the array size for the matrixes operation must be $1 \times N_{samples}$

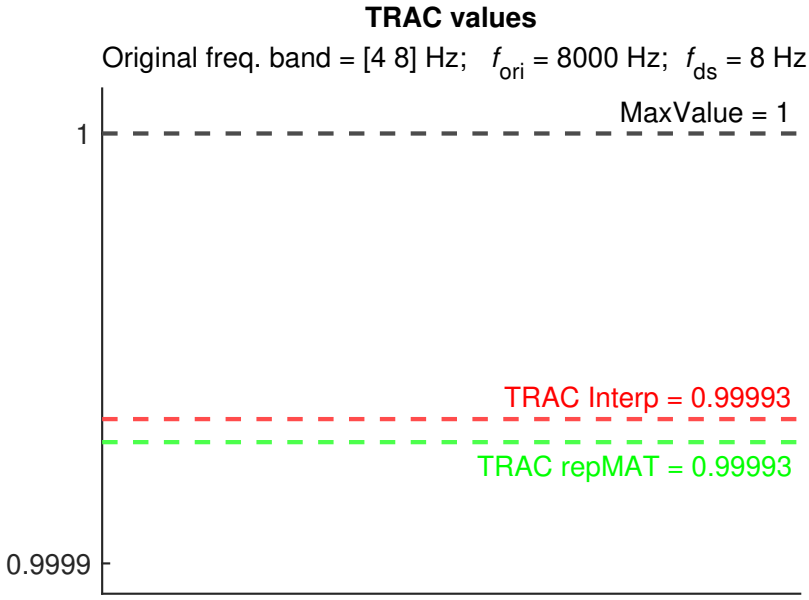

Figure 2.13.: TRAC for Interpolation method and repMat method reconstruction - Windowed Chirp $F_L = 4Hz$; $F_H = 8Hz$

The following examples are additional numerical validation performed.

Figure 2.15 is the reconstruction of the m_2 block displacement response of the MDOF system described in 2.9 analyzed using a windowed chirp excitation in the frequency band $[9.5\ 16.5]Hz$. Figure 2.16 is the reconstruction of a pseudorandom signal, generated in the frequency band $[75\ 100]Hz$. A pseudorandom signal is a bandlimited signal (in amplitude it is a rectangle) with a random phase.

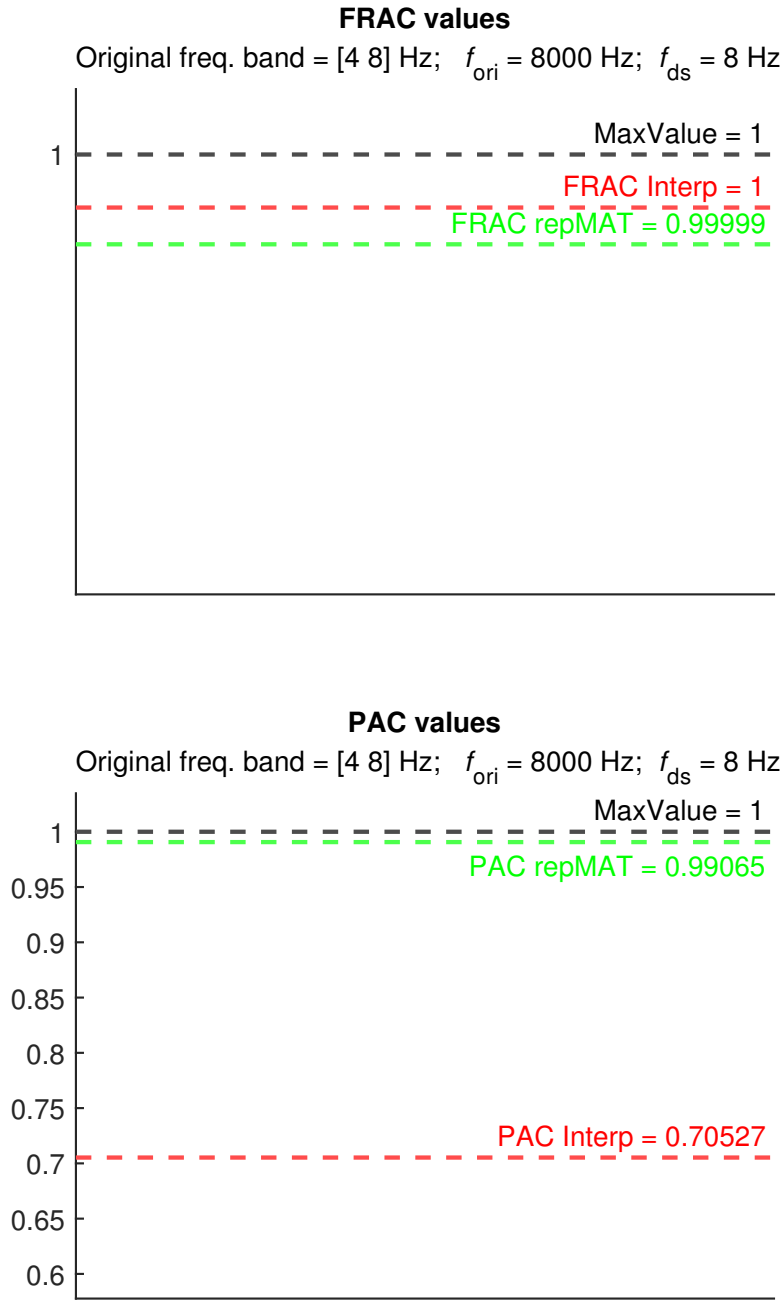

Figure 2.14.: FRAC and PAC for Interpolation method and repMat method reconstruction - Windowed Chirp $F_L = 4Hz$; $F_H = 8Hz$

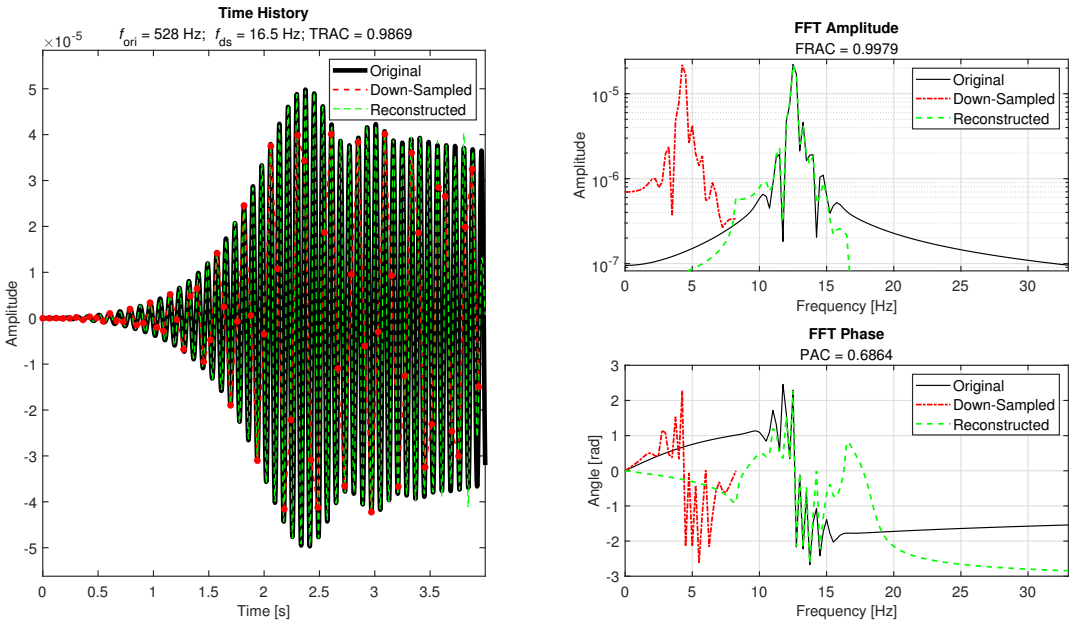

Figure 2.15.: Reconstructed signal via Interpolation method - MDOF excited via Windowed Chirp $F_L = 9.5Hz; F_H = 16.5Hz$

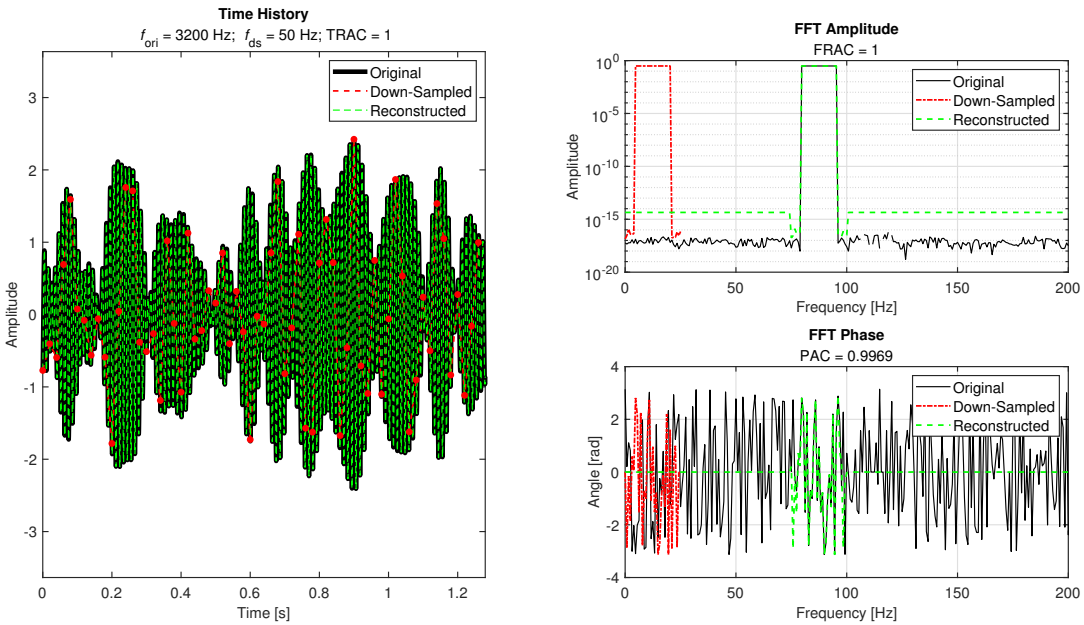

Figure 2.16.: Reconstructed signal via repMat method - Pseudorandom excitation $F_L = 75Hz; F_H = 100Hz$

Chapter 3.

Experimental Validation

This section illustrates the experimental implementation of the two studied algorithms discussed in section 2.2. The workflow follows these steps:

1. Define the acquisition parameters;
2. Set up the measurement chain;
3. Set up the synchronization signal between the cameras and the excitation signal;
4. Design the post-processing procedure with attention to the correct acquired data management.

3.0.1. Acquisition Parameters

To establish the acquisition parameters it is necessary to know which parameters characterize the single experiment and of course which parameters are obtained via computation of the previous ones.

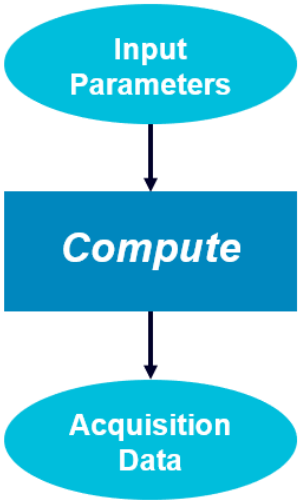

Figure 3.1.: "Abstract Oriented" diagram

Figure 3.1 is a generic diagram that schematizes the concept.

The **INPUT** parameters are:

- Observation band: **band**;
- Acquisition time: **dt**;
- Sampling frequency of the final reconstructed signal: **rightF**;
- Excitation band: **band_exc**

Note that the excitation band can be equal to the observation band or it can be a subset of the observation band. It is useful to define a margin variable that defines the amount of Hz to choose as inner gap for the excitation band with respect to the observation band (e.g. if observation band is $[20\ 40]Hz$ and excitation band is $[24\ 36]Hz$, the margin is $4Hz$). Using an excitation band as a subset of the observation band is recommended. In fact, the numerical validations showed that adopting an excitation band equal to the observation band, the down-sampling operation may alterate the spectrum at 0 Hz.

Using these parameters it is possible to compute the frame rate of the cameras (i.e. the down-sampling frequency) and the number of photos (i.e. the samples of the down-sampled signal).

The **OUTPUT** parameters are:

- Camera sampling frequency: **down_sampledF**;
- Number of photos: **k_elem**;

Specifically the camera frame rate is computed as explained in equation 2.27.
The number of samples is deduced using the acquisition time from the input, computing the $n_{photos} = f_{camera} \cdot dt$ equation[1]. In addition to these output parameters, also the $desired_{ratio}$ computed as explained in equation 2.30 and the number of samples N of the reconstructed signal are computed. These two last parameters are useful only during the reconstruction phase in post-processing.

However, the just described flow requires additional modification. In fact, there are some possible outcomes that might happen during the computation:

- ➢ Camera frame rate **down_sampledF** is periodic;
- ➢ Number of photos **k_elem** is NOT integer or NOT even;
- ➢ Acquisition time **dt** is periodic;

Where by "periodic" is meant also with many decimal digits. Regarding the frame rate of the cameras, it is better not to have a value with many decimal digits, because the hardware can not perform with such accuracy. In the same way, having a value of

[1] Using the coding variable names `k_elem = down_sampledF * dt`

the acquisition time that is not periodic, allows better accuracy in the post-processing phase. In addition the number of photos must be integer and even to correctly apply the "repMat" reconstruction method, as explained in section 2.3. It is necessary to check over each of the possible outcomes and to implement an optimization procedure over the input parameters, avoiding the "bad cases" listed above.

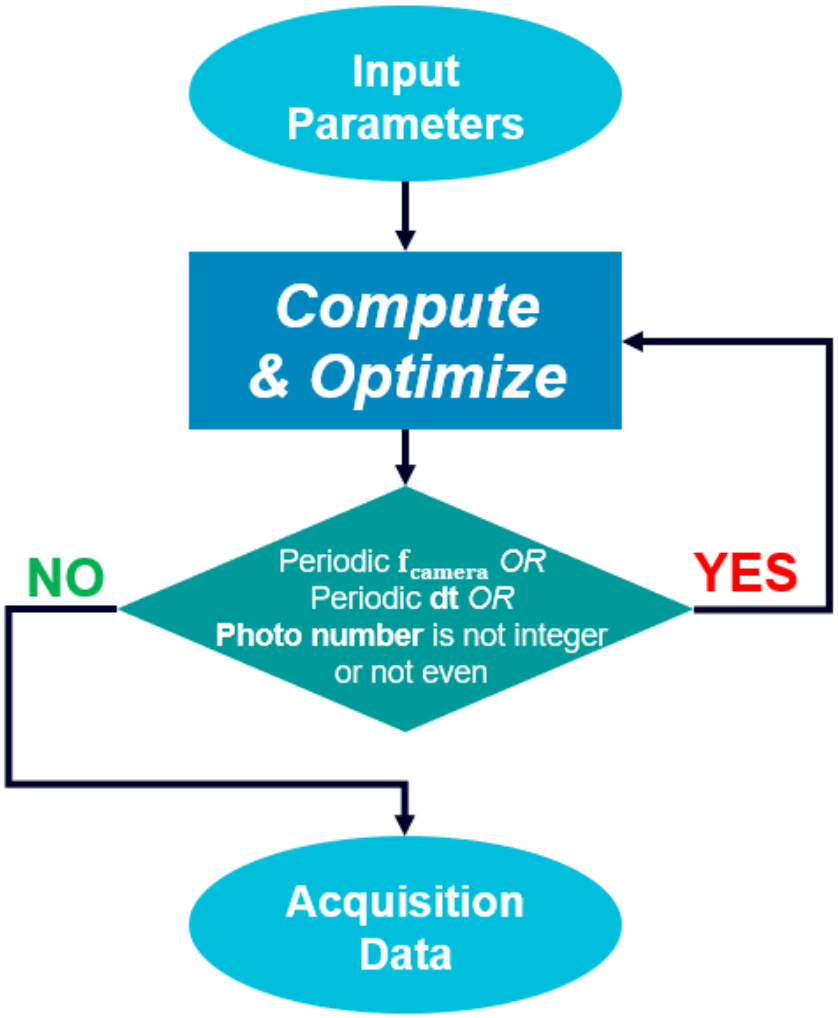

Figure 3.2.: Final workflow diagram with optimization and check implementation

Figure 3.2 is the final workflow diagram: the "Compute" block, as it was designed in figure 3.1, has become "Compute and Optimize", in fact further implementations have been developed to avoid the possible outcomes explained above. These implementations regard the camera frequency correction, the acquisition time correction and the number of photos correction.

The optimization starts by fixing the frame rate of the cameras.

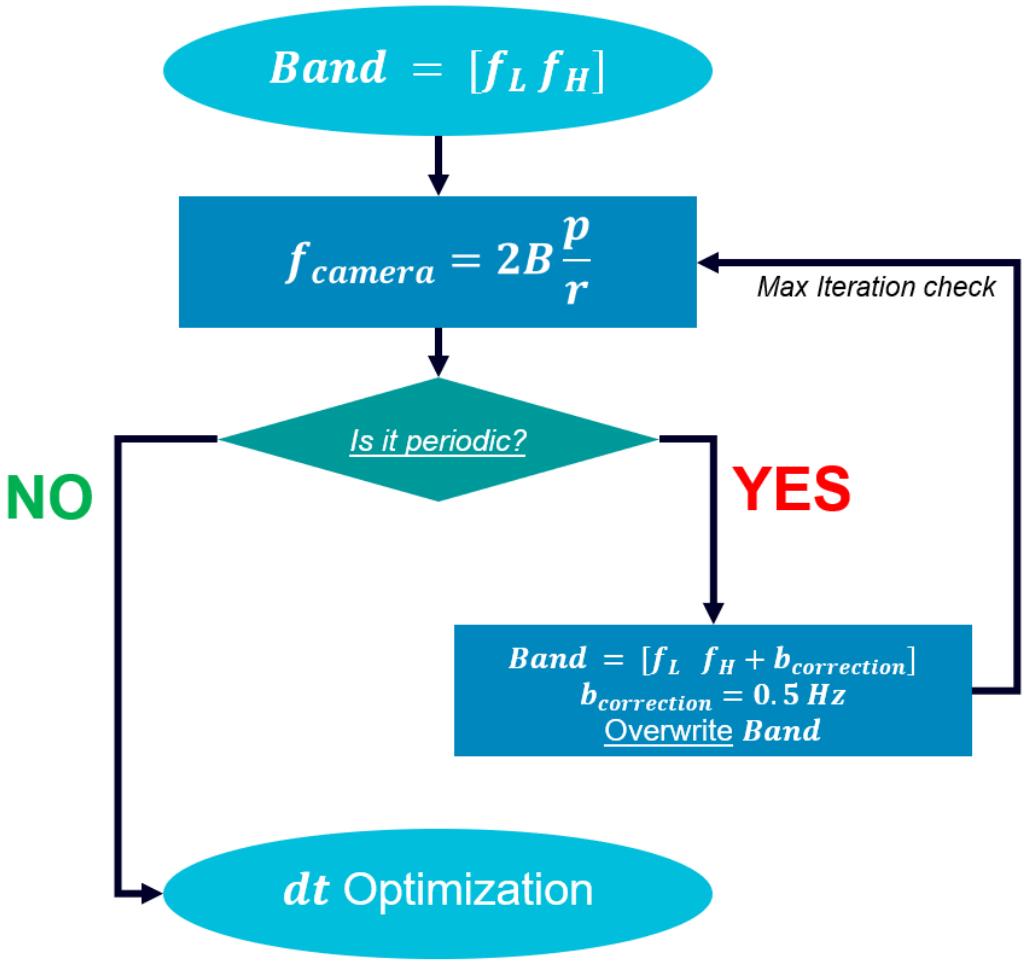

Figure 3.3.: Camera frequency correction - Diagram

The camera frame rate is computed using the observation band and the formula 2.27, if this value is periodic, the band input parameter is optimized such that the upper bound of the frequency range is increase by a band correction factor (set at $b_{correction} = 0.5Hz$) and the observation band is overwritten and the new camera frame rate is computed. This loop happens until the frame rate is not periodic or with many decimal digits. Figure 3.4 shows how with a setup of $[100\ 140]Hz$ the computation leads to a camera frame rate **down_sampledF** $= 93.3333Hz$ which is a periodic value. In figure 3.5 the band is optimized, and using $[100\ 141]Hz$ allows to have a frame rate **down_sampledF** $= 94Hz$ which is perfectly suitable for the experiment and can be set for the hardware. The loop is controlled over a max number of iteration (set to 100). For the experimental validation, discussed in the next sections, the optimization required at max 6 iterations, i.e. increasing the upper bound by at max 3 Hz.

```
STARTING SETUP
INPUT band = [100 140] Hz
INPUT dt = 2.6 s


Band Parameters Optimization
Attempt n. 1
Band = [100 140] Hz
fl = 100 Hz
fh = 140 Hz
B = 40 Hz
p = fh/B = 3.5
p IS NOT an INTEGER!
r = 3
B' = 46.6667 Hz
fc = 120 Hz
fc' = 116.6667 Hz
Computed down_sampledF with this band is 93.3333 Hz
down_sampledF is periodic and not usable!
```

Figure 3.4.: Camera frequency correction - Script Output (frame rate not suitable)

```
Attempt n. 3
Band = [100 141] Hz
fl = 100 Hz
fh = 141 Hz
B = 41 Hz
p = fh/B = 3.439
p IS NOT an INTEGER!
r = 3
B' = 47 Hz
fc = 120.5 Hz
fc' = 117.5 Hz
Computed down_sampledF with this band is 94 Hz
down_sampledF can be used for experiment!
```

Figure 3.5.: Camera frequency correction - Script Output (frame rate is suitable)

Once the frame rate of the cameras has been set and fixed, the optimization of the number of photos and of the acquisition time need to be performed.

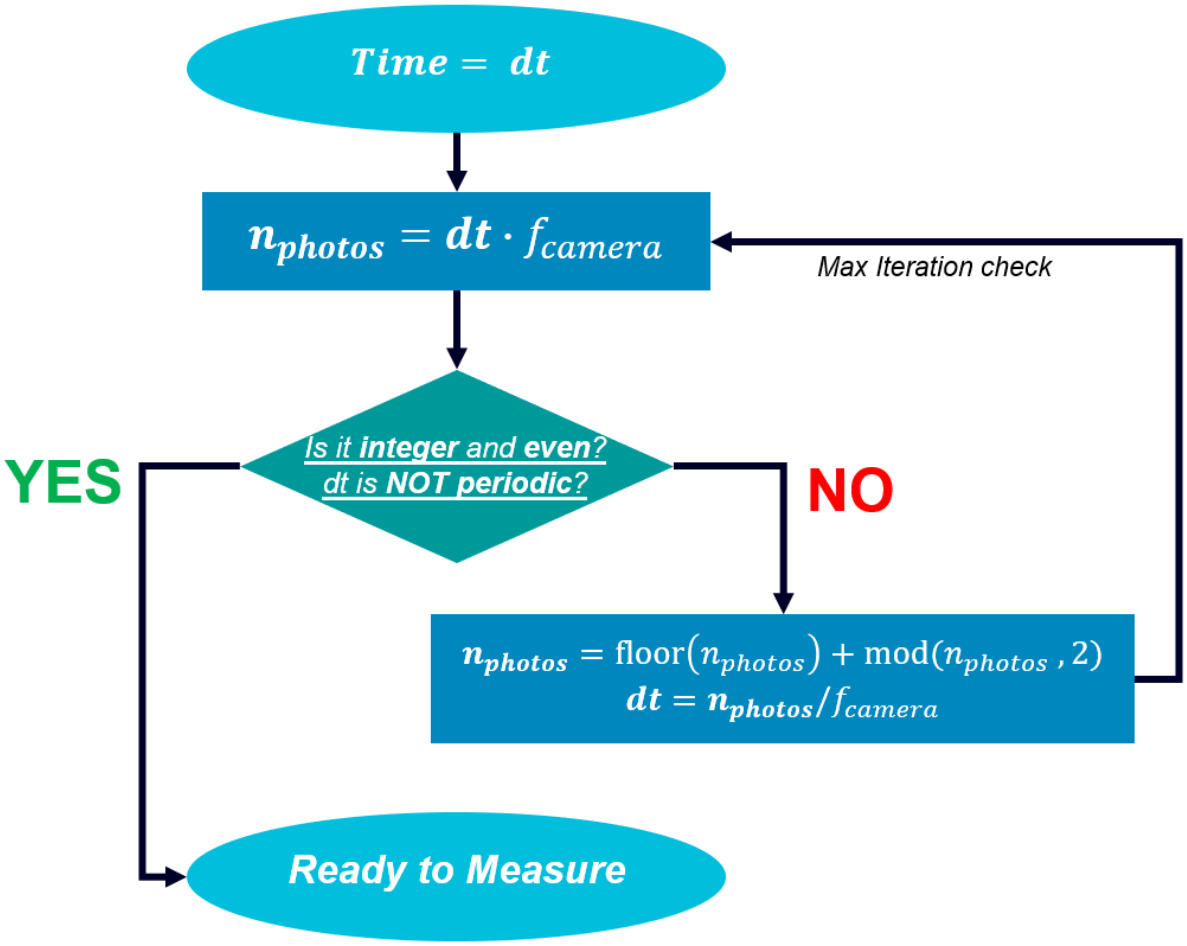

Figure 3.6.: Correction of the acquisition time and of the number of pictures - Diagram

Starting from the acquisition time, as an input parameter inserted by the user, it is possible to compute the number of samples, by multiplying the acquisition time with the frame rate of the cameras (fixed in the previous cycle). After the computation a first check over the number of photos is performed. If the number is not integer it is rounded at the closest even number using the equation $n_{photos} = \text{floor}(n_{photos}) + \text{mod}(n_{photos}, 2)$. From this number the new acquisition time is recomputed via the inverse formula $dt = n_{photos} \cdot f_{camera}$. Looping over the number of photos, incrementing it by +2 during each cycle, the operation stops when a suitable acquisition time is reached.

Figure 3.7 and 3.8 show the results of the iterations. Initially the number of photos is computed as 244.4 and it is corrected to the closest integer even number (i.e. 244). The new acquisition time is computed and the number of photos is increased by +2 until the value of the acquisition time reaches a not periodic (or with many decimal digits) value.

```
Samples Settings
k_elem = dt*down_sampledF = 244.4
k_elem is not integer or not an even number
k_elem is corrected to the value: k_elem = 244
Attempt n. 1
k_elem = 244
dt_new is a periodic time! dt_new = 2.5957 s
k_elem is corrected to the value: k_elem = 246
- - - - - - - - - - - - - - - - - - - - - - - - - - - - - -
Attempt n. 2
k_elem = 246
dt_new is a periodic time! dt_new = 2.617 s
k_elem is corrected to the value: k_elem = 248
- - - - - - - - - - - - - - - - - - - - - - - - - - - - - -
Attempt n. 3
k_elem = 248
dt_new is a periodic time! dt_new = 2.6383 s
k_elem is corrected to the value: k_elem = 250
- - - - - - - - - - - - - - - - - - - - - - - - - - - - - -
Attempt n. 4
k_elem = 250
dt_new is a periodic time! dt_new = 2.6596 s
k_elem is corrected to the value: k_elem = 252
- - - - - - - - - - - - - - - - - - - - - - - - - - - - - -
Attempt n. 5
k_elem = 252
dt_new is a periodic time! dt_new = 2.6809 s
k_elem is corrected to the value: k_elem = 254
- - - - - - - - - - - - - - - - - - - - - - - - - - - - - -
```

Figure 3.7.: Correction of the acquisition time and of the number of pictures - Script Output (the number of pictures is not integer and the acquisition time is periodic)

```
- - - - - - - - - - - - - - - - - - - - - - - - - - - - - - - -
Attempt n. 15
k_elem = 272
dt_new is a periodic time! dt_new = 2.8936 s
k_elem is corrected to the value: k_elem = 274
- - - - - - - - - - - - - - - - - - - - - - - - - - - - - - - -
Attempt n. 16
k_elem = 274
dt_new is a periodic time! dt_new = 2.9149 s
k_elem is corrected to the value: k_elem = 276
- - - - - - - - - - - - - - - - - - - - - - - - - - - - - - - -
Attempt n. 17
k_elem = 276
dt_new is a periodic time! dt_new = 2.9362 s
k_elem is corrected to the value: k_elem = 278
- - - - - - - - - - - - - - - - - - - - - - - - - - - - - - - -
Attempt n. 18
k_elem = 278
dt_new is a periodic time! dt_new = 2.9574 s
k_elem is corrected to the value: k_elem = 280
- - - - - - - - - - - - - - - - - - - - - - - - - - - - - - - -
Attempt n. 19
k_elem = 280
dt_new is a periodic time! dt_new = 2.9787 s
k_elem is corrected to the value: k_elem = 282
- - - - - - - - - - - - - - - - - - - - - - - - - - - - - - - -
New Acquisition Time is computed: dt_new = 3 s
```

Figure 3.8.: Correction of the acquisition time and of the number of pictures - Script Output (the number of pictures is increased by +2 to get a suitable acquisition time)

The acquisition parameters are then fixed and set for the experiment. A final recap is provided with all the useful necessary data to set up the experiment. Importantly, the observation band, the frame rate of the cameras, the acquisition time and the number of photos are the main parameters that characterize the experiment.

```
Final Acquisition Data Recap
Observation band = [100 141] Hz
Excitation band = [103 137] Hz
TestLab sampling frequency: rightF = 3200 Hz
Cameras sampling frequency: down_sampledF = 94 Hz
Computed sampling frequencies ratio = 3200/94 = 34.0426
Acquisition Time: dt_new = 3 s
Number of photos: k_elem = 282
Number of samples of original signal: N = 9600
```

Figure 3.9.: Final acquisition data

The values are saved in the workspace, they will be use to generate the excitation signal to provide to the shaker and the pulse and trigger signals to provide to the cameras. Figure 3.9 shows the acquisition data for the case analyzed in the previous figures.

3.0.2. Experimental Setup

The setup for the experimental validation is shown is figure 3.10. Measurements will be performed over a cantilever beam (dimensions $= 400 \times 40 \times 5\ mm$). The beam is indeed clamped in one extremity on a mass block.

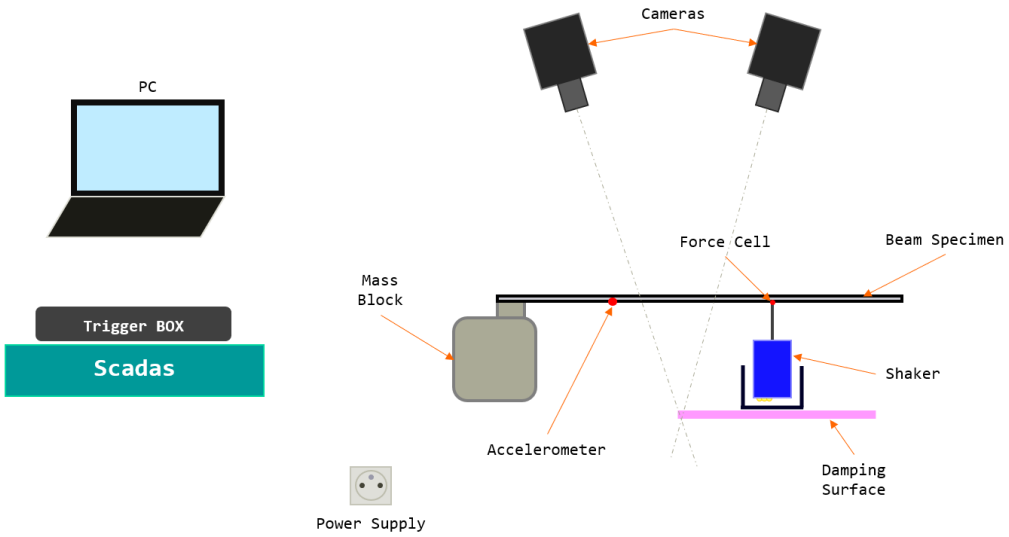

Figure 3.10.: Experimental Setup - Instrumentation

The excitation happens via a shaker. A damping surface, in this case a foam panel, is placed between the shaker and the floor. The driving point is located at 2/3 of the beam length from the clamped edge. A force cell is connected to the harmonic stinger of the shaker and attached to the structure in the driving point. Two cameras in stereo vision configuration are facing towards the top of the specimen where the speckle pattern is located[2]. The cameras are connected to the laptop and to the trigger box which is used for the synchronization. An accelerometer is shown as the red dot represented in figure 3.10 and 3.11. During the test, 10 accelerometers were used for the validation.

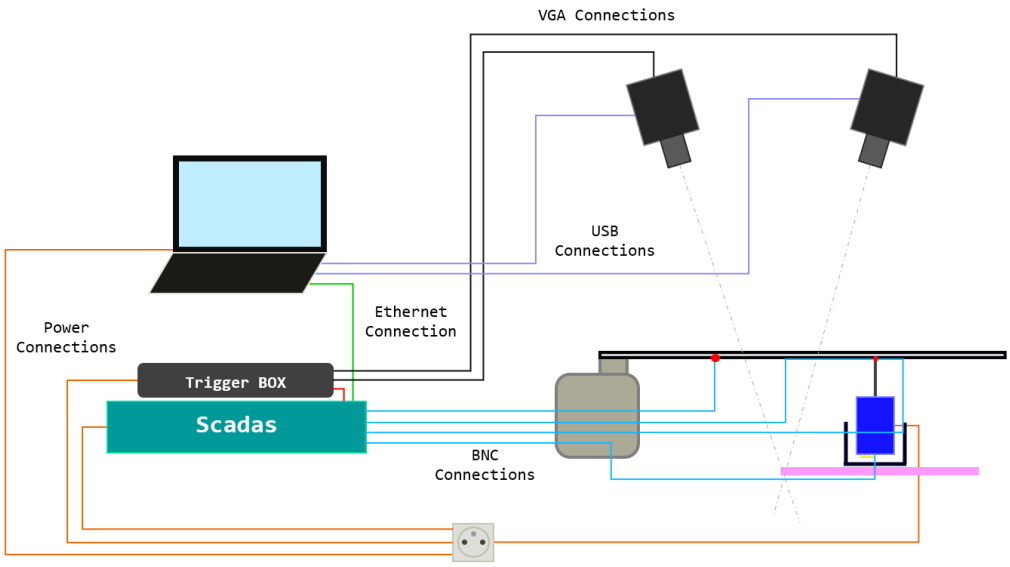

Figure 3.11.: Experimental Setup - Cabling&Connections

The Scadas is the acquisition system provided by Siemens where all the sensors (accelerometers, force cell), actuator (shaker) and the trigger box are connected via BNC co-axial connectors. The cameras are connected to the computer via USB and to the trigger box via VGA connections.
A total number of 13 channels are used:

- 10 channels for the accelerometers;
- 1 channel for the force cell in the driving point;
- 1 channel for the sync signal trigger for the cameras;
- 1 channel to measure the signal which is being given in input to the shaker.

This last channel is a verification channel that allows to check if the generated signal (via MatLab) given in input to the shaker is effectively the same that TestLab processes and sends to the shaker itself.

[2]Note that the beam itself has also an additional speckle pattern on its bottom surface as shown in figure 3.13 for other uses not relevant for this study

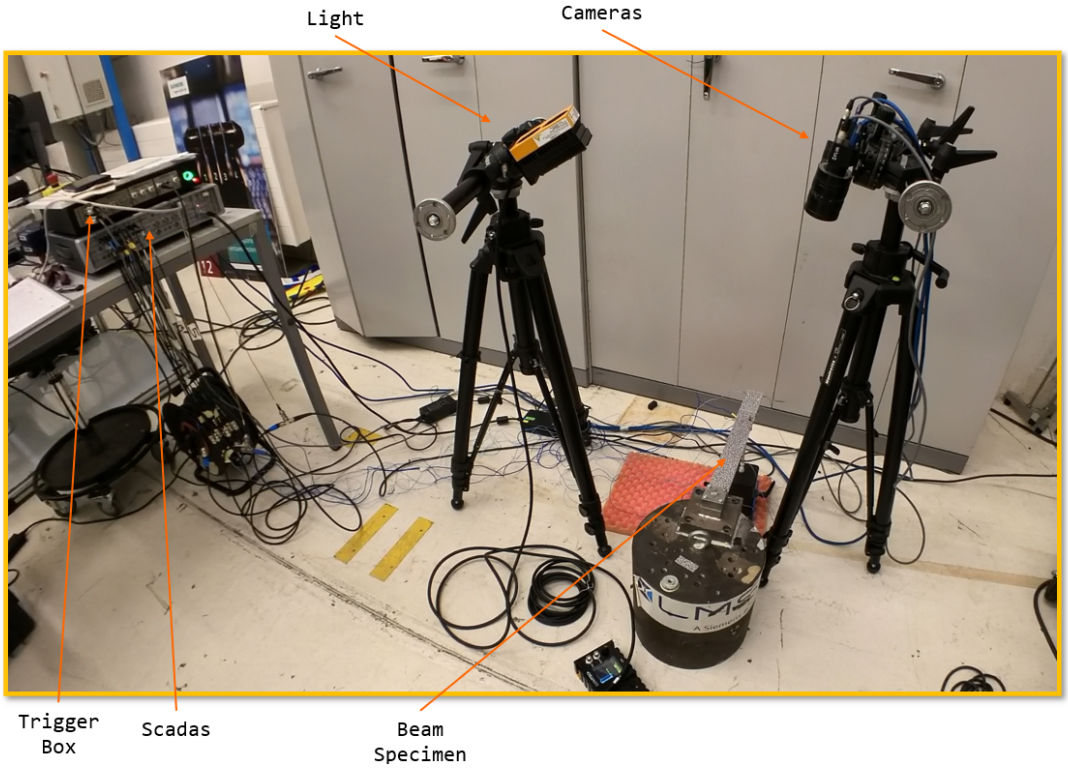

Figure 3.12.: Experimental Setup - Global view

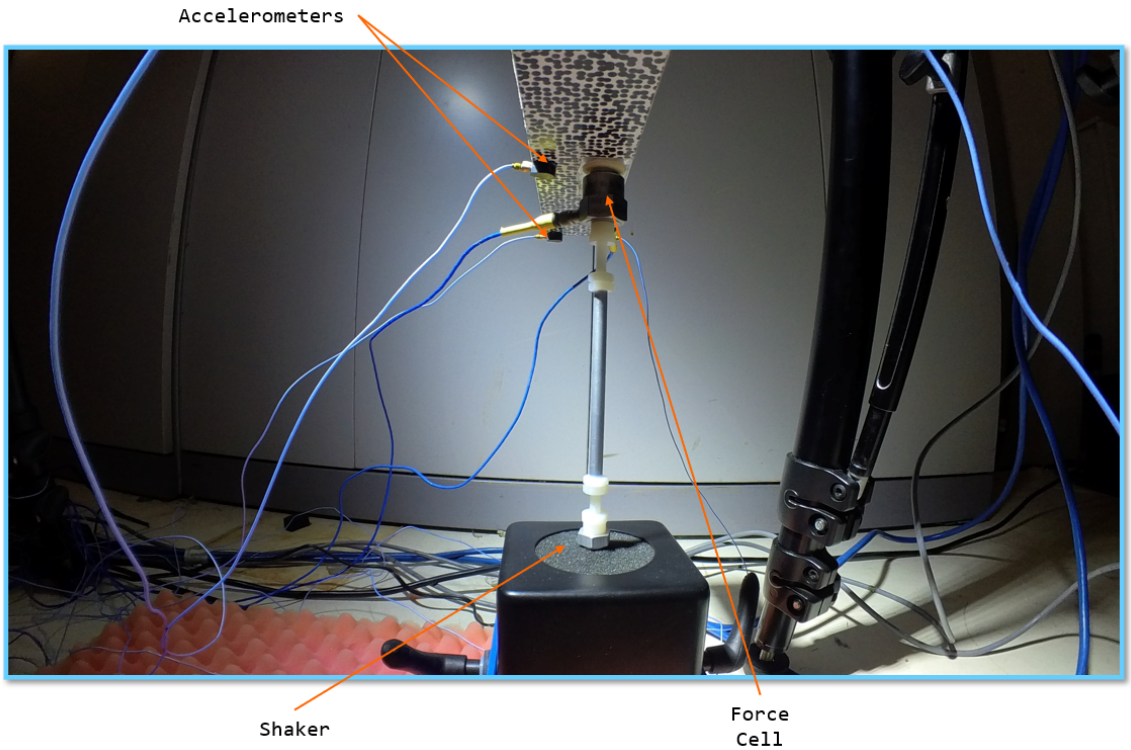

Figure 3.13.: Experimental Setup - Side view (beam and shaker)

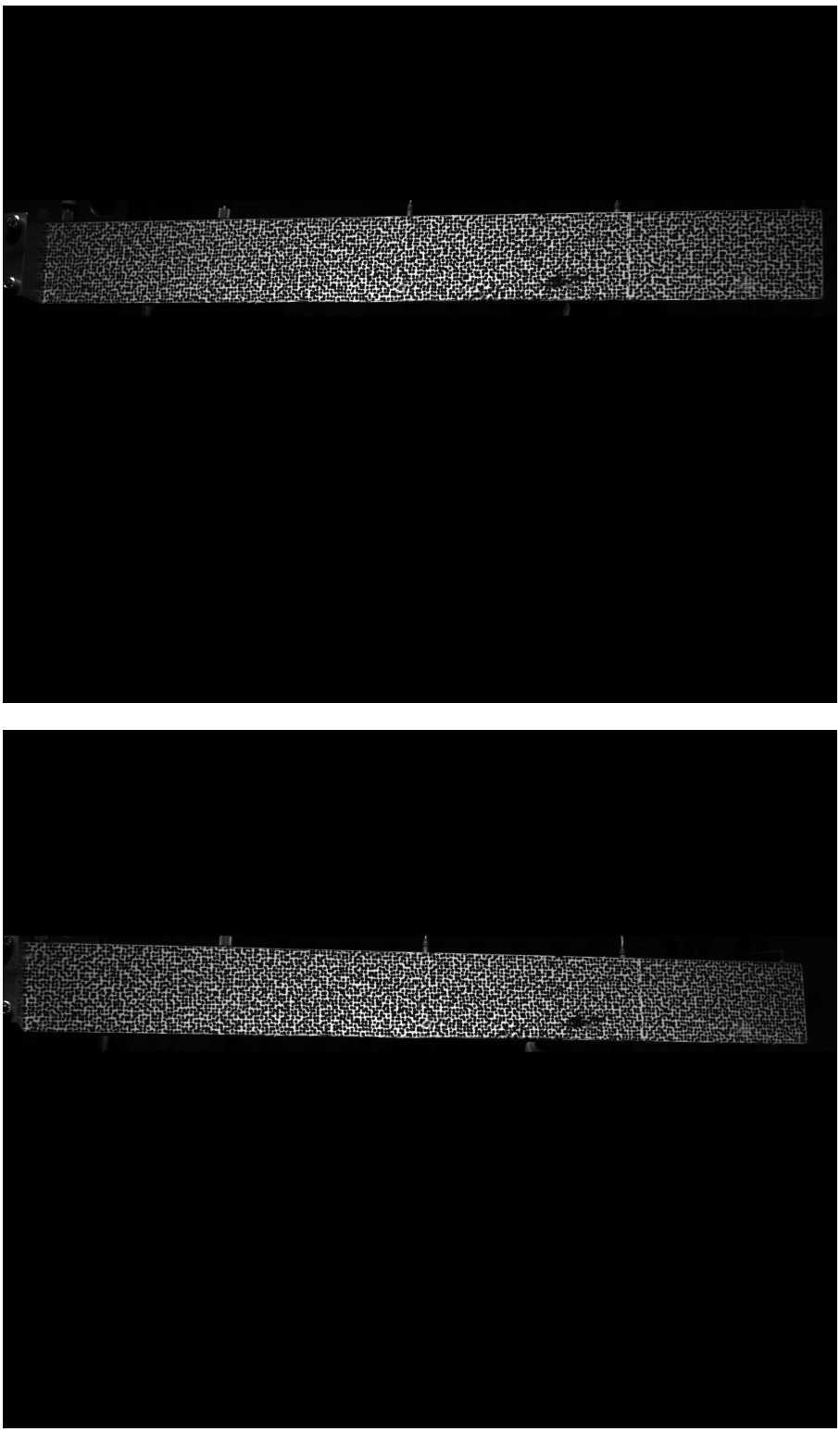

Figure 3.14.: View of the cameras[3], left and right; The ROI is cropped such that only the beam is analyzed (reduce area, improve frame rate)

3.0.3. Experimental Procedure

The experimental procedure involves the following steps, illustrated in figure 3.15.

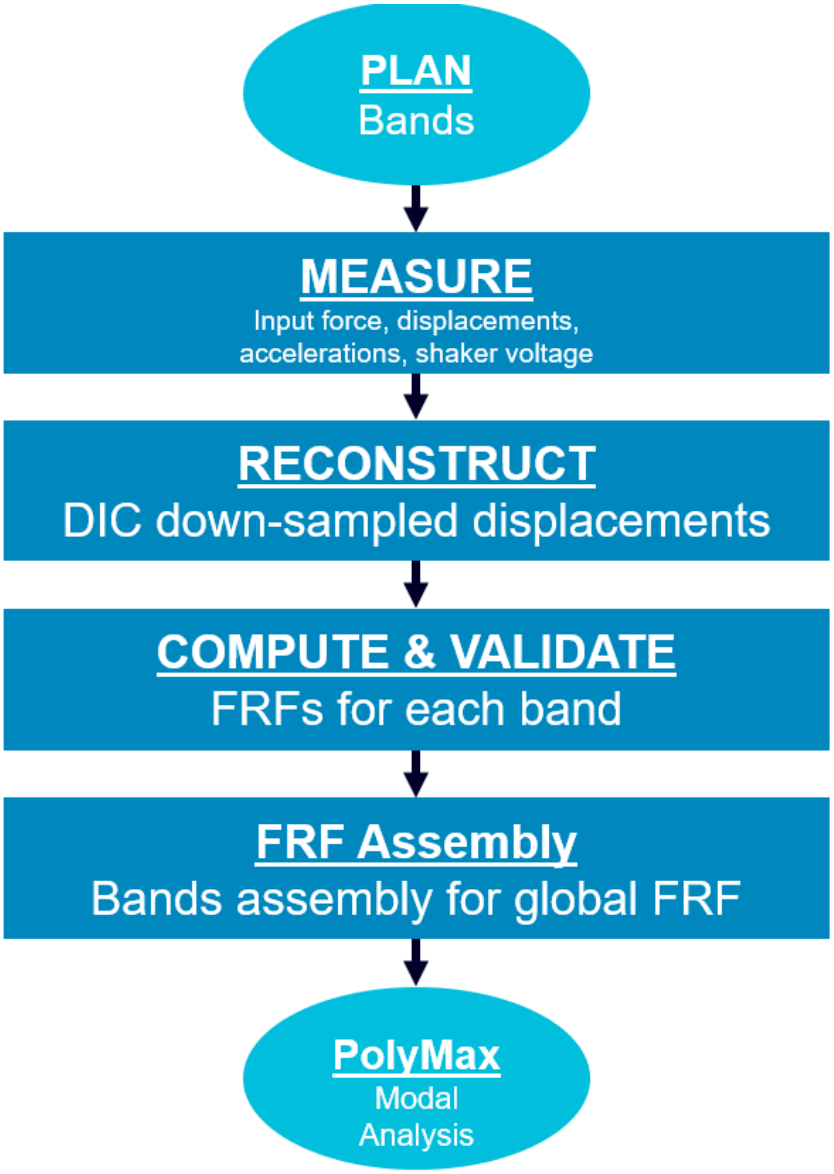

Figure 3.15.: Experimental Procedure - Diagram

Initially a planning phase where all the bands to analyze are decided: for each band the set up algorithm for the computation of the acquisition parameters is performed (for each band the camera frame rate and the number of photos are computed) and a table as the one showed in figure 3.16 will contain the results of the computation.

[3]Backfly Low Speed - BFS-U3-51S5M-C: 5,0 MP, 75 FPS: `https://www.flir.it/products/blackfly-s-usb3/?model=BFS-U3-51S5M-C&vertical=machine+vision&segment=iis`

Depending on the planned type of measurements it is of course possible to personalize the planning of the bands using for example overlapped bands, sectorial or consecutive bands in specific frequency ranges. One frequency band corresponds to one "run", all the runs together represent one test.

BAND		p	r	down_sampledF	desired_fs_ratio	k_elem	k_elem*n_av	n	dt	Run Name
0	40	1	1	80	40	80	480	1	1	Run_exc4-36_over0-40_dt1_desRa40
20	60	1.5	1	120	26.66666667	120	720	2	1	Run_exc24-56_over20-60_dt1_desRa26.667
40	80	2	2	80	40	80	480	3	1	Run_exc44-76_over40-80_dt1_desRa40
60	100	2.5	2	100	32	100	600	4	1	Run_exc64-96_over60-100_dt1_desRa32
80	120	3	3	80	40	80	480	5	1	Run_exc84-116_over80-120_dt1_desRa40
100	141	3.439024	3	94	34.04255319	94	564	6	1	Run_exc104-137_over100-141_dt1_desRa34.043
120	160	4	4	80	40	80	480	7	1	Run_exc124-156_over120-160_dt1_desRa40
140	180	4.5	4	90	35.55555556	90	540	8	1	Run_exc144-176_over140-180_dt1_desRa35.556
160	200	5	5	80	40	80	480	9	1	Run_exc164-196_over160-200_dt1_desRa40
180	220	5.5	5	88	36.36363636	88	528	10	1	Run_exc184-216_over180-220_dt1_desRa36.364
200	240	6	6	80	40	80	480	11	1	Run_exc204-236_over200-240_dt1_desRa40
218	258	6.45	6	86	37.20930233	86	516	12	1	Run_exc222-254_over218-258_dt1_desRa37.209
240	280	7	7	80	40	80	480	13	1	Run_exc244-276_over240-280_dt1_desRa40
260	301	7.341463	7	86	37.20930233	86	516	14	1	Run_exc264-297_over260-301_dt1_desRa37.209
280	320	8	8	80	40	80	480	15	1	Run_exc284-316_over280-320_dt1_desRa40
300	340	8.5	8	85	37.64705882	102	612	16	1.2	Run_exc304-336_over300-340_dt1.2_desRa37.647
320	360	9	9	80	40	80	480	17	1	Run_exc324-356_over320-360_dt1_desRa40
340	382.5	9	9	85	37.64705882	102	612	18	1.2	Run_exc344-378.5_over340-382.5_dt1.2_desRa37.647
360	400	10	10	80	40	80	480	19	1	Run_exc364-396_over360-400_dt1_desRa40
380	420	10.5	10	84	38.0952381	84	504	20	1	Run_exc384-416_over380-420_dt1_desRa38.095
400	440	11	11	80	40	80	480	21	1	Run_exc404-436_over400-440_dt1_desRa40
420	462	11	11	84	38.0952381	84	504	22	1	Run_exc424-458_over420-462_dt1_desRa38.095
440	480	12	12	80	40	80	480	23	1	Run_exc444-476_over440-480_dt1_desRa40
463	504	12.29268	12	84	38.0952381	84	504	24	1	Run_exc467-500_over463-504_dt1_desRa38.095
480	520	13	13	80	40	80	480	25	1	Run_exc484-516_over480-520_dt1_desRa40
504	546	13	13	84	38.0952381	84	504	26	1	Run_exc508-542_over504-546_dt1_desRa38.095
520	560	14	14	80	40	80	480	27	1	Run_exc524-556_over520-560_dt1_desRa40
542	585	13.60465	13	90	35.55555556	90	540	28	1	Run_exc546-581_over542-585_dt1_desRa35.556
560	600	15	15	80	40	80	480	29	1	Run_exc564-596_over560-600_dt1_desRa40
585	624	16	16	78	41.02564103	78	468	30	1	Run_exc589-620_over585-624_dt1_desRa41.026
600	640	16	16	80	40	80	480	31	1	Run_exc604-636_over600-640_dt1_desRa40
624	663	17	17	78	41.02564103	78	468	32	1	Run_exc628-659_over624-663_dt1_desRa41.026
640	680	17	17	80	40	80	480	33	1	Run_exc644-676_over640-680_dt1_desRa40
664	702	18.47368	18	78	41.02564103	78	468	34	1	Run_exc668-698_over664-702_dt1_desRa41.026
680	720	18	18	80	40	80	480	35	1	Run_exc684-716_over680-720_dt1_desRa40
699	738	18.92308	18	82	39.02439024	82	492	36	1	Run_exc703-734_over699-738_dt1_desRa39.024
720	760	19	19	80	40	80	480	37	1	Run_exc724-756_over720-760_dt1_desRa40
738	782	17.77273	17	92	34.7826087	92	552	38	1	Run_exc742-778_over738-782_dt1_desRa34.783
760	800	20	20	80	40	80	480	39	1	Run_exc764-796_over760-800_dt1_desRa40
780	820	20.5	20	82	39.02439024	82	492	40	1	Run_exc784-816_over780-820_dt1_desRa39.024

Figure 3.16.: Planning of the bands - Table results

In the studied test case a planning of 40 bands (40 runs) with length around 40 Hz overlapped each other by 50% is computed. With the purpose to cover the global range [0 820]Hz including all the five modes identified with a preliminary test discussed in section 4.1. For each run we take six times the amount of photos, to have later the possibility to average over six reconstructed displacement signals.

Once all the runs are planned and the respective band-limited signal have been generated, it is possible to start measuring. The measuring phase involves the acquisition of the input force on the beam via the force cell (it will be useful to compute the FRF for the modal analysis in post processing), the accelerations via the 10 accelerometers placed on the beam as showed in figure 3.19 and via the cameras the displacements of each geometry point of the beam computed by the DIC algorithm are measured, they are the down-sampled signal needed to be reconstructed.

Figure 3.17 shows on the top row the excitation signal, a schroeder band limited signal which is a pseudorandom signal (i.e. band limited spectrum in amplitude and random phase). Two signals are showed overlapped: in fact the generated signal is compared to the measured voltage that goes in output from the Scadas and in input to the shaker. This happens as a check if the shaker receives in input the correct signal. The same comparison can be also appreciated in frequency domain where also the band-limited spectrum of the schroeder is visible in figure 3.18.

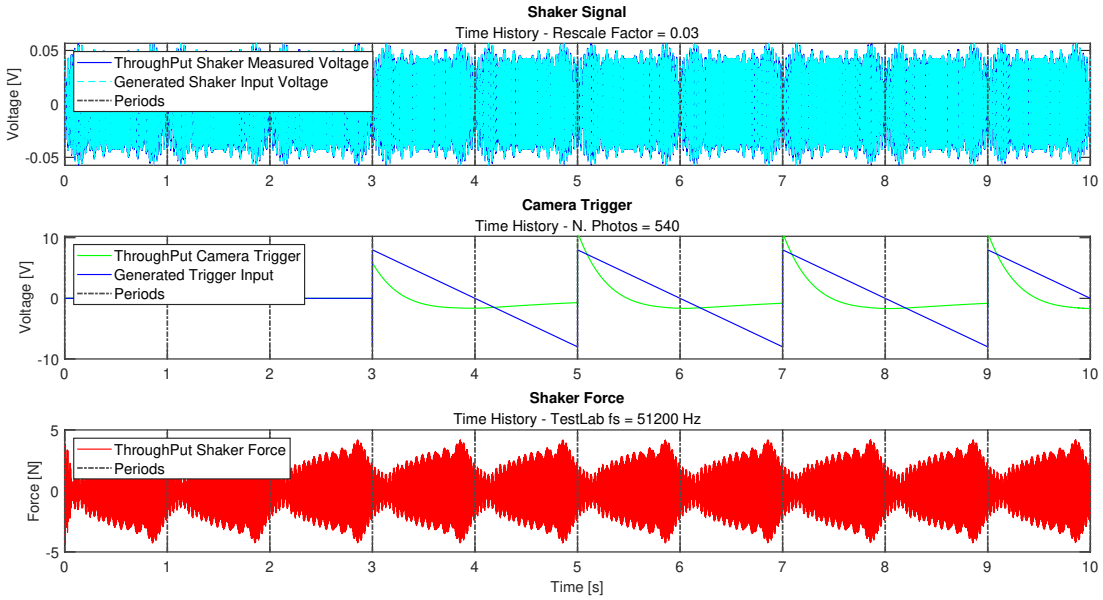

Figure 3.17.: Measured Data: Run band $[140\ 180]Hz$

The second row of figure 3.17 shows the syncronization signal. The syncronization signal is the blue saw-tooth signal which is used as a trigger for the cameras only to start the acquisition at the exact time. In fact, in the case of figure 3.17, the acquisition time is of $1s$ and the first 3 periods are ignored to avoid measuring transient behaviors. As a matter of fact the acquisition with the cameras starts at $3s$ and it ends at $9s$, measuring the 6 periods for the averaging procedure. The cameras are triggered because an high voltage peak (of around $8V$) is given in input by the trigger box. This high voltage peak is represented with the first high slope, located at $3s$, in the saw-tooth. The others voltage variation are not relevant for this case study. The green signal is the actual signal read by the trigger box, while the blue one is the signal genereted via MatLab and given in input to TestLab.

The last row is the measured data by the force cell, of course it will be necessary to consider only the part of the red signal in the range $[3\ 9]s$ to compute then the FRFs. An important note is on the sampling frequency set on TestLab to manage both the force signal and the trigger saw-tooth. This sampling frequency is infact the highest possible available on the software (in this case $51.2kHz$). The goal is to grant better accuracy in terms of synchronization time steps for the saw-tooth. Having a lower sampling frequency for the saw-tooth can cause a non-smooth digitalization of the saw-tooth itself. Consequently the cameras can react with delay with respect to the excitation.
Figure 3.19 shows the signals of the 10 accelerometers already cut in the right time range $[3\ 9]s$ while on the right side the beam geometry discretization is showed.

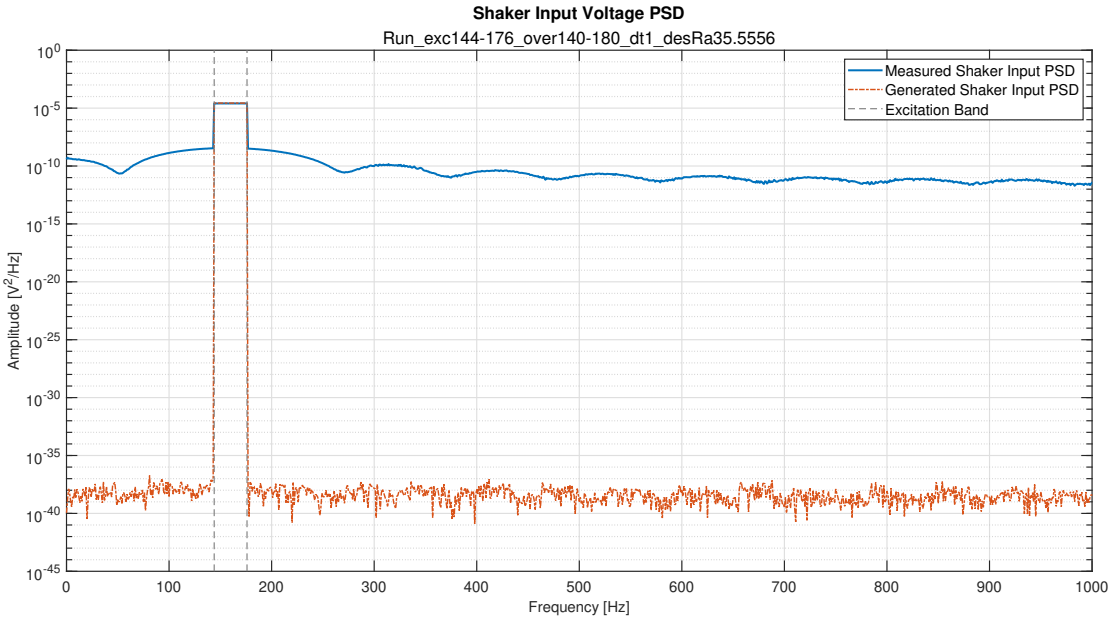

Figure 3.18.: Spectrum of band-limited excitation schroeder signal

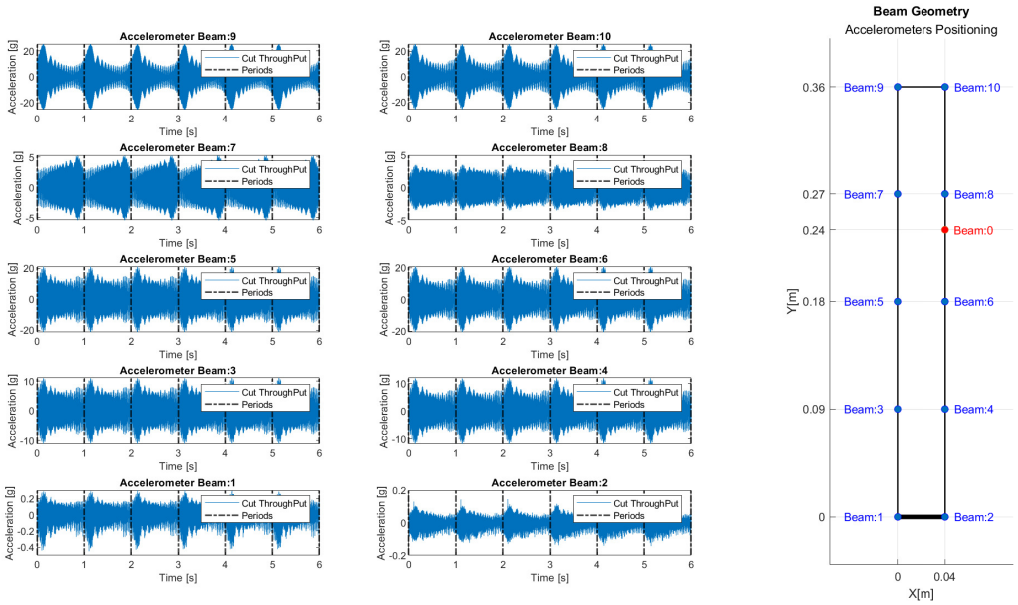

Figure 3.19.: Accelerometers signals: Run band $[140\ 180]Hz$

After the measuring phase where all the needed data are collected, the post processing phase begins. Firstly the down-sampled displacements need to be computed via the DIC algorithm (this is done by using the Siemens Software "DIC Analysis") for each run. Successively all the down-sampled displacements are reconstructed via the application of the algorithms discussed in section 2.2. Of course the DIC discretizes the structure in a certain number of points (in this case 2123 points): this means that for each run the number of down-sampled signals is equal to the number of points (i.e. the reconstruction algorithm is applied $= 40\ runs \times 2123\ points$ times).

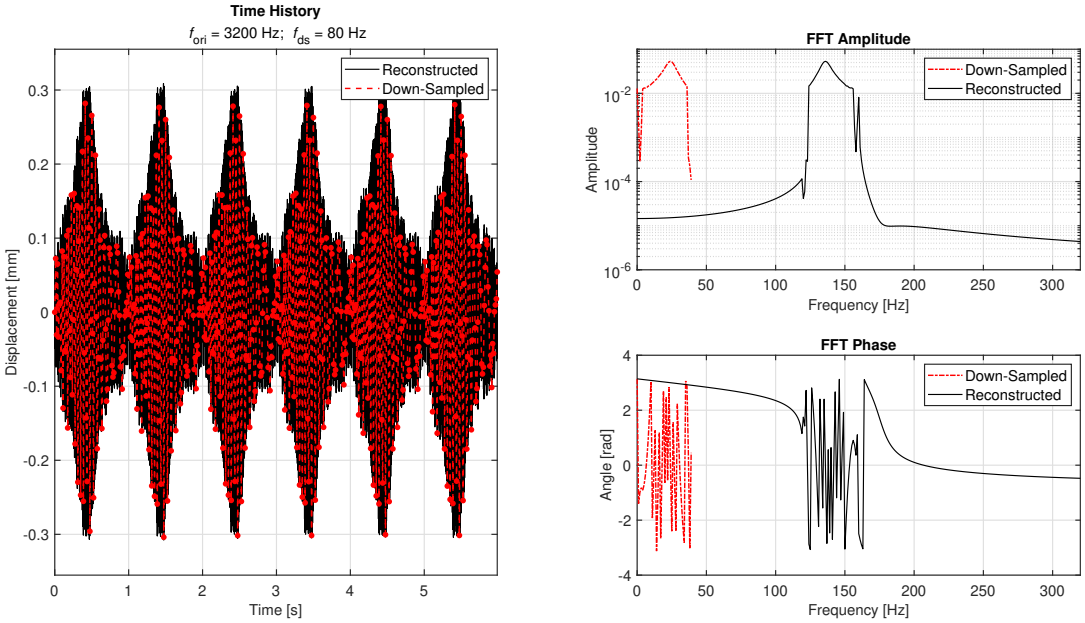

Figure 3.20.: Interpolation Reconstruction
Schroeder excitation $[124\ 156]Hz$; Geometry point #5

Figure 3.20 shows the reconstruction output of the interpolation method. On the left side there is the signal time history where also the six periods are detectable by the periodic trend of the signal during its duration. On the right side there is the reconstructed spectrum obtained via an FFT operation of the average of the six sub-time histories of the reconstructed signal.

Figure 3.21 shows the results of the repMat algorithm 2.3. Happening only in the frequency domain, no time histories are showed. The spectrum of the down-sampled signal is the red dotted line,the blue dashed line is the repeated spectrum computed by the algorithm while the blacl line is the spectrum chosen for the reconstruction.

The computational speed of the reconstruction procedure is very acceptable. The repMat method is faster than the Interpolation method, because the operation of the algorithm are actually very simple for the computer (only matrix shifting and selection), the reconstruction of a single band requires between 1 and 2 minutes for all the 2123 points. The interpolation method takes between 3 and 5 minutes for the reconstruction of a single run. This is not only due to the fact that the operations happen in time domain, but also that the math operations perfomed by the computer are more complex (sine and cosine multiplication, sum, and iteration, see section 2.2).

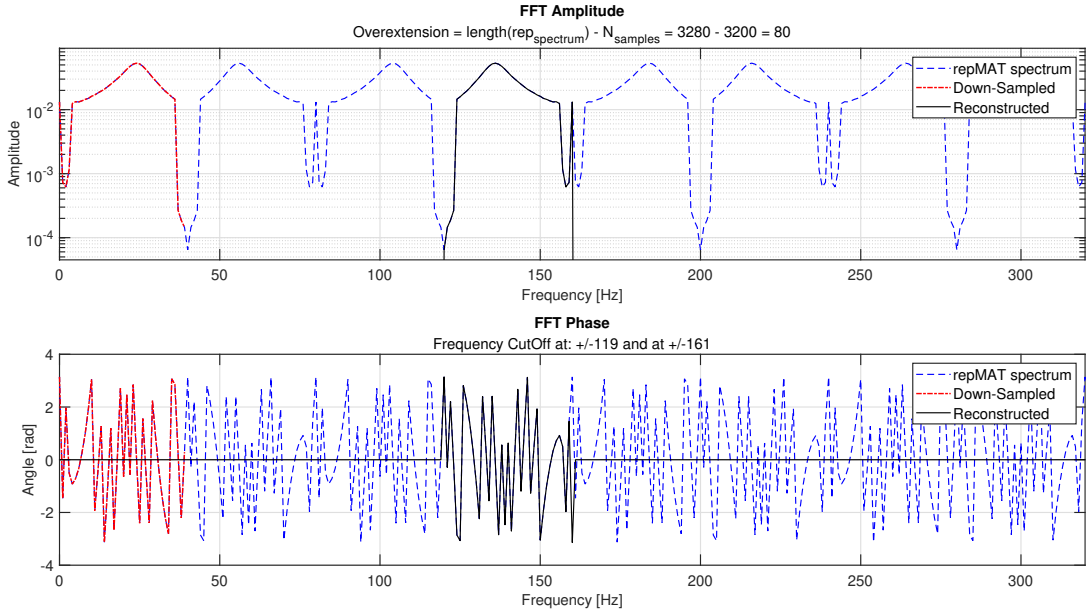

Figure 3.21.: repMat Reconstruction
Schroeder excitation [124 156]Hz; Geometry point #5

Now that the displacement signals are reconstructed the computation of the FRF can be performed. The reconstructed signal is the output and the force measured by the force cell is the input. Theory and forumlas are well explained in [17].

- For the "Interpolation Reconstruction" FRF and Coh, for each band, are computed starting from the time histories, and using the H_1 estimator;
- For the "repMat Reconstruction" the FRF, for each band, are computed directly via the spectrums, using aswell the H_1 estimator;

Calling $X(\omega)$ the FFT of the reconstructed displacements and $F(\omega)$ the FFT of the input force: G_{FF} is the autospectrum of the force, G_{XX} is the auto spectrum of the displacement and G_{XF} is the cross spectrum ($G_{XF} = G_{FX}$). The FRF is computed as follow:

$$H(\omega) = \frac{X(\omega)}{F(\omega)} \frac{F^*(\omega)}{F^*(\omega)} = \frac{G_{XF}}{G_{FF}} \tag{3.1}$$

The coherence is computed with its formula:

$$\gamma^2(\omega) = \frac{\left|\hat{G}_{FX}\right|^2}{\hat{G}_{FF}\hat{G}_{XX}} \tag{3.2}$$

where

$$\begin{aligned} \hat{G}_{FF} &= \frac{1}{N_{av}} \sum_{n=1}^{N_{av}} (G_{FF})_n \\ \hat{G}_{FX} &= \frac{1}{N_{av}} \sum_{n=1}^{N_{av}} (G_{FX})_n \\ \hat{G}_{XX} &= \frac{1}{N_{av}} \sum_{n=1}^{N_{av}} (G_{XX})_n \end{aligned} \tag{3.3}$$

$\gamma^2(\omega)$ is then averaged over the number of points:
$(2123\ points \times 1601\ freq.axis \longrightarrow 1 \times 1601\ freq.axis)$
The coherence will be used as a choice criteria during the FRF assembly procedure discussed in section 4.4 between two overlap zones.

Chapter 4.

Analysis of the Results

4.1. Preliminary Test Only Accelerometers

A preliminary test is performed on the beam. This test is an investigation over the structure to understand which are the modes that the experimental procedure discussed in section 3.0.3 aims at. The beam is then excited with a periodic chirp in the frequency range [10 1000]Hz and the response in measured only with the 10 accelerometers placed on the structure (as showed in figure 3.19). In figure 4.1 the single FRF for each accelerometer are showed.

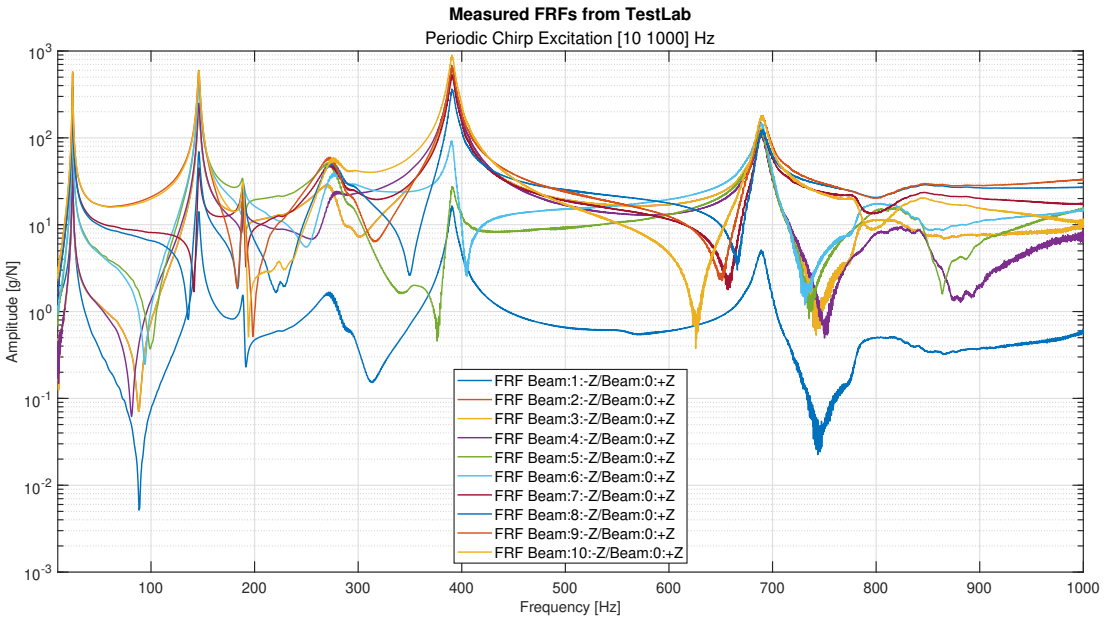

Figure 4.1.: Only Accelerometers Preliminary Test

Figure 4.2 shows the FRF sum of the 10 in figure 4.1. For each mode the mode shape is also computed, table 4.1 summarizes the modal parameters for each mode.

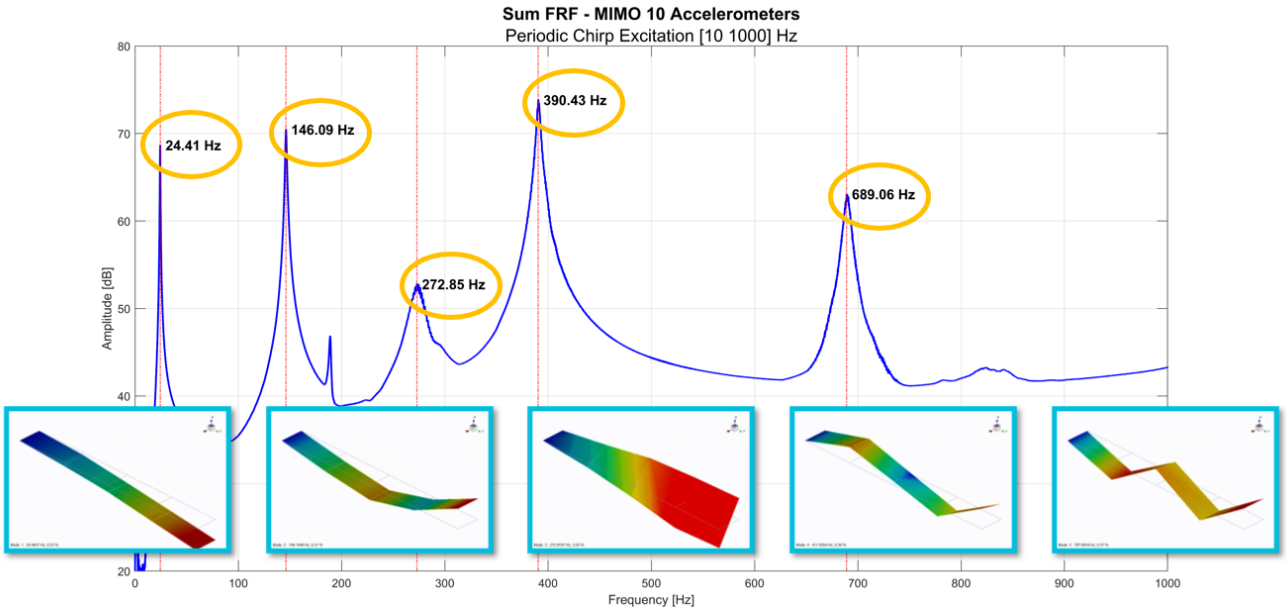

Figure 4.2.: FRF Sum of the preliminary test and the computed mode shapes

Mode	Frequency	Damping	Type
1	24 Hz	1.07%	1^{st} bending
2	146 Hz	0.67%	2^{nd} bending
3	273 Hz	3.72%	1^{st} torsional
4	390 Hz	0.61%	3^{rd} bending
5	689 Hz	0.64%	4^{th} bending

Table 4.1.: Modal parameters detected with the preliminary test

This preliminary test helped for the sectorial band analysis discussed in the next section. In fact, once all the 40 bands have been planned and measured (see section 3.0.3) it is possible to choose first which band analyze. Knowing the location of the modes helps in the choice. Successively also the other bands will be analyzed for the FRF assembly procedure (section 4.4).

4.2. Sectorial Bands PolyMax & Validation

Once all the tool for the post processing of a single band have been developed and explained in chapter 2, it is possible to analyze the results.
The bands taken into study are: $[0\ 40]Hz$, $[120\ 160]Hz$, $[260\ 301]Hz$, $[360\ 400]Hz$ and $[664\ 702]Hz$. For each band two FRFs are computed: the FRF sum from the 10

accelerometers and the FRF sum (indicated as H_{sum} in equation 4.1) of the 2123 points of the DIC reconstructed displacements.

$$H_{\text{sum}} = \sum |\,\text{Re}[H]| + i \sum |\,\text{Im}[H]| \tag{4.1}$$

In addition, another FRF is showed: the integrated FRF of the accelerometers. In fact applying equation 4.2 to the FRF of the accelerometers it is possible to compare the two FRF for the validation.

$$H_{\text{integrated}} = \frac{H_{\text{sumAcc}}}{\omega^2} \tag{4.2}$$

The more the dashed light blue line (i.e. the integrated FRF) is overlapped to the solid blue line (i.e. the reconstructed displacements FRF) the better is the accuracy of the procedure. This means obtaining same FRF data both with accelerometers and with the low-speed cameras plus the reconstruction method. Note that in the following images, the displacements FRF (solid blue line) are all from the interpolation reconstruction method.
For each band the mode shapes in output from PolyMax[1] are also showed. Note that all the modes are computed as complex, and the results found are all real mode shapes. It is possible to appreciate the correct view of the mode shape from the DIC in comparison with the validation of the accelerometers and the advantage of the better discretization of the geometry that DIC does.

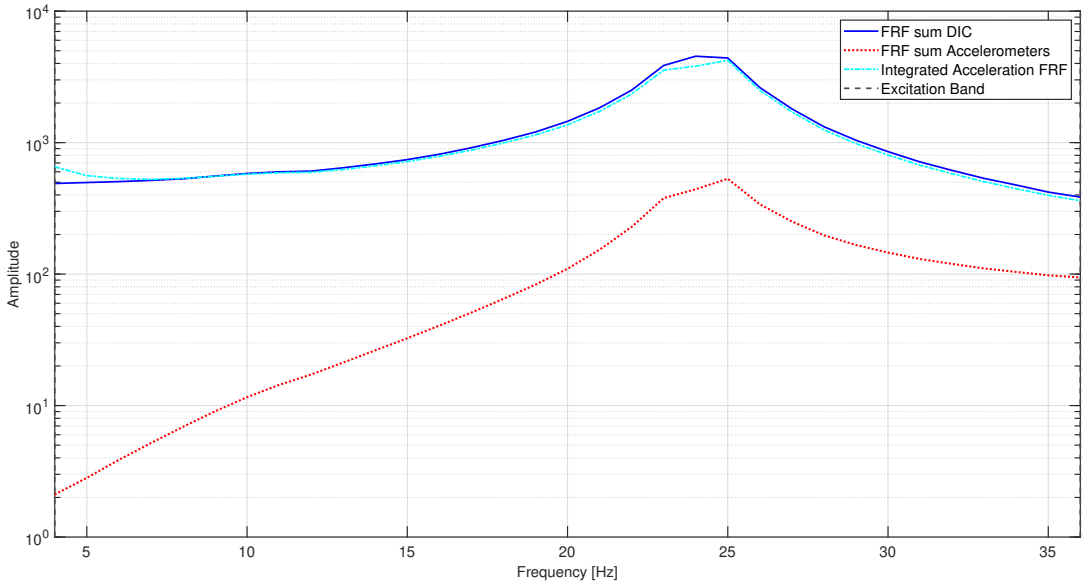

Figure 4.3.: Comparison Sum FRF Reconstructed Displacement and Sum FRF of Measured Acceleration: Band [0 40]Hz; Excitation [4 36]Hz

[1] polyreference least-squares complex frequency-domain method for modal parameters estimation[18]

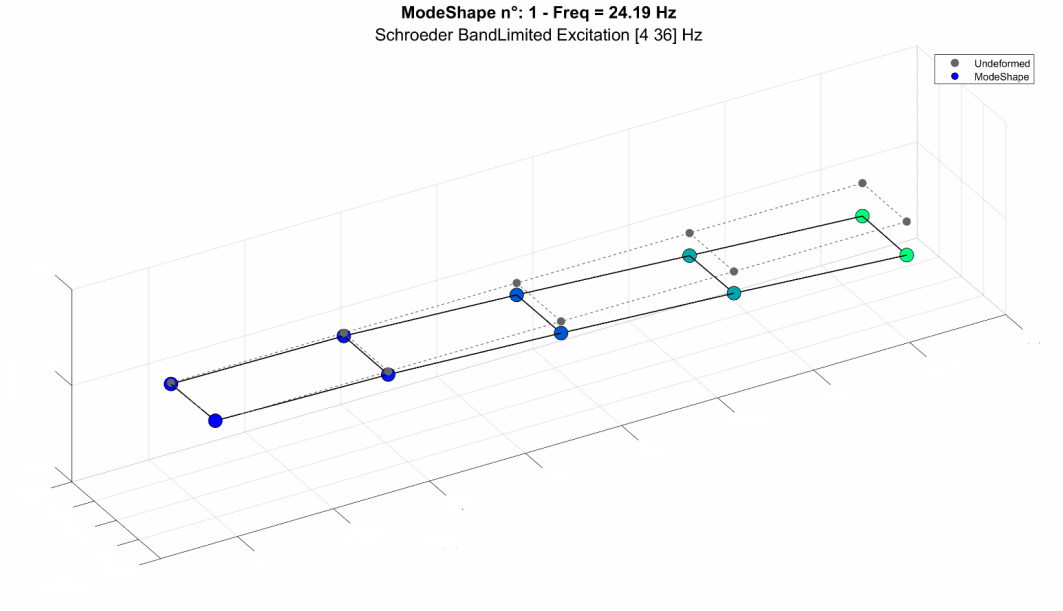

Figure 4.4.: 1^{st} bending computed from the FRF of the 10 accelerometers - Schroeder Excitation $[4\ 36]Hz$

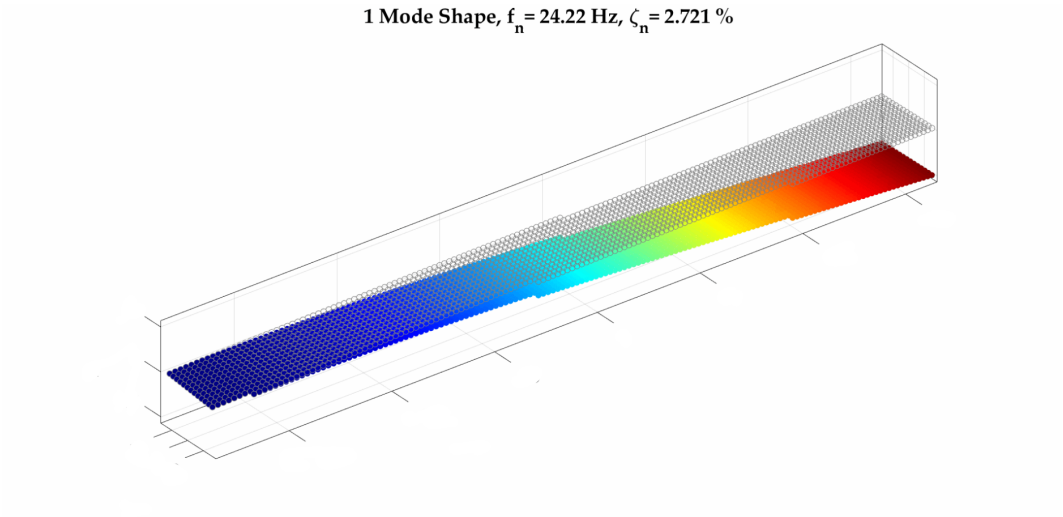

Figure 4.5.: 1^{st} bending computed from the FRF of the DIC reconstructed displacements - Schroeder Excitation $[4\ 36]Hz$

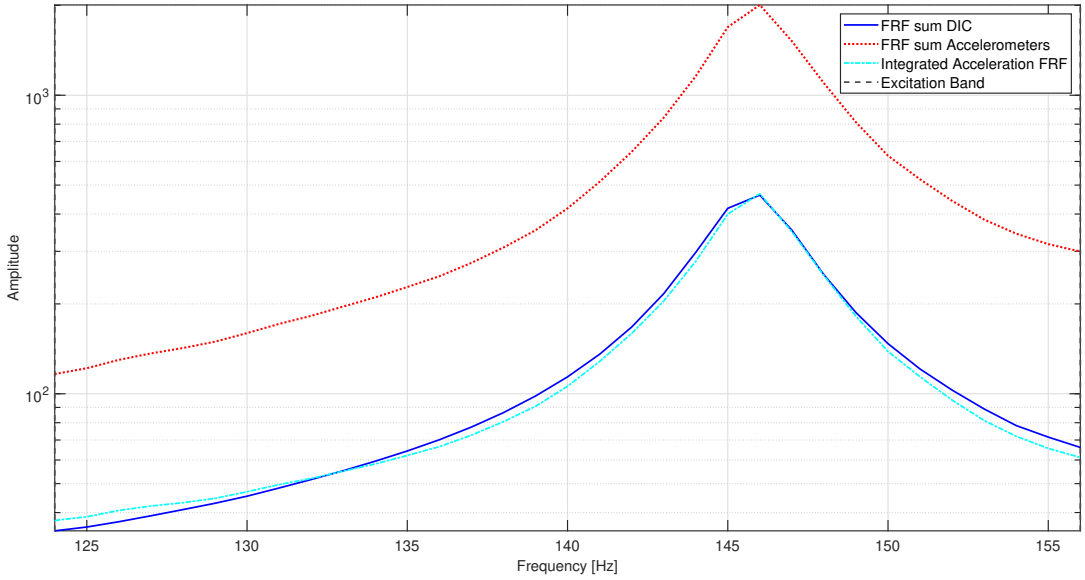

Figure 4.6.: Comparison Sum FRF Reconstructed Displacement and Sum FRF of Measured Acceleration: Band [120 160]Hz; Excitation [124 156]Hz

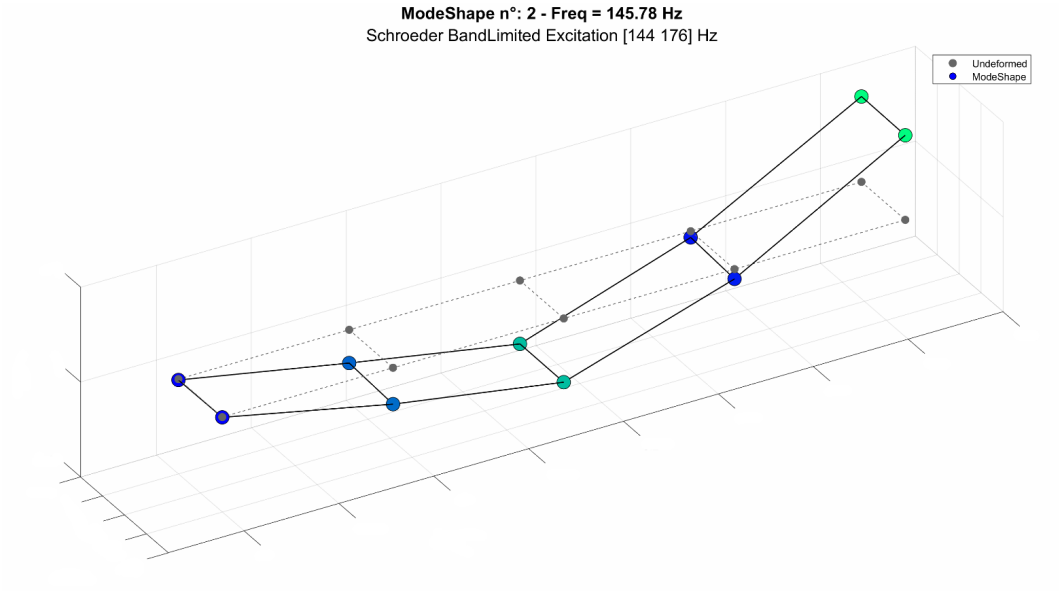

Figure 4.7.: 2^{nd} bending computed from the FRF of the 10 accelerometers - Schroeder Excitation [124 156]Hz

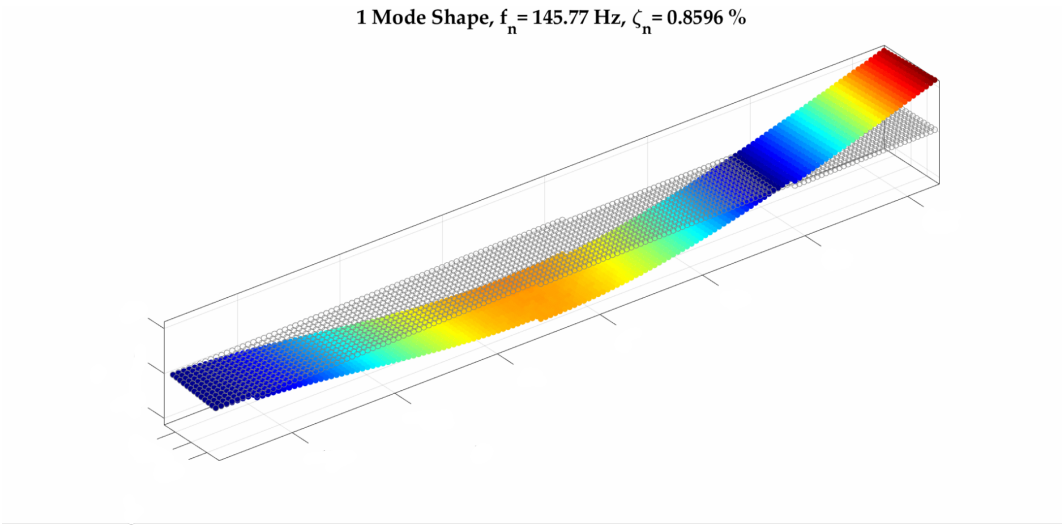

Figure 4.8.: 2^{nd} bending computed from the FRF of the DIC reconstructed displacements - Schroeder Excitation [124 156]Hz

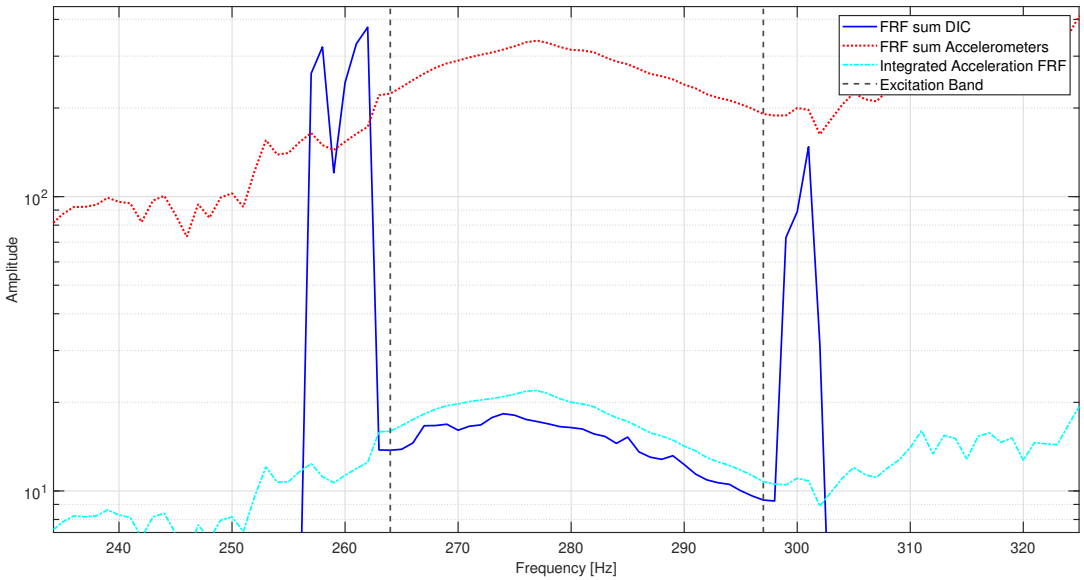

Figure 4.9.: Comparison Sum FRF Reconstructed Displacement and Sum FRF of Measured Acceleration: Band [260 301]Hz; Excitation [264 297]Hz

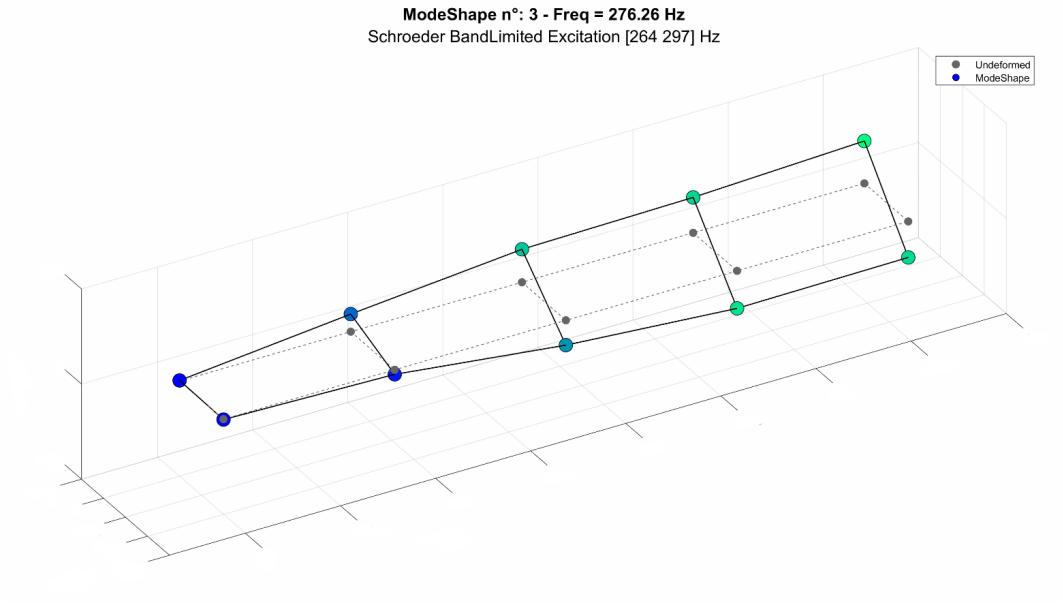

Figure 4.10.: 1^{st} torsional computed from the FRF of the 10 accelerometers - Schroeder Excitation $[264\ 297]Hz$

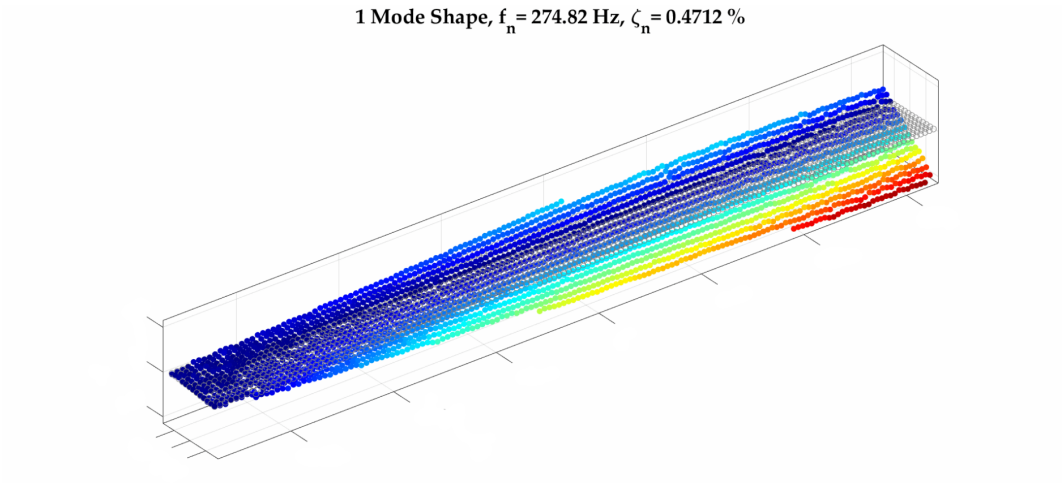

Figure 4.11.: 1^{st} torsional computed from the FRF of the DIC reconstructed displacements - Schroeder Excitation $[264\ 297]Hz$

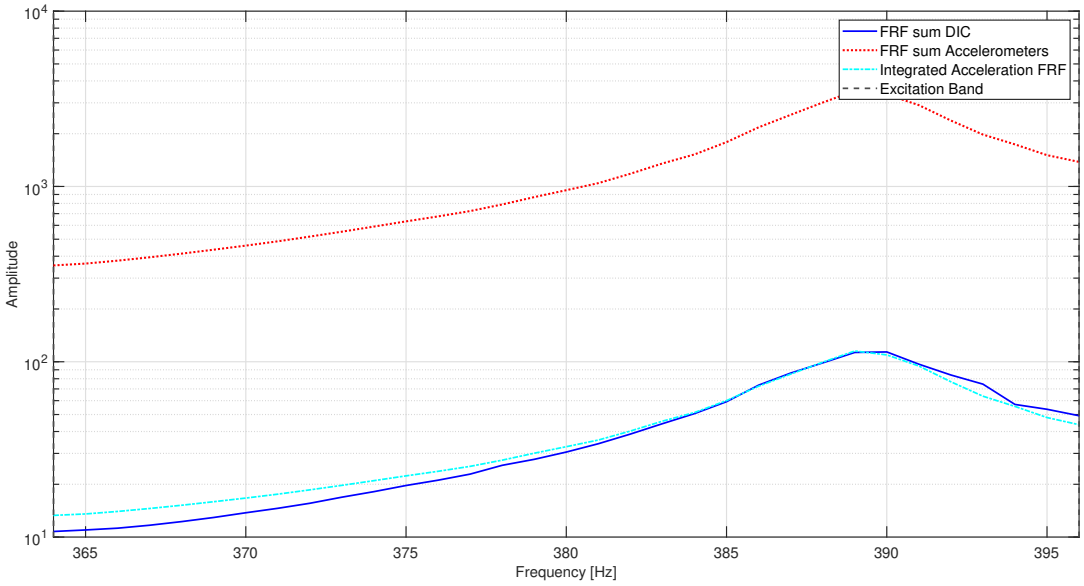

Figure 4.12.: Comparison Sum FRF Reconstructed Displacement and Sum FRF of Measured Acceleration: Band [360 400]Hz; Excitation [364 396]Hz

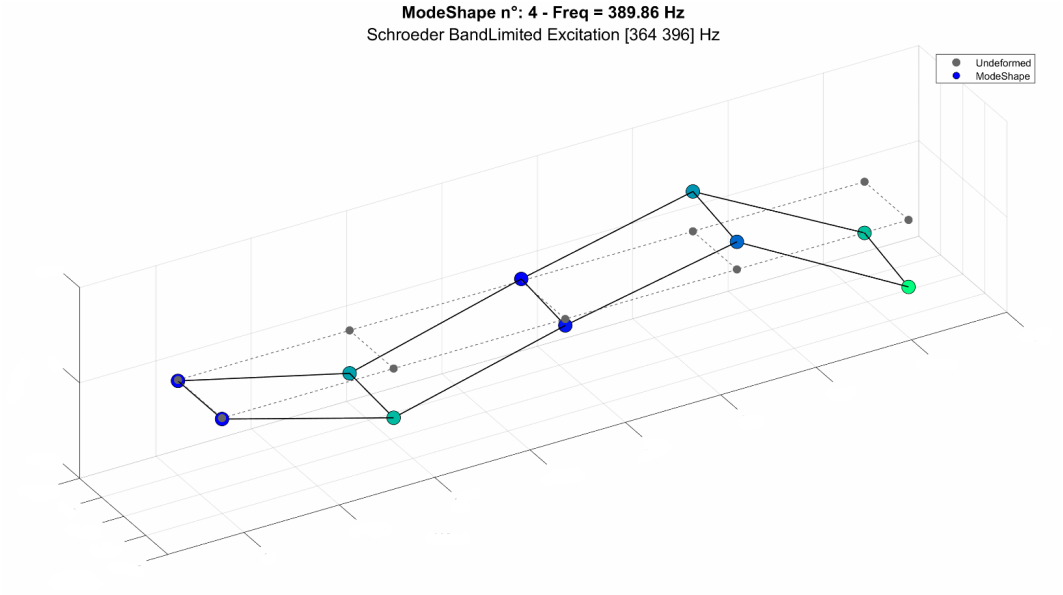

Figure 4.13.: 3^{rd} bending computed from the FRF of the 10 accelerometers - Schroeder Excitation [364 396]Hz

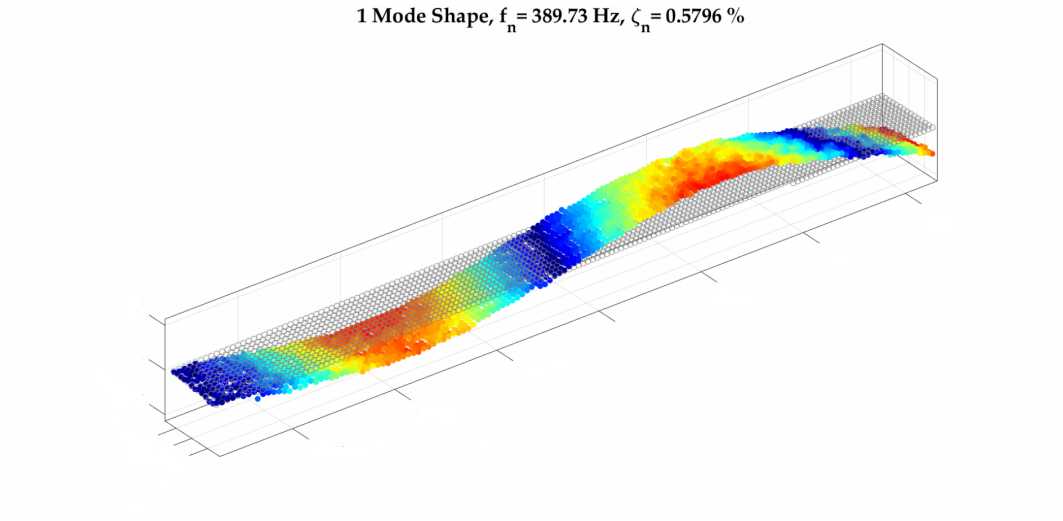

Figure 4.14.: 3^{rd} bending computed from the FRF of the DIC reconstructed displacements - Schroeder Excitation $[364\ 396]Hz$

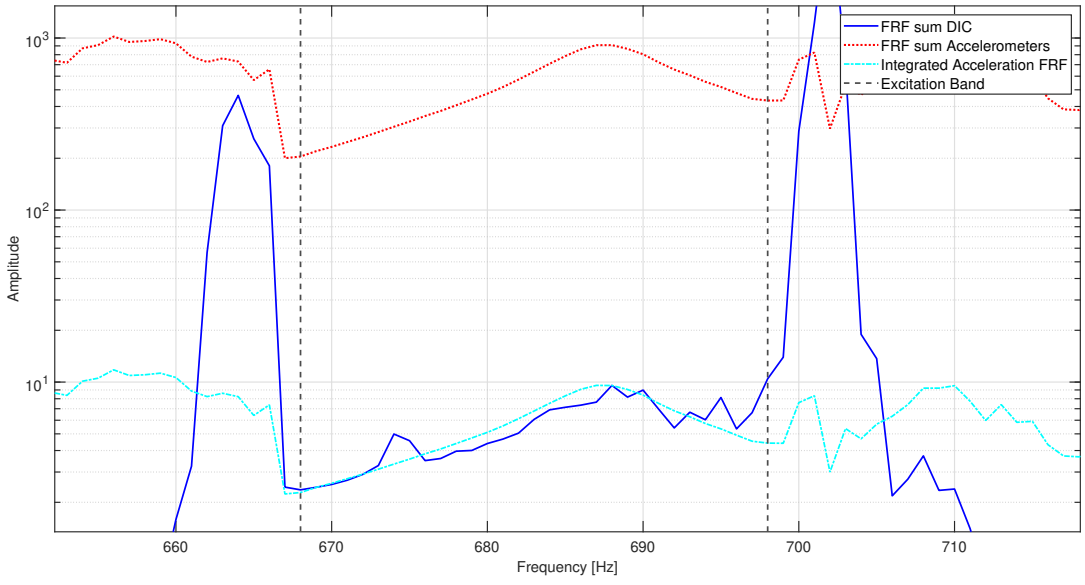

Figure 4.15.: Comparison Sum FRF Reconstructed Displacement and Sum FRF of Measured Acceleration: Band $[664\ 702]Hz$; Excitation $[668\ 698]Hz$

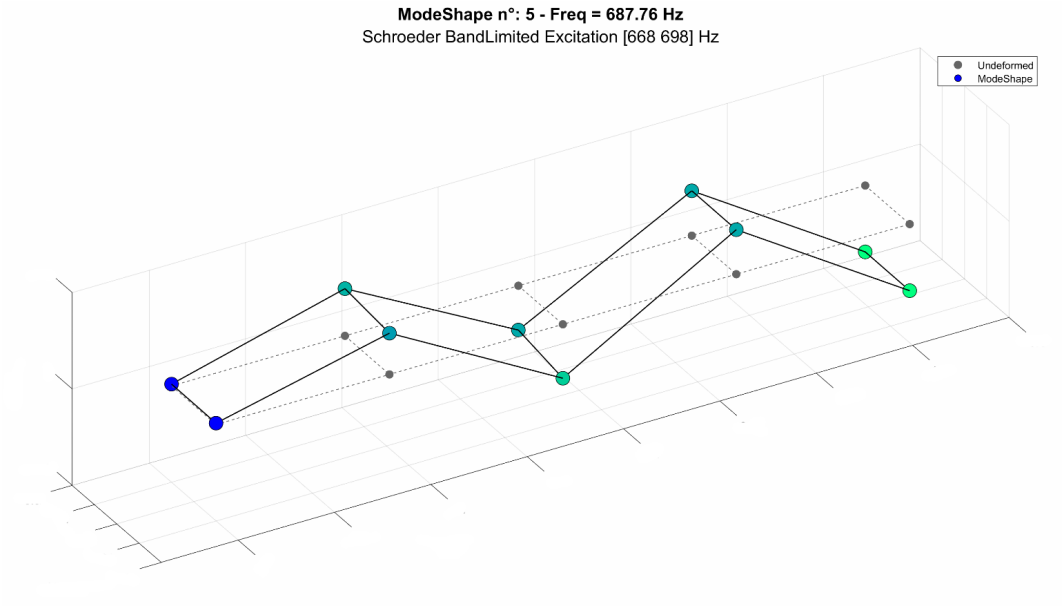

Figure 4.16.: 4^{th} bending computed from the FRF of the 10 accelerometers - Schroeder Excitation $[668\ 698]Hz$

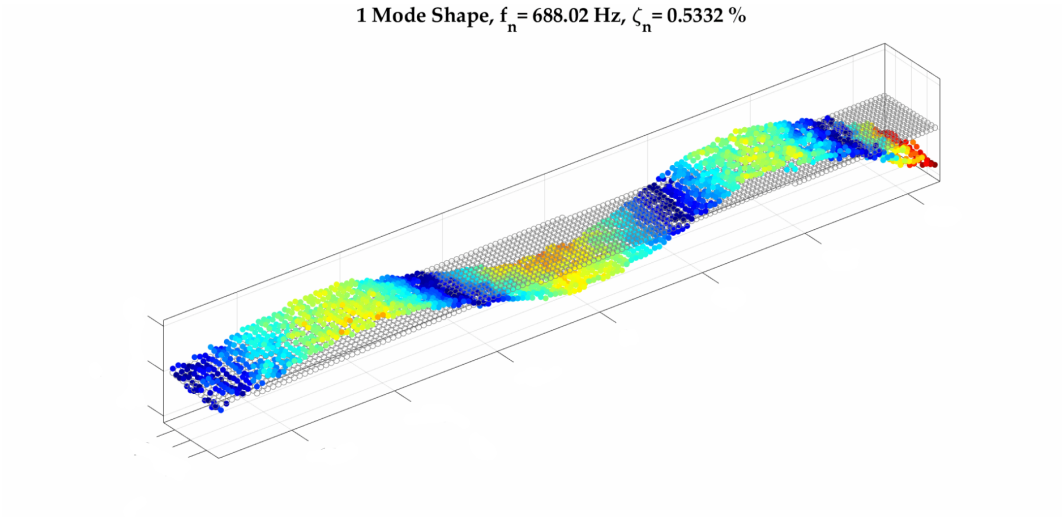

Figure 4.17.: 4^{th} bending computed from the FRF of the DIC reconstructed displacements - Schroeder Excitation $[668\ 698]Hz$

4.3. Noise Floor Evaluation

To get a numerical quantification of the noise floor, some static images of the beam are used. The DIC algorithm is performed on those static images and the standard deviation of the variable of interest "Out of Plane W [mm]" displacements is extracted. Its value is $\sigma \approxeq 0.004$.

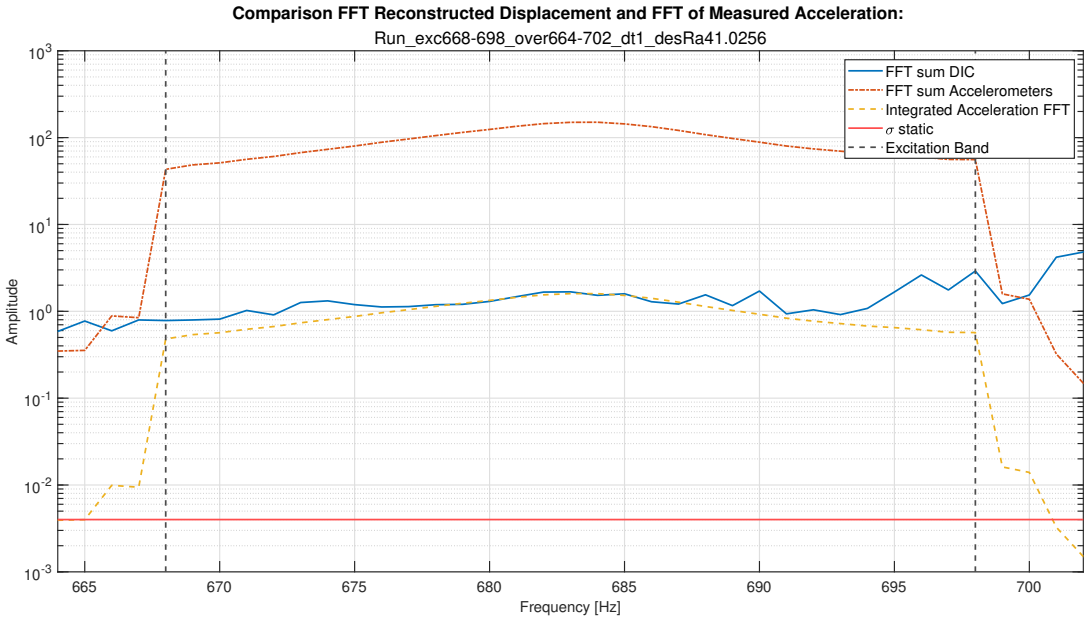

Figure 4.18.: Standard deviation σ level extracted from static image correlation analysis compared to the FFT amplitude of the reconstructed displacements of the band $[664\ 702]Hz$

Figure 4.18 shows the FFT sum of both the 10 accelerometers, its integrated version, and the FFT of the reconstructed displacements. Together with these data there is also the sigma value in amplitude set as an horizontal line. The gap between the FFT of the reconstructed displacements and the standard deviation of the displacements of the static images (i.e. the noise floor estimation) is sufficient to create a displacement readable by the cameras.

Of course performing the same analysis over bands at lower frequencies increases the gap, being the displacement a lower frequencies much more evident by the cameras.

4.4. FRF Bands Assembly

A general dynamic procedure for FRF branches assembly has been developed, the procedure follows these steps:

1. Choose the reconstruction method;
2. Load the FRFs and the Coherences for all the bands;
3. Cut FRF and Coherence according to excitation;
4. Identify overlap zones;
5. Choose best Coherence branch on the overlap zones;
6. Concatenate all branches;

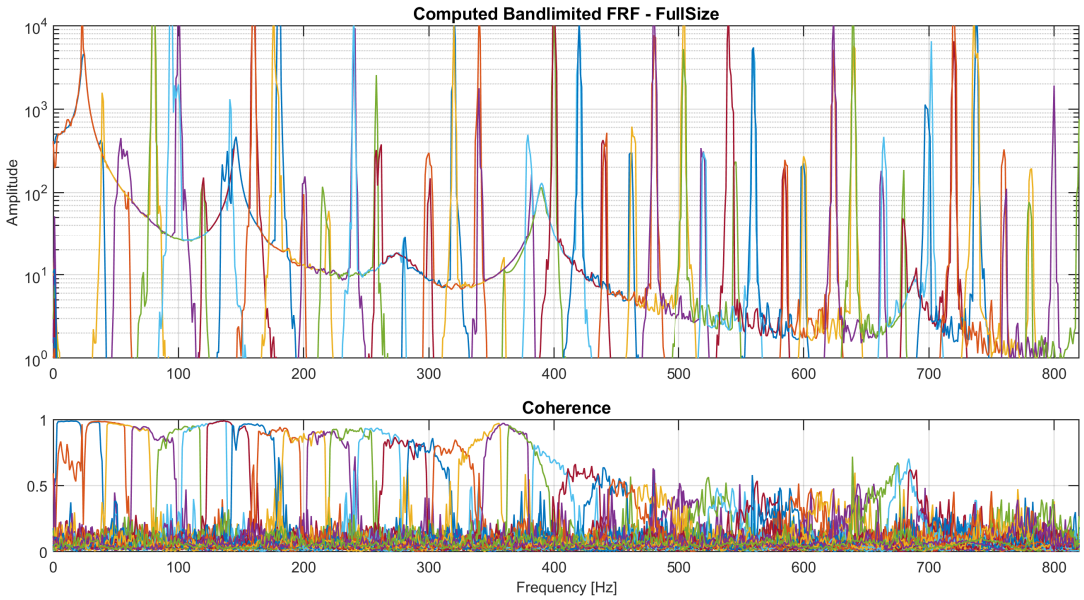

Figure 4.19.: All the FRFs and the Coherences of the chosen bands are loaded

Figure 4.19 is what shows up when loading simultaneously all the FRF and coherence results of the 40 bands. Of course the FRF need to be considered in the excitation band. Once loaded, before passing to the next step, all the FRF need to have the same frequency resolution. This is because after the concatenation a general fixed frequency axis will be defined with a fixed resolution. All the FRF branches should be referred to this fixed frequency axis. The developed assembly algorithm counts the occurrences of how many different frequency axis there are in the loaded bands data. The fixed resolution will be the one that the majority of the bands have. The bands with a different frequency resolution (i.e. a different acquisition time) are equalized over the fixed resolution. This happens via an interpolation of the "old" FRF data over the new frequency axis. The same procedure needs to be applied to

the coherence too.

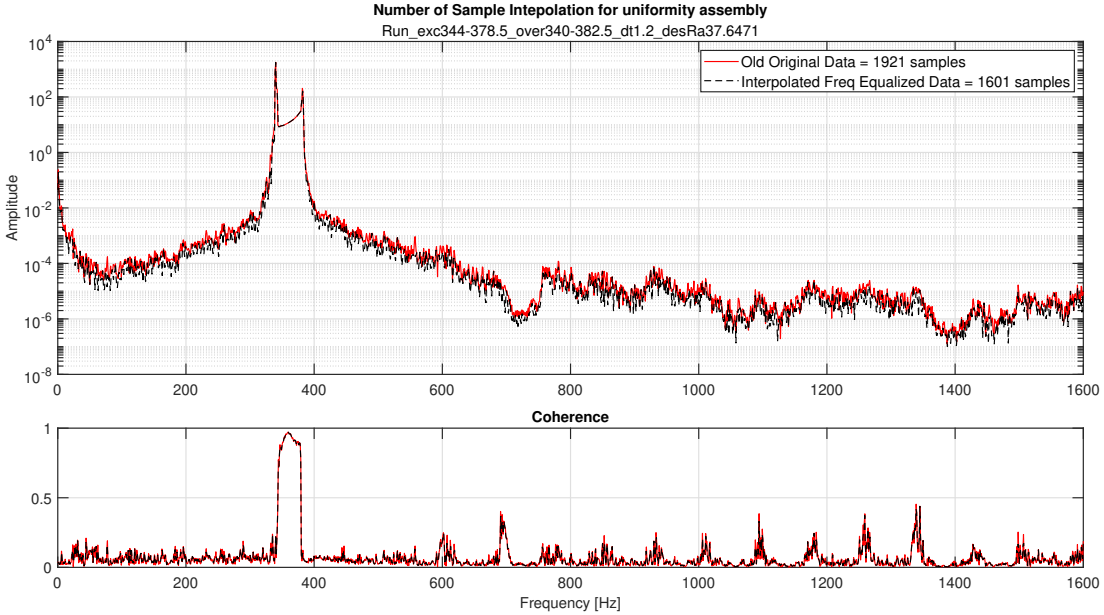

Figure 4.20.: Manage frequency resolution equalization of Band [340 382.5]Hz

Figure 4.20 shows the interpolation results of the FRF data of the band [340 382.5]Hz. In the case study planned as discussed in section 3.0.3 there are only 2 cases that need the frequency resolution equalization bands [300 340]Hz and [340 382.5]Hz that have an acquisition time of 1.2s with respect to all the others 38 bands that have been set with an acquisition time of 1s (i.e. 1 Hz resolution).

Figure 4.21 is the result obtained selecting the specific FRF branches for each band only in the excitation range, basically "cleaning" the previous plot in figure 4.19. In Figure 4.21 it is also showed the phase of the FRF. The phase trend shows phase inversion in correspondence of the resonance peaks. On the other hand the phase not always bounds smoothly like the amplitude (e.g. at 50 Hz, 200 Hz, 370 Hz). This phenomena has been investigated during the study using several approaches to understand it. Firstly this phase behaviour it is visible with both the reconstruction methods (possible exclusion of the reason being the reconstruction process). Secondly, the analysis has been conducted using as the reference image in the DIC algorithm the first deformed image of the stack and also, in a separate study, using a static image as the reference and removing the last deformed image, in both cases the results are the same. Of course the not perfectly continuous trend of the phase may influence the PolyMax computation, results are discussed in section 4.4.2. The reason of a not perfect bounding in phase it is still uncertain, and further investigations are needed.

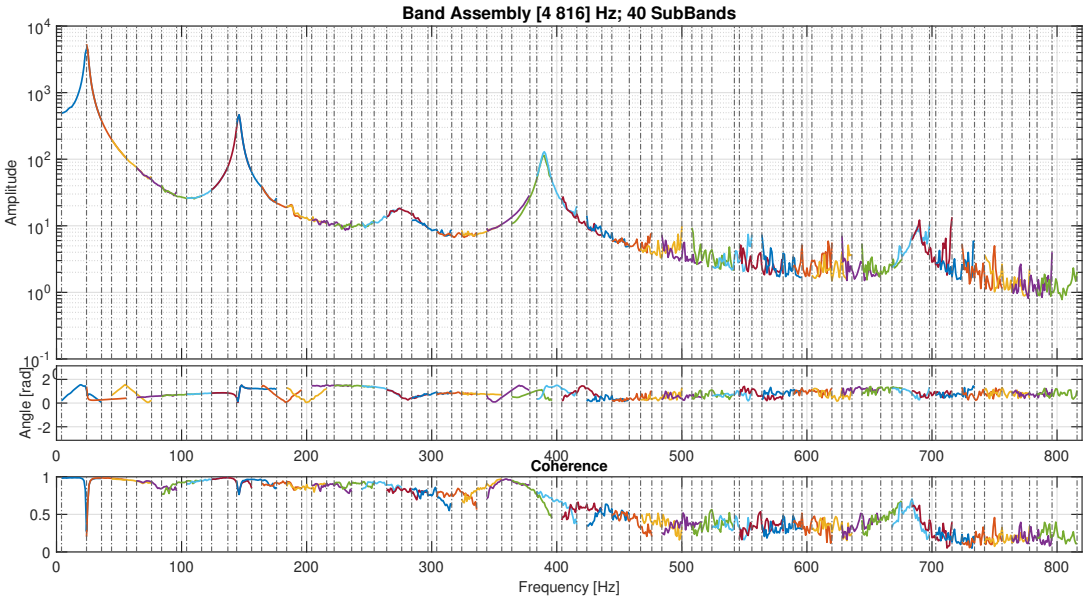

Figure 4.21.: Every FRF and Coh are considered only in the excitation frequency range (delimited by the dashed black vertical lines)

Additionally the global phase trend going up-hill can indicate a not perfect synchrony between the force and the response. Coherence drops at higher frequencies, there the FRF both in amplitude and in phase is noisy.

To define which FRF branch will be chosen for the final concatenation, the coherence is used as a key factor. Indeed, once the overlap zones are identified by the script, the average coherence value for each branch in the overlap zone is computed. The chosen FRF branch will be the one with the highest average coherence value in the zone. The final FRF obtained is a complex double matrix dataset, that can be post-processed in PolyMax to perform modal analysis. Figure 4.22 shows the results of the concatenation.

4.4.1. Comparison and Validation with preliminary test FRF

A very good comparison is the one showed in figures 4.23 and 4.24. The blue dotted FRF is the first FRF measured with only accelerometers during the preliminary test discussed in section 4.1. This FRF is expressed in acceleration over force. If the double integration (see equation 4.2) is performed (moving towards displacements over force), the black dotted line is obtained. The integrated FRF matches accurately the FRF obtained with the reconstruction process. Noise is observed at higher frequencies, this can be due to some noise in the cameras or to a non completely accurate time-step provided by the cameras.

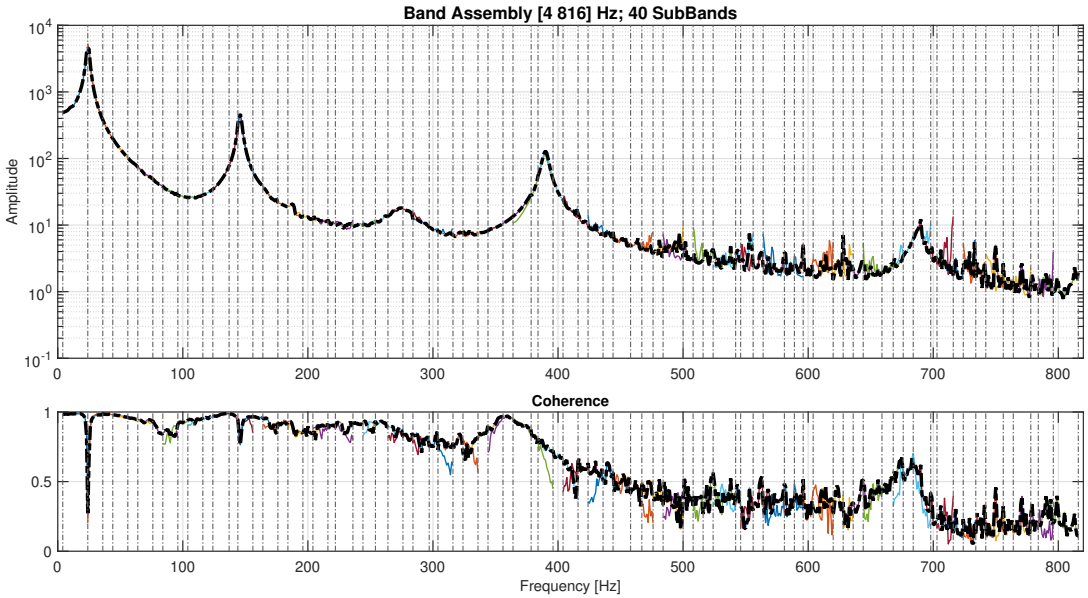

Figure 4.22.: The chosen branches are concatenated choosing the best coherence branch in the overlap zones

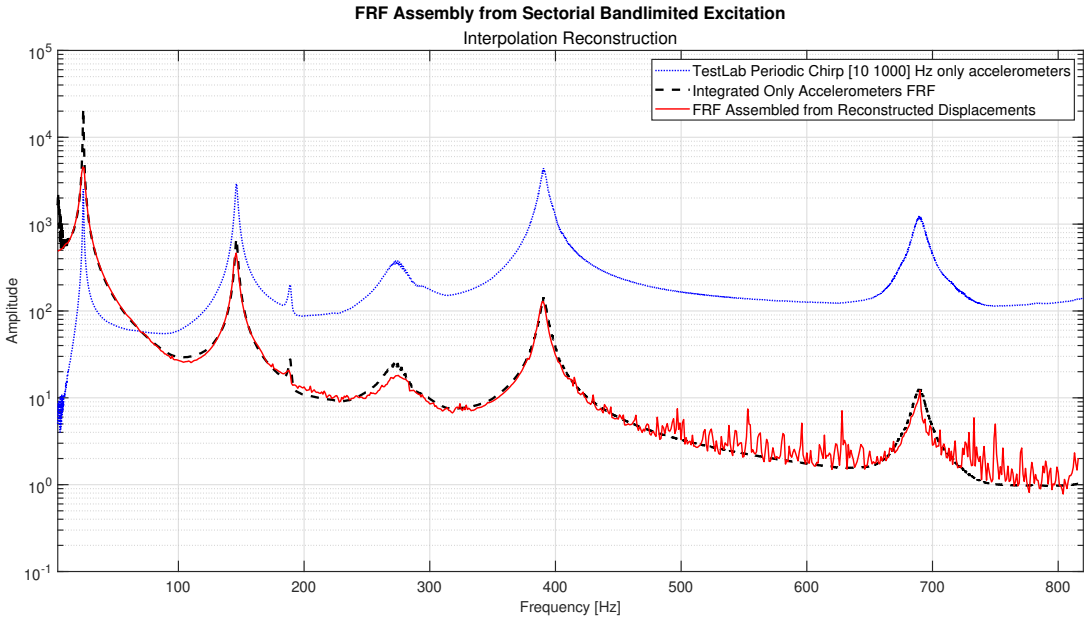

Figure 4.23.: FRF Assembly from Sectorial Bandlimited Excitation - Interpolation Reconstruction

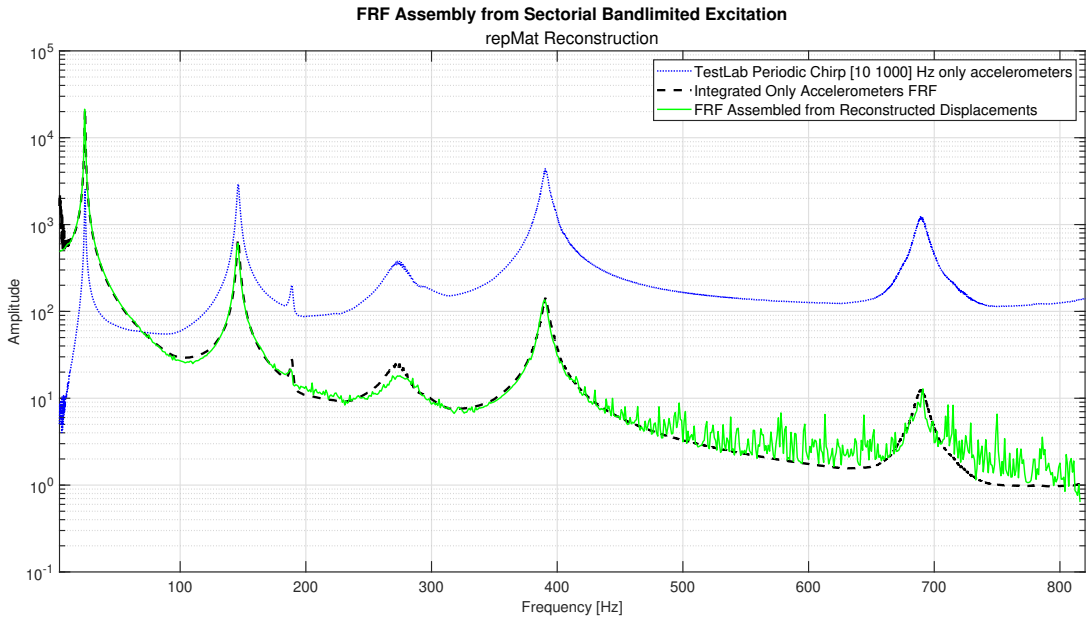

Figure 4.24.: FRF Assembly from Sectorial Bandlimited Excitation - repMat Reconstruction

4.4.2. PolyMax Plus Computation

The final FRF can be studied entirely with PolyMax, in this case, its "Plus" version available on TestLab is used. Figure 4.25 is the stabilization diagram obtained. The algorithm stabilize correctly the first four modes with an order of 50. The last mode is stabilized only increasing the order of PolyMax or sectorializing the analysis on a subset of the entire band $[4\ 816]Hz$ for example $[600\ 816]Hz$. In the first case the mode shape is visible with also a rigid mode component, see figure 4.30. In the second case it is visualized correctly, see figure 4.31.

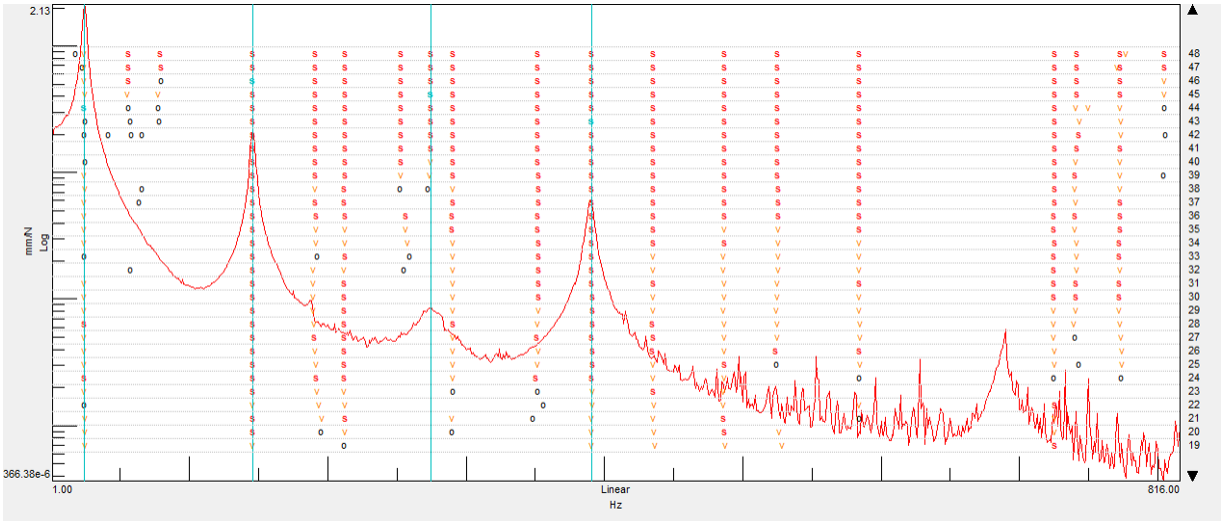

Figure 4.25.: Stabilization Diagram of the assembled FRF

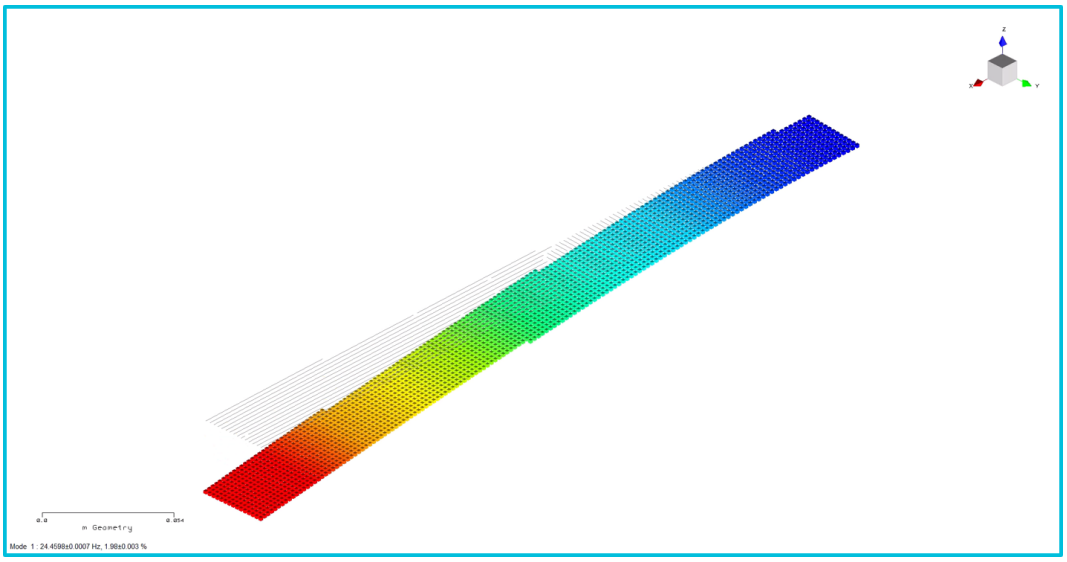

Figure 4.26.: 1^{st} bending computed from the assembled FRF of the DIC reconstructed displacements

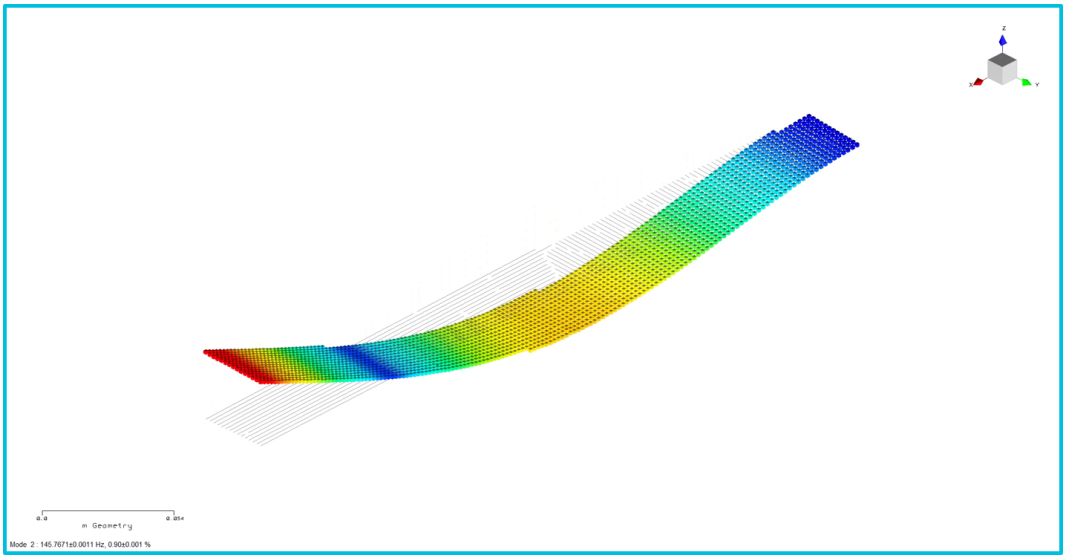

Figure 4.27.: 2^{nd} bending computed from the assembled FRF of the DIC reconstructed displacements

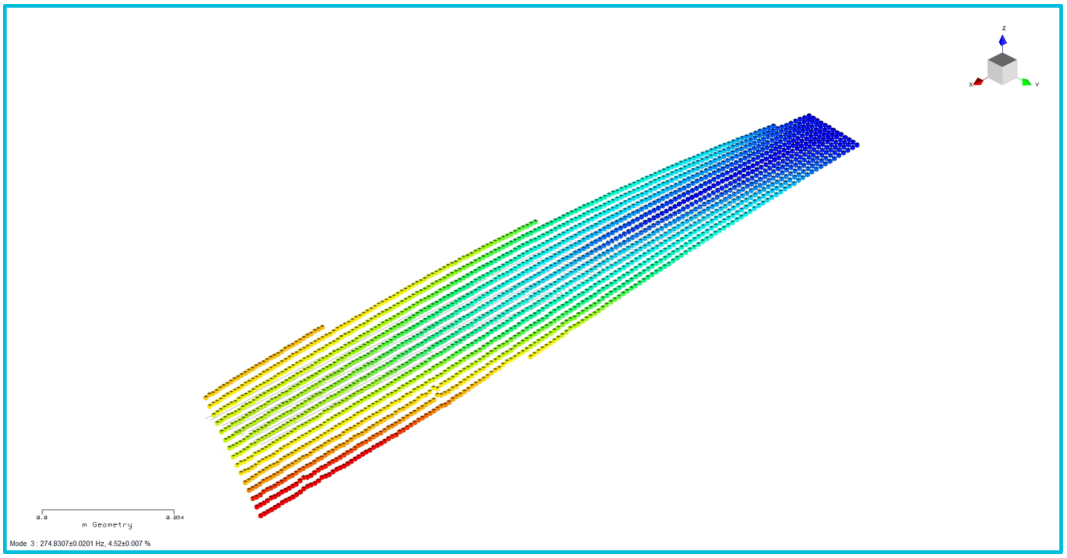

Figure 4.28.: 1^{st} torsional computed from the assembled FRF of the DIC reconstructed displacements

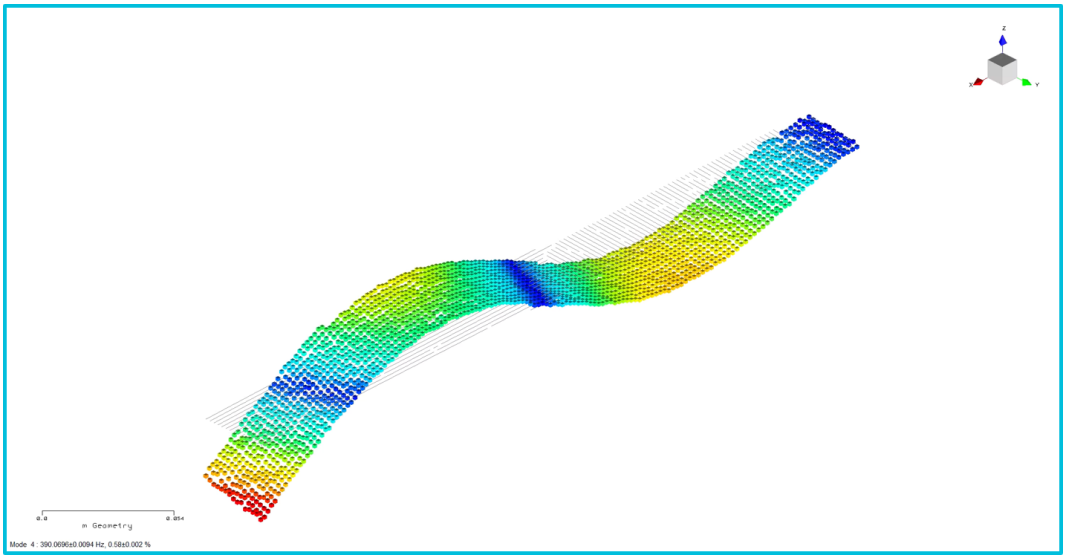

Figure 4.29.: 3^{rd} bending computed from the assembled FRF of the DIC reconstructed displacements

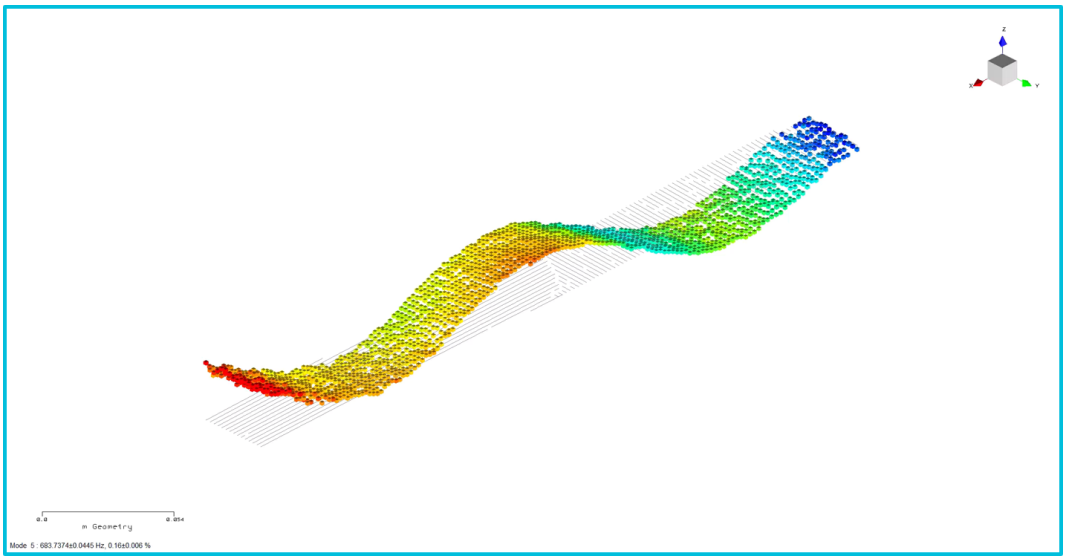

Figure 4.30.: 4^{th} bending computed from the assembled FRF of the DIC reconstructed displacements - PolyMax Order $\approx$ 200

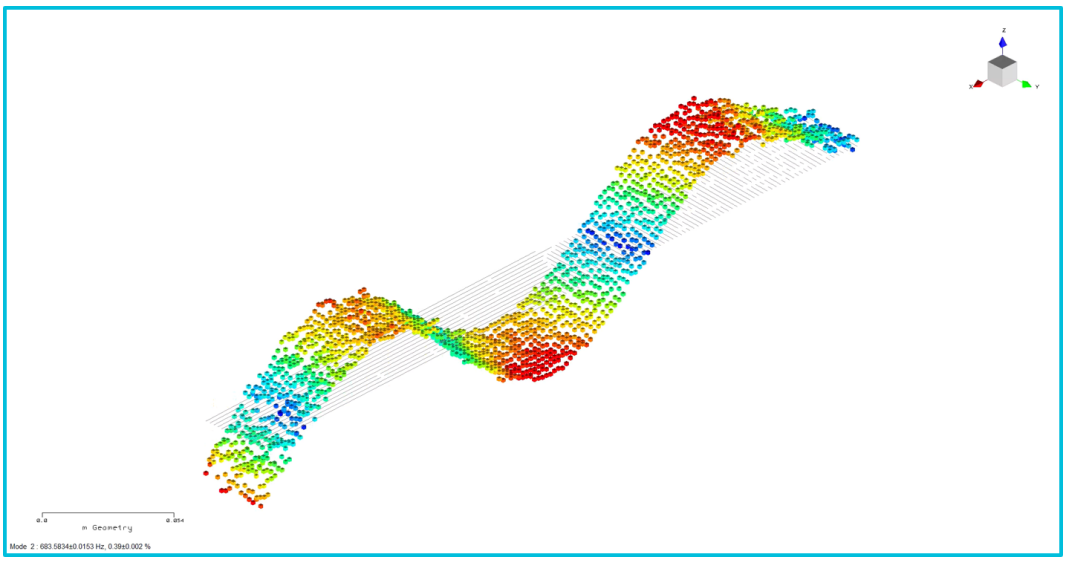

Figure 4.31.: 4^{th} bending computed from the assembled FRF of the DIC reconstructed displacements - Band analyzed [600 816]Hz

Chapter 5.

Conclusions

In conclusion, this study lead to a in depth analysis over the implementation and the development of reconstruction algorithms for down-sampled displacements computed via Digital Image Correlation for vibration measurements. They allowed to measure at high frequencies using low-speed cameras and having higher resolution.

5.1. Summary of Results

Here a summary of the main objectives achieved with this thesis work:

- Two different reconstruction algorithms have been studied and numerically validated (using also numerical estimation) over simple signals and over simulated Multi DOF system;
- The developed set up algorithms for the measuring parameters allowed a smooth and efficient data management and measurement set up;
- The algorithms have been applied on an experimental case, validation using piezo-accelerometers has been performed;
- A dynamic and parametric FRF assembly software algorithm has been developed to perform modal analysis after data collection of the band-limited runs;
- PolyMax Plus analysis showed good results and correct mode shape visualization in comparison with the accelerometers;

5.2. Future Works

The post-processing time needs improvements, especially in terms of script interaction: a systematic and iterative script development can be investigated in the future to compact the post-processing activity with an eye on future company software developments. The noise at higher frequencies remains an issue, high-speed cameras validation can indeed be performed to investigate together with further validation over more complex structures. Generally the activity showed significant results capturing almost full dynamics of a structure using low-speed cameras, no contact-cabled sensors, and having smaller dataset size, going beyond the Nyquist theorem.

Appendix A.

Compressed Sensing reconstruction

This appendix illustrates a practical implementation of Compressed Sensing for a PseudoRandom/Schroeder signal. The algorithm is first explained in detail and finally, practical numerical results are shown.
The analysis has been conducted over the study published on Matworks [19], and mathematically analyzed providing a summary of the solution for the l_1 minimization via convex programming of [20].

A.1. Theory on Compressed Sensing

Compressed sensing (also known as compressive sensing, compressive sampling, or sparse sampling) is a technique to recover a signal starting from some of its random samples. In the following section the theory summarized by Cleve Moler in [19] is reported for a better understanding of the test showed in section **??**.

A.1.1. Computational Problem Formulation

A raw signal can be regarded as a vector $\boldsymbol{f}$ with millions of components. We assume that $\boldsymbol{f}$ can be expressed as a linear combination of basis function.

$$\boldsymbol{f} = \boldsymbol{\Psi c} \tag{A.1}$$

Where $\boldsymbol{\Psi}$ is the discrete cosine transform application, and $\mathbf{c}$, the coefficients vector. It is sparse, i.e. most of the $\mathbf{c}$ coefficients are effectively zero.
A discrete cosine transform (DCT) expresses a finite sequence of data points in terms of a sum of cosine functions oscillating at different frequencies (there are multiples math formulations).

Sampling the signal involves the operator Φ which is a subset of the rows of the identity operator:

$$b = \Phi f \tag{A.2}$$

Where, as a consequence, b represents a few random samples of the original signal f. The signal reconstruction consist in recovering $\boldsymbol{c}$ solving:

$$\boldsymbol{Ax} = \boldsymbol{b} \tag{A.3}$$

Where:

$$\boldsymbol{A} = \boldsymbol{\Phi\Psi} \tag{A.4}$$

It is possible then to recover the signal itself by computing:

$$\boldsymbol{f} \approx \boldsymbol{\Psi x} \tag{A.5}$$

A is a rectangular matrix (Φ is rectangular), therefore the system is underdetermined, i.e. there are many more unknowns than equations.
To solve the problem we impose a non-linear regularization involving the l_1 norm.

A.1.2. Concept of "Regularization"

A very intuitive and clear example to understand the concept of what is a regularization is the famous "World's Simplest Impossible Problem" [21] by Cleve's Corner. The question states: *"If the average of two numbers is three, what are the numbers?"*.

The solution to this problem is not unique, and the problem is ill-defined.
"2 and 4" is one of the most common answer, but by answering in this way means imposing a kind of regularization that requires the result to be two distinct integers.
This problem is a 1-by-2 system with: $A = [1/2\ 1/2]$ and $b = 3$.
MatLab can answer in these ways:

- $y = pinv(A) \times b \rightarrow y = \{3, 3\}$ (minimum norm least squares);
- $x = A \backslash b \rightarrow x = \{6, 0\}$ ("sparse" solution);

A.1.3. Final Problem

A larger instance of the same task is the signal reconstruction procedure. Being the problem underdetermined, there is a huge number of possible solutions, to pick the right ones we need to use the vector norms.
These are 3 different "Non-Linear" regularization.

$$\begin{aligned} \text{norm}(x, 2) &= \sqrt{\sum_i x_i^2} \quad \text{"Euclidean" norm } l_2 \\ \text{norm}(x, 1) &= \sum_i |x_i| \quad \text{"Manhattan" norm } \boldsymbol{l_1} \\ \text{norm}(x, 0) &= \sum_i (x_i \neq 0) \quad \boldsymbol{l_0} \text{ norm} \end{aligned} \tag{A.6}$$

The two fundamental keys to apply compressed sensing are sparsity and the l_1 norm. Practically the objective is to exploit the sparsity of the c vector to then use the l_0 regularization, counting non-zeros items. But this problem has impractical computational complexity.

As a matter of fact, studies, such as the ones of David Donoho, Emmanuel Candés, and Terence Tao shows that l_0 can be replaced by l_1, and that with high probability the two problems have the same solutions.
The l_1 is practical because it can be solved as a linear programming problem. The comptutation and math behind the solution of a primal dual algorithm fo the linear programming problem is presented in [20]. Figure A.1 shows a synthetical diagram of the working principle of the compressed sensing reconstruction. It is also showed where an ideal experimental approach may start, i.e. when the random sampling operation is firstly performed.

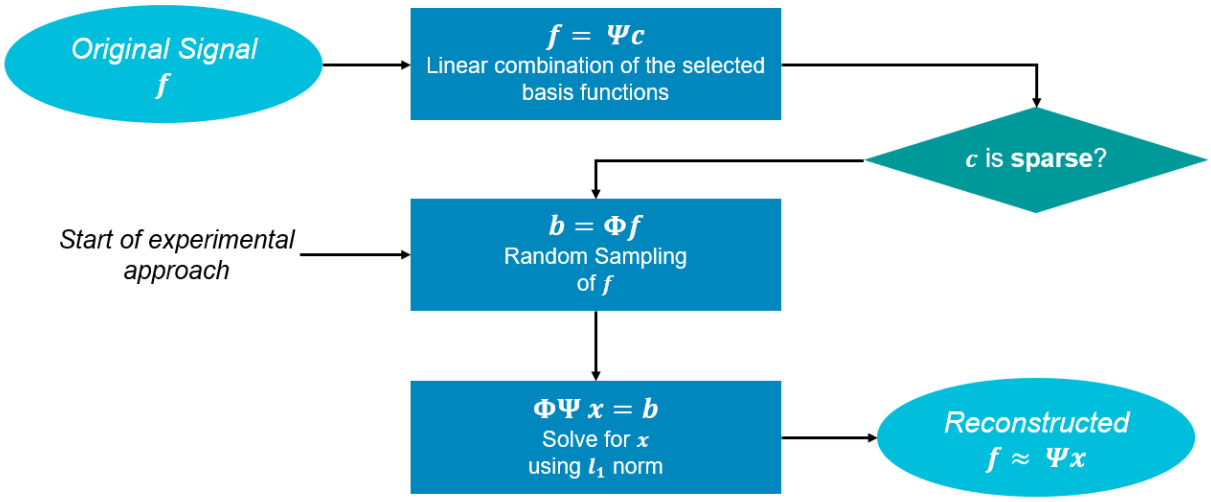

Figure A.1.: Schematic procedure of compressed sensing

A.1.4. Script Implementation Case

Following the theory of the previous sections the following procedure has been adopted:

i Generation of the signal (in this case a pseudorandom schroeder signal with excitation band $[30\ 50]Hz$);

ii Define compressed sensing parameters (a scaling factor for random selection; the number of iteration for the l_1 calculation)

iii Generate the random samples of the signal as showed in figure A.2;

iv Build the A matrix as in equation A.4;

v Compute l_1 solution of the Primal Dual algorithm [20], figure A.3 shows how the cumulative value of l_1 tends to be minimized with the increasing of the iterations;

vi Reconstruction validation (elaborate TRAC index with original signal) as showed in figure A.4.

In conclusions compressed sensing can be a nice approach to reconstruct signals with a shorter number of samples in comparison with the original signal.

One main constraint is that the scaling factor can not be too much big, i.e. the number of samples reduction advantage needs to be taken into consideration. Pseudorandom signals, such as Schroeder and Pseudorandom performs very well for the developed script implementation.

Future steps can be, trying to optimize the procedure finding a good combination of the starting parameters to have the maximum possible scaling factor gain over the numerical random sampling simulation. Practical tests and validation can be performed.

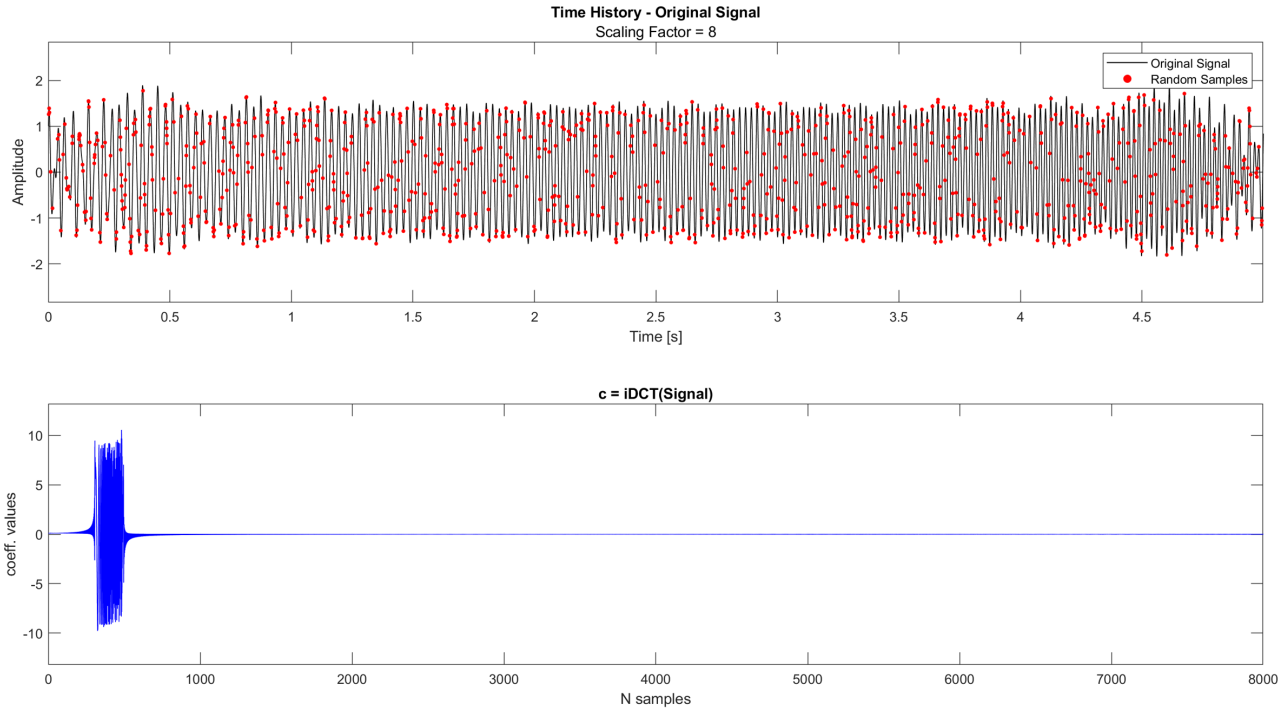

Figure A.2.: Compressed Sensing - Setup: Original samples = 8000; Random samples = 1000; Scaling factor = 8

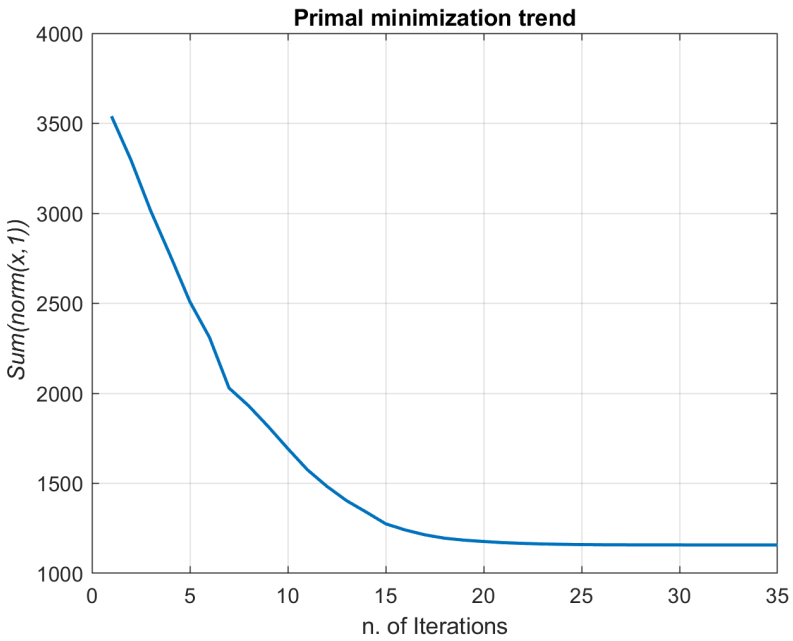

Figure A.3.: Primal minimization trend - Cumulative value of l_1 norm

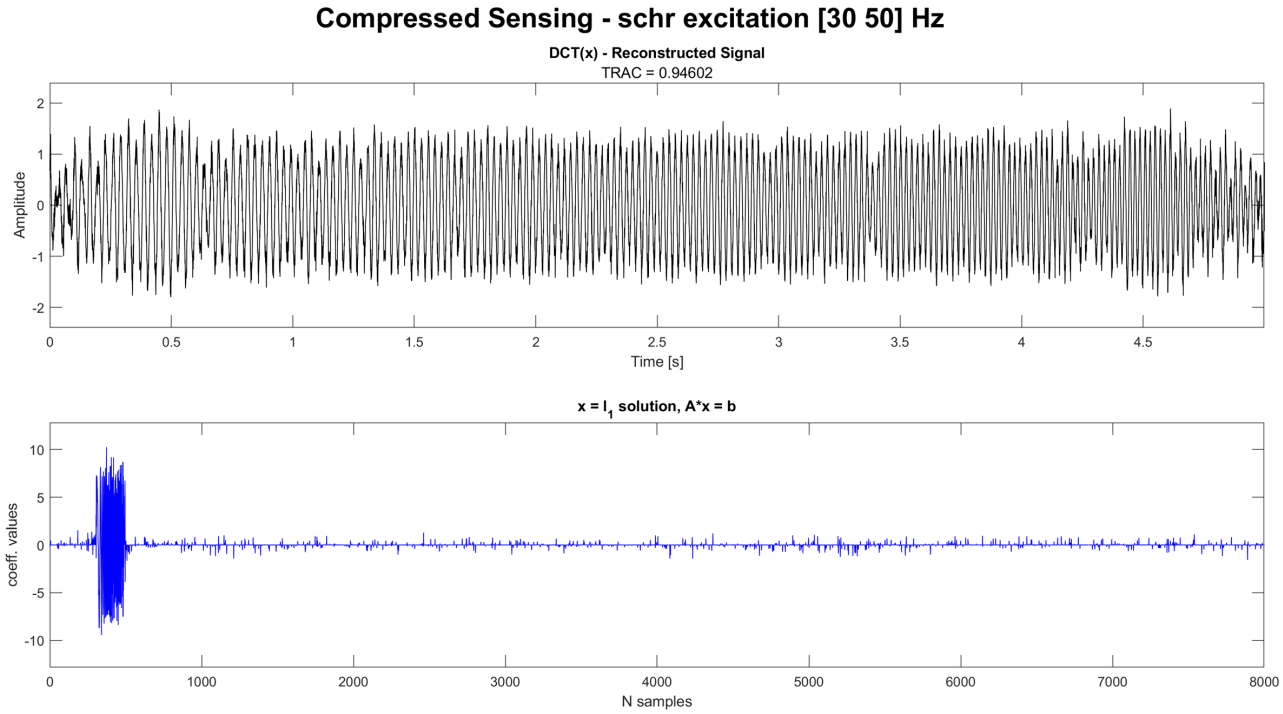

Figure A.4.: Reconstructed signal as the DTC of the solution of equation A.3

Bibliography

[1] Paolo Neri. Frequency-band down-sampled stereo-DIC: Beyond the limitation of single frequency excitation. *Mechanical Systems and Signal Processing*, 172:108980, June 2022.

[2] John G. Proakis and Dimitris G. Manolakis. *Digital signal processing: principles, algorithms, and applications*. Prentice Hall, Upper Saddle River, N.J, 3rd ed edition, 1996.

[3] Siemens Digital Industry Software NV. Digital Image Correlation: Camera Considerations.

[4] Bart Peeters, Wim Hendricx, Jan Debille, and Hector Climent. Modern solutions for ground vibration testing of large aircraft. *Sound and vibration*, 43(1):8, 2009.

[5] Tech Nexion. What is a High Frame Rate Camera? What are the Factors Affecting Frame Rate?

[6] Yonggang Wang, Felix Simeon Egner, Thijs Willems, Matteo Kirchner, and Wim Desmet. Camera-based experimental modal analysis with impact excitation: Reaching high frequencies thanks to one accelerometer and random sampling in time. *Mechanical Systems and Signal Processing*, 170:108879, 2022.

[7] Yongchao Yang, Charles Dorn, Tyler Mancini, Zachary Talken, Satish Nagarajaiah, Garrett Kenyon, Charles Farrar, and David Mascareñas. Blind identification of full-field vibration modes of output-only structures from uniformly-sampled, possibly temporally-aliased (sub-nyquist), video measurements. *Journal of Sound and Vibration*, 390:232–256, 2017.

[8] Jaka Javh, Janko Slavič, and Miha Boltežar. Experimental modal analysis on full-field dslr camera footage using spectral optical flow imaging. *Journal of Sound and Vibration*, 434:213–220, 2018.

[9] E Di Lorenzo, P Lava, R Balcaen, S Manzato, and B Peeters. Full-field modal analysis using high-speed 3d digital image correlation. In *Journal of Physics: Conference Series*, volume 1149, page 012007. IOP Publishing, 2018.

[10] Marcos Tan Endo, Arlindo Neto Montagnoli, and Rodrigo Nicoletti. Measurement of shaft orbits with photographic images and sub-sampling technique. *Experimental Mechanics*, 55:471–481, 2015.

[11] Sandro Barone, Paolo Neri, Alessandro Paoli, and Armando Viviano Razionale. Low-frame-rate single camera system for 3d full-field high-frequency vibration measurements. *Mechanical Systems and Signal Processing*, 123:143–152, 2019.

[12] Sandro Barone, Paolo Neri, Alessandro Paoli, Armando V Razionale, Leonardo Bertini, and Ciro Santus. Optical stereo-system for full-field high-frequency 3d vibration measurements based on low-frame-rate cameras. In *Design Tools and Methods in Industrial Engineering: Proceedings of the International Conference on Design Tools and Methods in Industrial Engineering, ADM 2019, September 9–10, 2019, Modena, Italy*, pages 155–164. Springer, 2020.

[13] Yihao Liu, Hongjian Gao, James Zhuge, and Jeff Zhao. Research of undersampling technique for digital image correlation in vibration measurement. In *Shock & Vibration, Aircraft/Aerospace, Energy Harvesting, Acoustics & Optics, Volume 9: Proceedings of the 35th IMAC, A Conference and Exposition on Structural Dynamics 2017*, pages 49–58. Springer, 2017.

[14] J Javh, M Brumat, J Slavic, and M Boltezar. A high-speed camera measurement set-up for deflection shape analysis. *Proceeding of ISMA2016-USD2016*, pages 1043–1050, 2016.

[15] Paolo Neri, Alessandro Paoli, Ciro Santus, et al. Bandpass high frequency blisk vibration measurements by down-sampled stereo-dic acquisitions. In *Proceedings of ISMA2022 International Conference on Noise and Vibration Engineering*, pages 2892–2903, 2022.

[16] Peter Avitabile and Pawan Pingle. Prediction of Full Field Dynamic Strain from Limited Sets of Measured Data. *Shock and Vibration*, 19(5):765–785, 2012.

[17] P. Sas, W. Heylen, S. Lammens, and Katholieke Universiteit Leuven Faculteit der Toegepaste Wetenschappen Departement Werktuigkunde Afdeling Toegepaste Mechanica en Energieconversie. *Modal Analysis: Theory and Testing*. Katholieke Universiteit Leuven. Faculty of Applied Sciences. Mechanical Engineering Department, 1997.

[18] Bart Peeters, Herman Van Der Auweraer, Patrick Guillaume, and Jan Leuridan. The PolyMAX Frequency-Domain Method: A New Standard for Modal Parameter Estimation? *Shock and Vibration*, 11(3-4):395–409, 2004.

[19] MathWorks By Cleve Moler. "Magic" Reconstruction: Compressed Sensing.

[20] Emmanuel Candes, Justin Romberg, et al. l1-magic: Recovery of sparse signals via convex programming. *URL: www. acm. caltech. edu/l1magic/downloads/l1magic. pdf*, 4(14):16, 2005.

[21] Cleve's Corner. The World's Simplest Impossible Problem.